

# **Nephronectin regulates cardiac valve development via BMP4-HAS2 signaling in zebrafish**



Dissertation

for attaining the Doctorate degree  
of Natural Sciences

submitted to the Faculty of Biological Science.  
of the Johann Wolfgang Goethe University  
in Frankfurt am Main

by

**Chinmoy Patra**

From Bankura, India

Max Planck Institute for Heart and Lung Research

Bad Nauheim, Germany, 2011

(D 30)

Accepted by the Faculty of the .....

Johann Wolfgang Goethe University as a dissertation.

Dean: ...

Expert assessor:

Date of the disputation

## **SUPERVISED BY**

Dr. Felix B. Engel, Ph.D  
Department of cardiac development and regeneration  
Max Planck Institute for Heart and Lung Research  
Bad Nauheim, Germany

## **REVIEWER**

Prof. Dr. Anna Starzinski-Powitz, Ph.D.  
Dean  
Institute for Cell Biology and Neuroscience  
Molecular Cell Biology and Human Genetics  
Johann Wolfgang Goethe University  
Frankfurt am Main, Germany

and

Prof. Dr. Dr. Thomas Braun, M.D., Ph.D.  
Department of cardiac development and regeneration  
Max Planck Institute for Heart and Lung Research  
Bad Nauheim, Germany

DEDICATED TO MY  
PARENTS AND GRANDPARENTS

*Whose perpetual affection and blessing always*

*Inspired me for higher ambition in life*

## **DECLARATION**

The work described in this thesis is original and has not previously been submitted for a degree or diploma in any other University or College, and to the best of my knowledge, does not contain material previously published or presented by another person, except where due reference is made in the text.

Chinmoy Patra

## Contents

<b>1.</b>	<b>Introduction</b>	<b>1</b>
1.1	Congenital heart disease	1
1.2	Cardiac valve development	2
	1.2.1 Key regulatory pathways	4
1.3	Zebrafish heart development	7
	1.3.1 Atrioventricular canal morphogenesis	10
1.4	Nephronectin	12
1.5	Aim of the study	15
<b>2.</b>	<b>Materials</b>	<b>16</b>
2.1	Equipment	16
	2.1.1 Miscellaneous equipment	16
	2.1.2 Microscopes	17
	2.1.3 Centrifuges	17
2.2	Miscellaneous materials	18
	2.2.1 Disposables	18
	2.2.2 Non-disposables	19
2.3	Chemicals	19
2.4	Enzymes	21
2.5	Oligonucleotides	22
2.6	Antibodies	23
2.7	Fish food	25
2.8	Buffer and solutions	25
2.9	kits	30
2.10	Antibiotics	31
2.11	Zebrafish lines	32
2.12	Plasmids	32
2.13	Morpholino-oligonucleotides	33
2.14	Growth media	34
2.15	Competent cells	35
2.16	Software	35

---

<b>3. Methods</b>	<b>36</b>
3.1 Zebrafish maintenance	36
3.2 RNA isolation and reverse transcription	37
3.3 cDNA amplification by PCR	37
3.4 Agarose gel electrophoresis	37
3.5 cDNA elution from agarose gel	38
3.6 Cloning	38
3.7 Preparation of competent <i>E. coli</i> cells	39
3.8 Transformation of <i>E. coli</i> competent cells	39
3.9 Plasmid DNA isolation	39
3.10 Determination of the concentration of nucleic acids	39
3.11 <i>In situ</i> hybridization	40
3.11.1 Probe synthesis	40
3.11.2 Fixation and storage of embryos	40
3.11.3 1 <sup>st</sup> day-hybridization	41
3.11.4 2 <sup>nd</sup> day-unbound probe removal	41
3.11.5 3 <sup>rd</sup> day-unbound antibody removal and staining	42
3.12 Embedding and documentation	42
3.13 Capped <i>npnt</i> mRNA synthesis	42
3.13.1 Linearized template generation	42
3.13.2 <i>In vitro</i> capped RNA synthesis	43
3.14 Manipulation of gene expression	43
3.15 BMP signaling inhibition	43
3.16 Protein extraction from whole zebrafish embryos	44
3.17 Determination of protein concentration	44
3.18 Western blot analysis	44
3.19 Histological analysis	45
3.20 Immunohistochemistry	46
3.21 Isolation of neonatal heart cells	47
3.22 Microscopy and morphological analysis	48
3.23 Statistical analysis	49

---

<b>4.</b>	<b>Results</b>	<b>50</b>
4.1	<i>npnt</i> is transiently expressed during mammalian heart development	50
4.2	Cloning for in situ probe and full length <i>npnt</i> synthesis	51
4.3	<i>npnt</i> is transiently expressed in the heart during zebrafish development	53
4.4	Npnt knockdown utilizing different morpholinos	54
4.5	Npnt knockdown disrupts heart development and is lethal	55
4.6	Npnt knockdown causes an extended AV canal	56
4.7	Microinjection of <i>npnt</i> mRNA rescues AV canal extension	58
4.8	Npnt depletion does not affect the total number of cardiomyocytes	60
4.9	Npnt depletion causes an expansion of myocardial AV canal gene expression	62
4.10	Npnt morphant hearts have an AV canal endocardium	63
4.11	Npnt knockdown causes abnormal expansion of the cardiac jelly	65
4.12	Npnt knockdown causes abnormal trabeculation	66
4.13	Has2 knockdown reduces the number of AV endocardial cells	67
4.14	Bmp4 and <i>cspg2</i> misexpression is not dependent on expanded <i>has2</i> misexpression	69
4.15	Diminished BMP signaling reduces AV canal expansion via inhibition of ectopic expression of <i>has2</i> and <i>cspg2</i>	70
4.16	Chemical inhibition of BMP signaling has no obvious effect on wild type zebrafish embryos hearts	72
4.17	Wnt/ $\beta$ catenin signaling is not the downstream target of Npnt	73
4.18	Npnt does not signal through integrin $\alpha 8$	74
<b>5</b>	<b>Discussion and outlook</b>	<b>76</b>
5.1	The ECM is critical for valve development	76
5.2	Npnt does not regulate Wnt signaling	77
5.3	Npnt-signals through the BMP4-Has2 axis	78
5.3.1	Receptor-mediated inhibition of Bmp4 expression	79



---

5.3.2	Npnt controls BMP4 bioavailability by limiting its diffusion	80
5.4	Npnt signals through growth factor receptors	81
5.5	Npnt depletion does not affect cardiomyocyte number	82
5.6	Conclusion	83
<b>6.</b>	<b>Summary</b>	<b>85</b>
<b>7.</b>	<b>References</b>	<b>87</b>
<b>8.</b>	<b>Appendices</b>	<b>95</b>
	Npnt amino acid sequence homology	95
	Sequential events during zebrafish heart development	96
	Acknowledgements	98
	Zusammenfassung	100
	Curriculum vitae	109
	Publications	110

**Abbreviations**

ALPM	Anterior lateral plate mesoderm
AMP	Adenosine monophosphate
AP	Alkaline phosphatase
ATP	Adenosine 5'triphosphate
AV	Atrioventricular
BMP	Bone morphogenic protein
BSA	Bovine serum albumin
cAMP	Cycline adenosine monophosphate
cDNA	Complementary DNA
CHAPS	3-((3-Cholamidopropyl)dimethylammonium)-1-propanesulfonate
CHD	Congenital heart disease
DAPI	4,6-diamino-2-phenylindole
dH <sub>2</sub> O	Distilled water
DEPC	Diethylpyrocarbonate
DMEM	Dulbeco's modified eagle medium
DMSO	Dimethyl sulfoxide
DNA	Deoxyribonucleic acid
dNTP	Deoxyribonucleotide triphosphate
dpf	Days post fertilization
DTT	Dithiothreitol
E	Embryonic day
EC	Endocardial cushion
ECL	Enhanced chemiluminiscence
<i>E.coli</i>	<i>Escherichia coli</i>
EDTA	Ethylenediaminetetraacetic acid
EGTA	Ethylene glycol tetraacetic acid
EGFP	Enhanced green fluorescent protein
EMT	Epithelial-Mesenchymal Transformation
ERK	Extracellular receptor kinase
EST	Expressed sequence tag
EtBr	Ethidium bromide
FCS	Fetal calf serum

---

<i>g</i>	Acceleration of gravity
g	Gram
GAPDH	Glyceraldehydes-3-phosphate dehydrogenase
GFP	Green fluorescent protein
GST	Glutathione S-transferase
HA	Hyaluronan (hyaluronic acid)
Has	Hyaluronan synthase
HCl	Hydrochloric acid
hpf	Hours post fertilization
HEPES	4-(2-hydroxyethyl)-1-piperazineethanesulfonic acid
HRS	Horseradish peroxidase
HH	Hamburger Hamilton
IPTG	Isopropyl-D-1-thiogalactopyranoside
kDa	Kilodalton
KCl	Potassium chloride
KH <sub>2</sub> PO <sub>4</sub>	Potassium dihydrogen phosphate
l	Liter
ICC	Immunocytochemistry
IFT	Inflow tract
IHC	Immunohistochemistry
M	Molar
mg	Milligram
min	Minute
ml	Milliliter
mM	Millimolar
mmol	Millimol
MMLV	Moloney murine leukemia virus
mRNA	Messenger RNA
MgCl <sub>2</sub>	Magnesium chloride
MOPS	3-[N-morpholino] propanesulfonic acid
NaCl	Sodium chloride
NaN <sub>3</sub>	Sodium azide
Na <sub>2</sub> HPO <sub>4</sub>	Disodium hydrogen phosphate
NaOH	Sodium hydroxide

---

NP40	Nonidet P40
ng	Nanogram
OD	Optical density
OFT	Outflow tract
P	Postnatal day
PBS	Phosphate buffered saline
PCR	Polymerase chain reaction
PIPES	Piperazine-1,4-bis(2-ethanesulfonic acid)
PKA	Protein kinase A
PKC	Protein kinase C
PMSF	Phenylmethanesulfonyl fluoride
PTU	N-phenylthiourea
PVDF	Polyvinylidenfluorid
pH	Negative logarithm of hydrogen ions concentration
q.s.	Quantum sufficiat (as much as suffices)
RNA	Ribonucleic acid
Rnase	Ribonuclease
rpm	Revolutions per minute
RT	Room temperature
RT-PCR	Reverse transcription followed by polymerase chain reaction
sec	Second
SDS	Sodium dodecyl sulfate
T <sub>a</sub>	Annealing temperature
Taq	<i>Thermus aquaticus</i>
TAE	Tris-acetate-EDTA
TBE	Tris-borate-EDTA
TBS	Tris buffered saline
TE	Tris-EDTA
TGFβ	Transforming Growth Factor β
Tricane	Ethyl-m-aminobenzoate methanesulfonate
tRNA	Transfer RNA
U	Unit
UTR	Untranslated region
UV	Ultraviolet

---

V	Volt
W	Watt
WB	Western blot
v/v	Volume/volume
w/v	Weight/volume
X-gal	5-bromo-4-chloro-3-indolyl-D-galactopyranoside

# 1. Introduction

## 1.1 Congenital heart disease

Abnormalities of the heart before birth are referred to as congenital heart disease (CHD). Around 1% of live births are affected (1). Moreover, heart defects are the leading cause of birth defect-related deaths. Depending upon which part of the heart is malformed CHD are classified into different categories (2) (Figure 1.1):

- a) **Cyanotic heart disease:** This disease includes all malformations that cause deoxygenated blood to bypass the lung entering the systemic circulation. This category includes Tetralogy of Fallot, transposition of the great arteries, Ebstein's anomaly of the tricuspid valve, tricuspid atresia, pulmonary atresia, double outlet right ventricle, total anomalous pulmonary venous connection and persistent truncus arteriosus.
- b) **Left-sided obstructive lesions:** In this category diseases are combined that are characterized by the failure of the left ventricle to efficiently pump oxygenated blood to all areas of the body. Defects include interrupted aortic arch, mitral stenosis, aortic stenosis, aortic coarctation and hypoplastic left heart syndrome.
- c) **Septation defects:** These defects result in a mixture of arterial and venous blood and results often in volume overload of the ventricles. Defects include atrial septation defects, ventricular septal defects and atrioventricular septal defects.
- d) **Other defects:** Bicuspid aortic valve and patent ductus arteriosus.

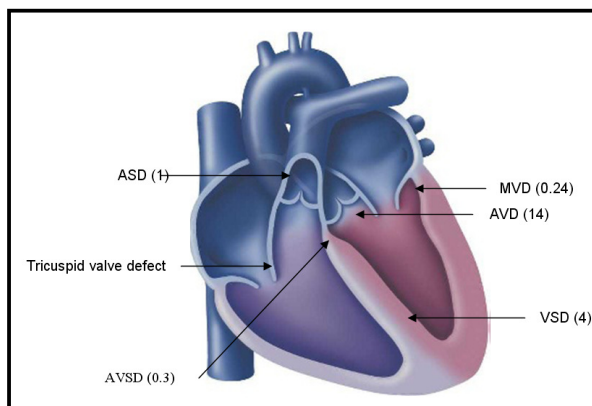


**Figure 1.1: Congenital heart disease.**

This diagram shows the different parts of the adult heart that are affected by congenital septal and valve disease. The number in parentheses indicates the estimated incidence of each disease per 1,000 live births. ASD, atrial septal defect; AVSD, atrioventricular septal defect; AVD, aortic valve defect; VSD, ventricular

septal defect; MVD, Mitral valve defect. Image and data adapted from Bruneau *et al.*, 2008 (2).

Due to its high mortality and morbidity it is important to determine the etiology of the different CHD, which requires a detailed understanding of heart development. This thesis focuses on the elucidation of molecular pathways governing cardiac valve development as congenital valve defects are with 20 to 30% the most common congenital cardiovascular malformations (3). It has been estimated that about 5% of live births carry congenital heart malformations if one also considers minor defects (1, 4). Defects in valve structure and function during development occur in several CHD like Holt–Oram, Marfan, Noonan and Williams syndromes for which the genetic cause has been identified (5). Mutations in the *tbx5* gene cause Holt–Oram syndrome (6). The Marfan syndrome is due to mutations in the *fibrillin1* gene, which encodes an extracellular matrix glycoprotein (7). The Noonan Syndrome is an autosomal dominant congenital disorder cause in most cases by mutations in the *ptn11* gene (8) and Williams syndrome is caused by a hemizygous deletion of about 26 genes in chromosome 7 (9). In addition, mutations of other genes like *notch1* (10) and *tbx20* (11) have been associated with valve malformation. However, in many diseases the underlying cause of valve malformation remains undiscovered. Thus, it is important to identify genes that play a crucial role in cardiac valve and septum formation as well as maturation.

## 1.2 Cardiac valve development

All vertebrate hearts, whether four- or two-chambered, have valves to enable unidirectional blood flow. Cell lineage analysis in mice as well as in birds have demonstrated that the majority of cells in the valves after birth originate from the endothelium (12-14) with little or no contribution from other regions of the heart like myocardium (12), proepicardium (14) or secondary heart field (especially in the outflow tract, OFT) (12).

In mouse the primitive heart tube is formed by fusion of the cardiac crescent along the embryonic midline at embryonic day (E) 8.0 (15). At this stage the primitive heart tube is composed of a myocardial and an endocardial layer, which is separated by a cell-free layer consisting of extracellular matrix (ECM) components called cardiac jelly. Subsequently, the heart tube bends (looping) and segmentation starts. Shortly after looping cardiac valve formation starts with the expansion of the cardiac jelly at the valve forming region i.e. at

the junction of the future atria and ventricle as well as at the endocardial ridges in the OFT. Endocardial cushions (EC) are formed by populating the expanded cardiac jelly with mesenchymal cells. These cells originate from the overlying endocardium by a process called Epithelial-Mesenchymal Transformation (EMT) (16, 17). During this process endocardial cells lose their epithelial characteristics, delaminate from the endocardial layer and migrate into the cardiac jelly and form cardiac cushion mesenchyme. In the atrioventricular (AV) canal EMT is initiated around E9.5 in mouse (18), HH17 in chicken (19), at stages 40-41 in frog (20, 21) and E31 to E35 in human (20). EMT in the OFT occurs slightly later (22).

Cross talk between endocardium and myocardium through the cardiac jelly is important for EC formation (23). At the valve forming region the myocardium secretes various signaling molecules, which drive ECM production and inhibit the transcription of chamber-specific genes (Figure 1.2A). The increased amount of ECM and the hydrophilic nature of proteoglycans in the ECM intensify the swelling of the cardiac jelly and protrusion of the endocardium into the lumen (24, 25), which allows unidirectional blood flow at this stage.

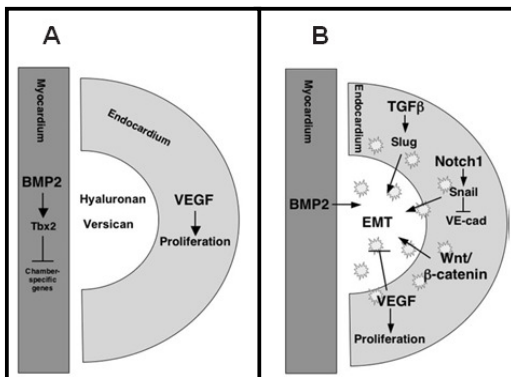


**Figure 1.2: Scheme representing the regulatory mechanisms that control EC formation (A) and EMT (B).** A, BMP2/4 induces transcription of *Tbx2* in the myocardium inhibiting chamber-specific gene expression and inducing deposition of hyaluronan and versican in cushion-forming regions of the AV canal and OFT. VEGF, expressed in endothelial cells, promotes

endothelial cell proliferation at EC. B, BMP2/4 expression in the myocardium adjacent to valve forming endocardium and multiple signals derived from endocardium promote EMT in EC (delamination and mesenchymal cells are indicated by white stars). TGF $\beta$  promotes EMT by signaling through Slug, whereas Notch1 suppresses VE-cadherin (VE-cad) expression by signaling through Snail promoting EMT. Wnt/ $\beta$ -catenin signaling promotes EMT in EC. After EC establishment, endocardial VEGF expression inhibits EMT and maintains endothelial cell proliferation at the valve forming region. Image and data adapted from Combs M.D. *et al.*, 2009 (26).



The molecular pathways and cellular morphogenesis are conserved in AV and OFT cushion development (27). EMT and EC morphogenesis depends on different signaling molecules from both myocardium and endocardium (Figure 1.2B). Participation of cells from the secondary heart field and neural crest derived cells add an additional level of complexity to OFT valve formation (26, 28).

### 1.2.1 Key regulatory pathways

**BMP signaling:** Bone Morphogenetic Proteins (BMPs) are multi-functional proteins that belong to the Transforming Growth Factor  $\beta$  (TGF $\beta$ ) superfamily. Several *in vivo* data suggest that myocardium-derived BMPs play a vital role during the early stage of EC formation and EMT (29-31). This is further supported by *in vitro* explant culture experiments (32) as well as primary cell culture data (33). Before the onset of EC formation BMP2 and BMP4 expression become restricted to the myocardium in the cushion-forming regions of the heart tube. Around E9.5 in mice BMP2 is expressed in the AV canal, OFT and atrial myocardium (27, 34) whereas BMP4 is only expressed in the AV canal and OFT myocardium (35). In chick BMP2 is also only expressed in the AV canal and OFT myocardium (36). In zebrafish BMP4 is expressed throughout the primitive heart tube and around 37 hours post fertilization (hpf) expression becomes restricted to the AV canal, OFT and inflow tract (IFT) (37).

BMPs signal through different serine/threonine kinase receptors including three type I subtypes [BMPR-IA (ALK-3), BMPR-IB (ALK-6) and type IA activin receptor (ActR-IA or ALK-2)] (38) and three type II subtypes [type II BMP receptor (BMPR-II), type II activin receptor (ActR-II) and type IIB activin receptor (ActR-IIB)] (39, 40). The transmembrane receptor betaglycan can enhance the binding of BMPs to their receptors (41). Activation of BMP receptors causes phosphorylation of its immediate downstream targets Smad1/5/8. Phosphorylated Smad1/5/8 proteins form a complex with Smad4 and translocate into the nucleus where they control the transcription of other genes vital for EC formation (Figure 1.3). BMP2/4 inhibits chamber-specific gene expression by inducing *Tbx2* transcription while promoting expansion of the cardiac jelly by inducing hyaluronan and versican deposition in the EC forming region (26).

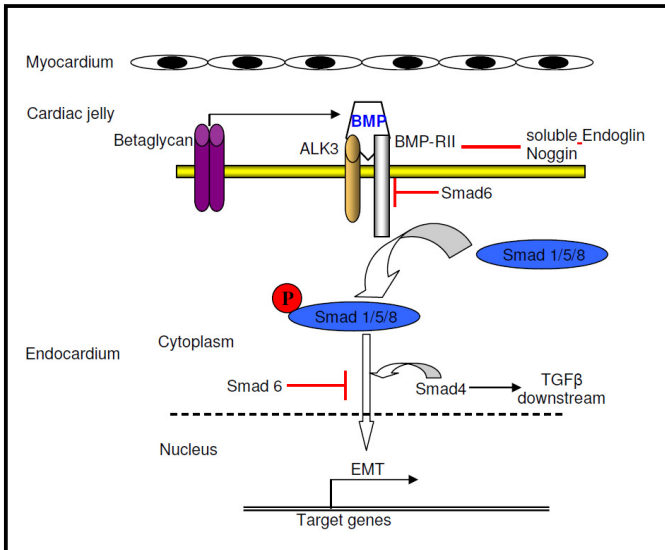


**Figure 1.3: Regulation of BMP signaling.** BMP ligands are secreted from the myocardium and are localized in the ECM. BMPs signal through heterodimerized ALK3/BMP-RII receptors on EC endocardial cells. BMP binding activates serine/threonine kinase activity of the receptors which results in phosphorylation of their downstream target molecules Smad1/5/8. Phosphorylated

Smad1/5/8 form a complex with Smad4 and subsequently translocate into the nucleus where they control the transcription of different transcription factors regulating EMT. Co-receptors like betaglycan enhance BMP binding to their receptors. Smad6 inhibits downstream of BMP signaling by antagonizing the phosphorylation of Smad1/5/8 and inhibiting the complex formation of phospho-Smad1/5/8 and Smad4. BMP antagonists like Noggin bind with BMP-2, -4 and -7 and block BMP signaling. Soluble Endoglin is thought to inhibit receptor binding of BMPs by sequestering them. BMP and TGF $\beta$  signaling cross talk via Smad4.

Several experiments have shown that the temporal and spatial control of BMP signaling is very important for the proper shape and function of the valves. Smad6 for example plays an important role as negative regulator of BMP signaling (Figure 1.3) (42, 43). Consequently, *Madh6* (encodes the Smad6 protein) mutant mice are characterized by excessive proliferation of mesenchymal cells causing hyperplastic ECs and thickened heart valves (44). Other inhibitors of BMP signaling are the secreted, glycosylated protein Noggin and the soluble Endoglin, which can bind with BMPs antagonizing the binding to their receptors (45, 46). BMP signaling inhibition results in downregulation of a number of genes including *tgf $\beta$* , *notch1*, basic helix loop helix transcription factor *twist1* and homeobox gene *msx2* which are related to EMT in AV canal EC development (34, 47).

Taken together, these data demonstrate that BMP signaling is crucial for cardiac valve formation by increasing production of ECM components, induction of endocardial EMT and patterning of the AV myocardium.

**Wnt/ $\beta$ -catenin signaling:** It has been demonstrated that the canonical Wnt/ $\beta$ -catenin cascade is important for EMT in mice as well as in zebrafish during cardiac valve development (48, 49). In mice both *Wnt4* and *Wnt9b* are expressed in endocardial cells underlying the EC forming region (26). Recently, it has also been demonstrated that in chick *Wnt9a* is expressed at the AV canal. Overexpression of *Wnt9a* results in hypercellular cushion and inhibition of Wnt signaling leads to lack of mesenchyme. In zebrafish lack of Wnt inhibition in *apc* mutants leads to an increase in the number of AV canal-like endocardial cells (49). Taken together it appears that the Wnt/ $\beta$ -catenin signaling cascade plays a major role during cardiac valve development.

**Signaling via ECM components:** The ECM of ECs is a hydrated scaffold that not only serves as a physical support for mesenchymal cell migration but also provides signaling cues initiating EMT (50). Before the onset as well as during the EC formation myocardial and endocardial cells secrete ECM components like ES/130 (a novel 130-kDa protein), hLAMP1 (lectin-associated matrix protein in the heart), fibronectin, versican and others that play crucial roles during EMT (51, 52).

The extracellular polysaccharide hyaluronan (HA) is a major component of the ECM in ECs that is synthesized by the enzyme Hyaluronan Synthase 2 (Has2). Has2 is expressed in the myocardium of the AV canal region, the endothelium of the OFT and by migratory mesenchymal cells (53). Around E9.5 cardiac jelly is rich in HA and versican. HA together with other interacting proteoglycans like aggrecan, versican, brevican, neurocan etc. gives proper hydrodynamic properties to the cardiac jelly. HA can also affect cellular events by interacting with cell surface receptors like CD44 and CD168 (Rhamm) transducing intracellular signaling through the Ras and ERK pathways (54, 55). In mice disruption of the *has2* gene prevents transformation of cardiac endothelial cells into mesenchyme (53). Interestingly, heterodimerized ErbB2/ErbB3 receptor in *Has2* mutant failed to phosphorylate. Using AV canal explant cultures Camenisch *et al.* could rescue this phenotype by adding the ErbB3 ligand, neuregulin (also known as heregulin-1). These data suggest that there is a link between hyaluronan and ErbB receptor-mediated signaling during EMT in ECs (28).

Versican, an extracellular matrix proteoglycan, plays an important role on cellular proliferation, migration and differentiation via interacting with cell surface receptors. In mice versican is expressed in the EC of the cardiac valve forming region (56). In zebrafish versican is expressed during early development throughout the cardiac myocardium and its expression becomes restricted at 37 hpf to the AV canal region (37). Versican can bind with CD44 and stabilizes its interaction with HA. It also has been suggested that versican can interact with  $\beta 1$  integrin and activate focal adhesion kinase, which promotes cell adhesion (57). However, a number of studies have shown that versican has anti-adhesive properties (58, 59). Mutation of the mouse *cspg2* gene encoding versican caused failure of endocardial cells to undergo EMT and to migrate into the cardiac jelly of cardiac valve primordia (56, 60).

Taken together, these data demonstrate that the components of the ECM play important roles during valve development beyond their function as physical support.

### 1.3 Zebrafish heart development

In this thesis we used the zebrafish as model system. Cardiogenesis in zebrafish starts at the early blastula stage (2.75 hpf, 512 cells) (see appendice, Table A1), when most cardiac progenitors are located at the marginal zone, midway between the dorso-ventral axis. At the pregastrula stage (5 hpf, 40% epiboly) atrial myocardial progenitors are ventrally and ventricular myocardial progenitors are more dorsally positioned. Endocardial progenitors are not spatially organized (61, 62). During gastrulation (5.5 hpf to 8 hpf) pre-cardiac cells involute and migrate towards the animal pole. At around the 6 to 8 somite stage (11.5 hpf) the migratory cardiac progenitor cells reach the embryonic axis and form part of the anterior lateral plate mesoderm (ALPM), that expresses the pre-cardiac marker *nkx2.5* (63). Around this stage *gata4* is expressed within rostral (anterior) and caudal (posterior) ALPM and *hand2* expression is restricted to the caudal portion of *gata4*-expressing ALPM. *nkx2.5* expression is observed within a medial portion of the caudal ALPM, but is excluded from the lateral and rostral ALPM (Figure 1.4) (64).

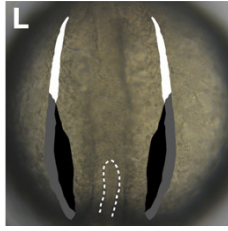


**Figure 1.4: Scheme of the ALPM superimposed onto a dorsal view of a live embryo at the 7 somite stage.** The tip of the notochord is outlined by dashes. The ALPM is divided in zones correlating with expression patterns described in the text: rostral (white), medial (black), and lateral (gray) ALPM. However during the 6 to 9 somite stage (11.5 hpf) ALPM morphology slightly varies. Modified image adapted from Schoenebeck *et al.*, 2007(64).

In between the somite stages 10 to 16 (14-16 hpf), the *nkx2.5*-positive cells migrate medially. The initiation of myocardial differentiation starts at somite stages 13 to 14 (15 hpf) and the cardiomyocyte-specific genes *cmlc2* and *vmhc* are expressed (65). Atrial-specific gene expression is first evident at the 19 somite stage. At the 16 somite stage cardiomyocyte progenitors form a pair of bilateral tubular primordia that are positioned on either side of the endocardial progenitor cells. The ventricular precursor cells (*vmhc*-positive) are medially and atrial precursors are laterally positioned. These lateral populations migrate towards the embryonic midline in an organized fashion (65). Proper myocardial differentiation and differentiation of the closely juxtaposed endodermal precursors are a prerequisite for the migration of both lateral myocardial populations (66-68). There are two possibilities: either endodermal precursors provide factors, which induce cardiomyocyte migration or they produce a substrate for migration. At around the 18 somite stage myocardial precursors reach the midline and begin to fuse at the posterior point to form a horseshoe-shaped structure (66). Around the somite stage 21 anterior cells migrate medially and the horseshoe transforms into a cone with a central lumen. At 22 hpf the cone shape gets transformed into a tube (66, 69). First the ventricular end of the heart tube organizes and then the atrial end. By 24 hpf, the tube lies along the anterioposterior axis with the atrial end anteriorly and ventral end posteriorly (Figure 1.5) (65).

After cardiac tube formation neural crest cells migrate to the linear heart tube and differentiate into cardiomyocytes. Incorporated cardiac neural crest cells express myocardial markers during the initiation of cardiac looping morphogenesis (30 hpf) (70, 71). Cardiac contraction begins at around the 27 somite stage (22 hpf). In zebrafish, after cardiac contraction begins, intra-cardiac hemodynamics and myocardial patterning play a crucial role for cardiac valve morphogenesis and trabeculation (72, 73). After primitive heart tube

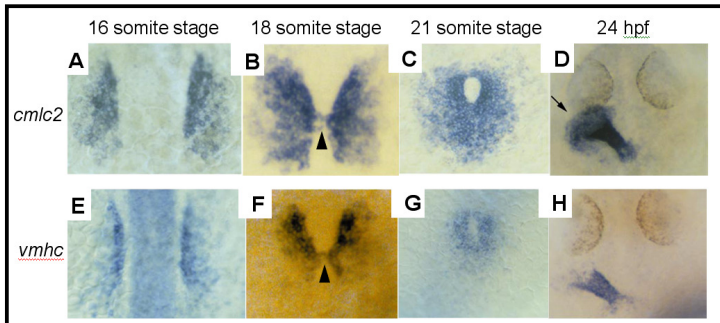


**Figure 1.5: Anatomical position of the myocardial progenitors during heart tube assembly. (A-H)**

Dorsal views anterior at the top showing the *cmlc2*-positive and on the bottom the *vmhc*-positive

myocardial population. At the 16 somite stage, *cmlc2*-positive cardiac precursors remain as two bilateral tubular primordia. Ventricular progenitors are positioned anteriorly. At the 18 somite stage, cardiac fusion begins via contact between two populations established at the posterior point (arrowheads in B,F) to form a horseshoe-shaped structure. At the 21 somite stage, anterior cells migrate medially and the horseshoe transforms into a cone with a central lumen. By 24 hpf, the cone is extended into a primitive heart tube. At this time point ventricular cells are almost completely assembled while the atrial precursors (arrow in D) are still scattered. Modified images are adapted from Yelon *et al.*, 1999.(65).

formation cardiac ballooning and looping starts and visibly distinct ventricular and atrial chambers are formed at around 30 hpf. At 3 days post fertilization (dpf) there are four visibly distinct chambers formed i.e. juxtaposed atrium and ventricle, sinus venosus, and bulbus arteriosus, which are separated by constrictions (Figure 1.6). Cardiac valve formation at the AV junction starts at 36 hpf with the initiation of cardiac jelly deposition and endocardial cell differentiation. Like mammalian and avian hearts the adult zebrafish heart contains a coronary vasculature and a third cellular layer surrounding the myocardium, the so-called epicardium (74). The myocardium remains devoid of an epicardium until 48 hpf. Like other vertebrates the epicardium in zebrafish develops from the proepicardial organ (PEO) (75). At 50 hpf there are two PEO visible in zebrafish hearts as clusters of cells. A similar structure has been described in mouse and avian PEO. One of the clusters is situated near the sinus venosus and the second one on the ventricular surface of the heart adjacent to the AV junction. On the third day of zebrafish development PEO cells start to migrate on the top of the myocardial layer and by 4 dpf the embryonic epicardium surrounds the myocardium (75). Signaling cues as well as cellular contribution from the epicardium are essential for proper coronary vasculature morphogenesis, ventricular trabeculation and overall myocardial growth and differentiation (76).

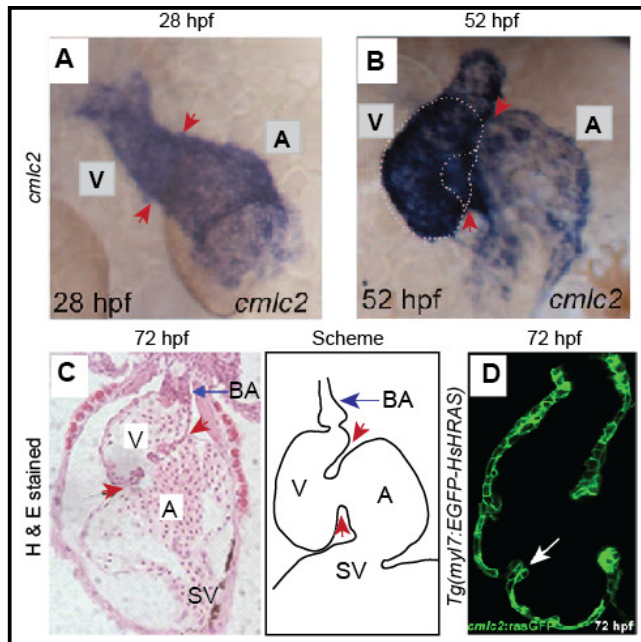


**Figure 1.6: Cardiac morphogenesis after primitive heart tube formation.** (A,B)

Brightfield images of the wild type embryos heart after whole-mount *in situ* hybridization with probe against *cm1c2*. (A) Around 30 hpf the primitive heart tube has become curved and visibly distinct ventricular and atrial chambers are formed. (B) A looped heart at 52 hpf, the ventricle is to the right and atrium to the left of the midline and constriction is evident at the AV boundary. (C) H & E stained

sagittal section of a heart from a wild type embryo at 72 hpf is showing four visibly distinct chambers formed in a series i.e. sinus venosus, atrium, ventricle, and bulbus arteriosus; blue arrow indicates the bulbus arteriosus. (D) Confocal image of the heart from *Tg(myI7:EGFP-HsHRAS)<sup>s883</sup>* embryos (EGFP localized in the cardiomyocyte membrane) at 72 hpf showing small clusters of cardiomyocytes (trabeculae) on the single layer of ventricular myocardium; indicated by arrow. Red arrows indicate the AV boundary. A; Atrium, V; Ventricle, SV; Sinus venosus, OFT; Outflow tract, IFT; Inflow tract. Modified images are adapted from Auman *et al.*, 2007 and Qu *et al.*, 2008 (77, 78).

In the zebrafish heart ventricular trabeculation is initiated at around 72 hpf. At this time point ventricular cardiomyocytes make small clusters of cells on the monolayered myocardium and protrude inside the ventricular lumen (Figure 1.6D). Afterwards they grow further and make complex finger like projections on the compact myocardial layer. A recent study has suggested that the initiation of ventricular trabeculation starts with cardiomyocyte delamination and migration. Later on trabecular growth depends on cell division (79). Every part of the adult zebrafish heart is evident at 5 dpf heart, i.e. epicardium, endocardium, myocardium, trabeculation of the ventricular wall as well as cardiac valves at the AV junction and OFT.

### 1.3.1 Atrioventricular canal morphogenesis

At 30 hpf the heart consists of a single layer of myocardium and a single layer of endocardium that are separated by cardiac jelly. At this time ventricular myocardial cells are cuboidal (80). In contrast, atrial myocardial cells are



squamous. Cardiomyocytes at the AV boundary have no obvious specific morphology. Endocardial cells are squamous throughout the endocardium (81).

Differentiation of the myocardial as well as endocardial cells at the AV boundary starts around 36 hpf. A single tier of endocardial cells starts to differentiate transforming into cuboidal shaped cells, whereas the rest of the endocardial cells remain squamous. Differentiating endocardial and myocardial cells express ECM components resulting in the swelling of the cardiac jelly at the AV boundary. The number of differentiated cuboidal endocardial cells at the AV boundary increases gradually. At 2 dpf a five to six cell-wide sheet of differentiated endocardial cells (cuboidal) lines the superior and inferior AV boundary regions. These differentiated cuboidal endocardial cells express Dm-grasp (Alcam), whereas squamous chamber endocardial cells are devoid of Dm-grasp. At this developmental stage this cellular structure prevents blood regurgitation (81).

The swelling of the cardiac jelly and the right combination of ECM components is crucial for AV canal differentiation and valve formation (16). The expression of genes important for AV canal differentiation and cardiac jelly swelling, like *has2*, *bmp4*, *cspg2*, *tbx2* and *notch1b*, becomes restricted to the AV boundary region during AV canal morphogenesis (37, 82). The differentiation of the AV endocardial cells is continued until 55 hpf. At 60 hpf differentiated AV endocardial cells start to form valve leaflets, which transform into functional leaflets at around 96 hpf (81, 83). During this invagination (60 to 96 hpf) cuboidal AV endocardial cells are round in appearance and lose their Dm-grasp expression (Figure 1.7) (81, 83).

There is a debate about the mechanism of valve leaflet development. Beis *et al.* have suggested that the zebrafish valve leaflet forms from a preexisting endocardial cushion similar to mammalian and avian (81). Recently, with the help of high-speed imaging of the zebrafish heart valve development Scherz *et al.* suggested that valve leaflets form directly by invagination of the endocardium but not by EMT (83). However, the structure of mature mammalian, avian, and amphibian AV valves is similar to adult zebrafish valves consisting of complex stratified connective tissue (74, 84) (Figure 1.7). Therefore it is likely, that the major molecular mechanisms and cellular events



in valve formation are conserved among species. This assumption has been substantiated by several experimental approaches (26, 74).

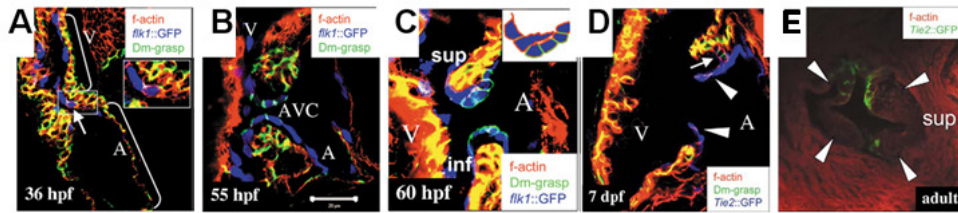


**Figure 1.7: AV valve morphogenesis between 36 hpf and 7 dpf.** (A,B,C) Confocal images of the heart is showing  $Tg(flk1:EGFP)^{S843}$  (pseudo-colored blue) embryos immunostained for Dm-grasp (pseudo-colored green) and stained with rhodamine phalloidin (red). (A) At 36 hpf the heart has partially looped and the endocardial cells are squamous, except one cell at the AV boundary, which is cuboidal expressing Dm-grasp (arrow). (B) At 55 hpf 5 cells in the superior AV canal and 4 cells in the inferior AV canal region exhibit a cuboidal shape and express Dm-grasp. In contrast, chamber endocardial cells are Dm-grasp-negative. Myocardial cells adjacent to the AV canal exhibit stronger Dm-grasp expression compared to the chamber myocardium. (C) At 60 hpf differentiated endocardial cells start to develop valve leaflets (inset shows schematic drawing of superior AV endocardial cells). (D) Confocal image of the heart is showing that at 7 dpf valve leaflets consist of two layers of  $Tg(Tie2:EGFP)^{S849}$  (pseudo-colored blue)-positive cells (arrowheads), which are devoid of Dm-grasp. (E) There are four valve leaflets in the adult zebrafish AV canal (arrowheads). A; Atrium, V; Ventricle, AVC; atrioventricular canal, sup; superior AVC, inf; inferior AVC. Modified images are adapted from *Beis et al.*, 2005 (81).

## 1.4 Nephronectin

We have recently discovered that Nephronectin is transiently expressed in the heart at the time of valve formation. Nephronectin (Npnt) is an ECM protein encoded by the gene *npnt*. Npnt contains: an N-terminal signal peptide for protein secretion,  $Ca^{2+}$ -binding EGF domains that can bind to growth factor receptors, a Mucin-like domain indicating that Npnt can be glycosylated, a RGD sequence that can bind to integrins and a C-terminal MAM domain suggesting an adhesive function (Figure 1.8). These domains are conserved among species, however, the number of EGF repeats are variable. Zebrafish Npnt has 65-70% homology compared to mammalian Npnt (see appendices, Figure A1). The predicted size of mouse Npnt is 63 kDa whereas the secreted Npnt runs on a denaturing gel like a protein of  $\approx 120$  kDa. This difference is probably due to glycosylation of the core protein (85, 86). Nephronectin has been described

as a ligand of integrin  $\alpha 8\beta 1$  having a higher affinity than the RGD motif-containing proteins fibronectin, vitronectin, osteopontin and tenascin-C (85). However, it can also bind with several other RGD-binding integrins (87).

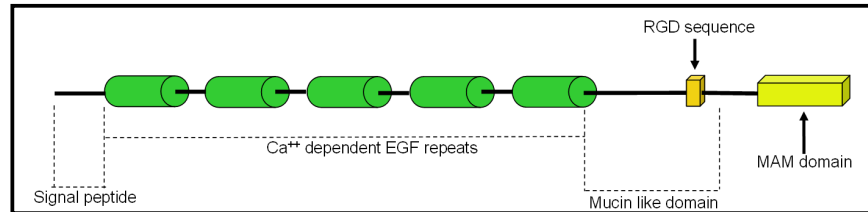


**Figure 1.8: Scheme representing different protein domains of Nephronectin.**

There are two variants of Npnt known in mammals. Both have the same domain structure, however, one variant has one more exon encoding  $\approx 18$  amino acids. There is no data available demonstrating that these variants behave differently. In zebrafish only one variant is known. Npnt is expressed in many developing organs like jaw, ear, eye, urogenital system, digestive tract, lung, branching epithelia etc. with a prominent expression in tissues undergoing EMT (87). Mouse lacking Npnt has shown delayed invasion of the metanephric mesenchyme by ureteric bud during early kidney development resulting in kidney agenesis or hypoplasia. This developmental problem in Npnt knockout mice is associated with the reduced expression of the TGF $\beta$  superfamily protein GDNF; a vital regulator of ureteric bud morphogenesis (88). It has also been shown that GDNF expression is reduced in integrin  $\alpha 8$  null mice (89). These data indicate that Npnt plays a vital role during ureteric bud mesenchyme migration by regulating GDNF expression via integrin  $\alpha 8\beta 1$  receptor. Another study suggests that Npnt is associated with tubular epithelium regeneration in nephrotoxic acute tubular necrosis (90). Furthermore, it has been associated with malignant melanoma. Stable Npnt overexpression in melanoma cell lines increased cell adhesion and decreased cell migration (91). *In vitro* data on the MC3T3-E1 osteoblast cell line has shown that TGF $\beta$  strongly inhibits Npnt expression by activating ERK1/2 and JNK pathway (92). Another study supports this by demonstrating that TGF $\beta$  inhibits Npnt-induced osteoblast differentiation (93). Subsequently, it has been suggested, that early osteoblast differentiation is dependent on EGF repeats of Npnt mediating ERK signaling (Figure 1.9) (94). Taken together Npnt is playing

an important role in cell migration and differentiation activating integrin and MAP kinase signaling pathways.

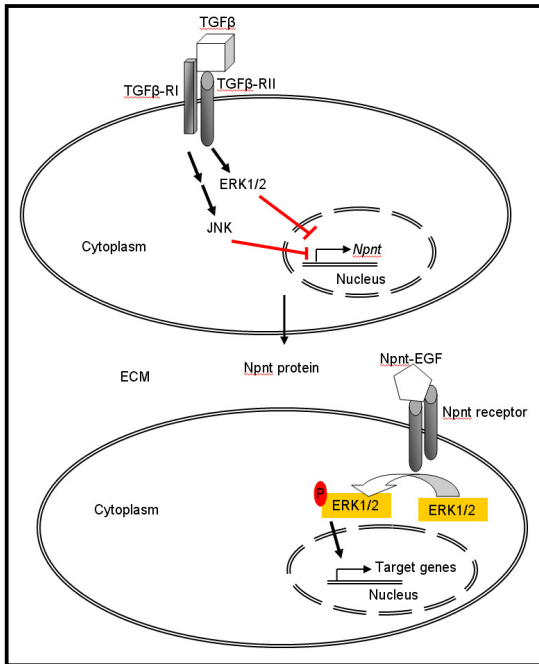


**Figure 1.9: Model of intracellular signaling via Npnt-EGF repeats and inhibition of Npnt expression by TGFβ.**

Binding of TGFβ ligand to its receptor activates ERK1/2 and JNK signaling cascade which inhibits Npnt expression. Extracellular Npnt can bind with its receptor via EGF repeats, results ERK1/2 phosphorylation and activation. Activated ERK1/2 regulates transcription of different genes vital for cellular differentiation.

## 1.5 Aim of the study

In order to better understand heart development Dr. Engel has performed a large scale expression study describing the expression of over 28000 genes during rat heart development from E11 to postnatal day P10.5. Genes that significantly changed in expression were clustered based on their temporal expression profile and could be associated to morphological changes. The goal of this approach is to identify novel regulators of heart development.

The aim of this thesis was to verify the hypothesis derived from the large scale expression study that Nephronectin is a novel regulator of heart development. As a model system the zebrafish was chosen due to the advantage that a zebrafish embryo develops externally, is translucent and continues to grow for several days despite developing a severely malformed, non functional heart. The specific aims of this study were:

- Aim 1:** Determining the spatiotemporal expression pattern of Npnt during mammalian and zebrafish heart development.
- Aim 2:** Assessing the function of Npnt during zebrafish heart development by utilizing morpholino-based antisense technology to knock down Npnt.
- Aim 3:** Elucidating the downstream signaling cascade of Npnt during heart development.

## 2. Materials

### 2.1 Equipment

#### 2.1.1 Miscellaneous equipment

The equipment listed in Table 2.1 was used in this work.

**Table 2.1:** Name, model and supplier of used equipment.

Equipment	Model	Supplier
Aliquoting pipette	Repeater Plus	Eppendorf
Agarose gel electrophoresis chamber	B2 Separationssystem	OWI
Aquatic system		Tecniplast
Bacterial incubator	InnOva 4200	New Brunswick Scientific
Balance	ALC 3100.2	Acculab
Belly dancer	The belly dancer	Stovall
Chemical hood	Vinitex Air	Vinitex
CO <sub>2</sub> incubator	Galaxy R	New Brunswick Scientific
CO <sub>2</sub> incubator	Innova co-170	New Brunswick Scientific
Heating block	Digital Heatblock	VWR
Homogenizer	Ultra turrax T8	IKA Werke
Hybridization oven	HB 1000 Hybridizer	UVP Laboratory Products
Injection pump	Pneumatic PicoPump PV820	World Precision Instruments
Laminar flow	Hearasafe KS	Heraeus
Luminescent Image analyzer	LAS-4000	FujiFilm
Magnetic heating plate	Combimag RCT	IKA Werke
Magnetic stirrer	Stirrer	VWR
Micromanipulator	MM33-right	World Precision Instruments
PCR cycler	Gene Amp PCR System 9700	Applied Biosystems
pH Meter	pH 221 Microprocessor pH Meter	HANNA Instruments

Equipment	Model	Supplier
Pipettes 2,5µL; 10µL; 100µL; 200µL 1000µL	Research	Eppendorf
Plate reader	NanoQuant	Tecan
Power supply	EV243; EV231	Consort
Real-time PCR cycler	CFX96 Real-Time System C1000 Thermal Cycler	BioRad
Roller mixer	SRT6	Stuart
Rotator	SB3	Stuart
SDS-PAGE electrophoresis chamber	X Cell Sure Lock	Invitrogen
Shaker	MHL20	HLC
Spectrophotometer	NanoDrop 2000c	PeqLab
Thermo-block	Digital heat block	VWR
Transfer chamber	X Cell II Blot Module	Invitrogen
Transilluminator	Gel ix DNA and Protein imager	Itas
Vacuumpump	Diaphragma Vacuum pump	Vacuubrand
Vortex	VV3	VWR
Waterbath	U3	Sulabo

### 2.1.2 Microscopes

The microscopes used in this study are listed in Table 2.2.

**Table 2.2:** Microscope type, model and supplier of used centrifuges.

Microscopes	Model	Supplier
Binocular	Leica S6	Leica
Confocal microscope	Axio Imager Z.1	Zeiss
Fluorescence	Leica DMI 3000 B	Leica
Fluorescence	Leica DM 6000 B	Leica
Microscope	Axiovert 25	Zeiss
Stereo microscope	Leica MZ 16FC	Leica

### 2.1.3 Centrifuges

The centrifuges used in this study are listed in Table 2.3.

**Table 2.3:** Centrifuge type, model and supplier of used centrifuges.

Centrifuge	Model	Supplier
Cooling centrifuge	Universal 320R	Hettich Zentrifugen
Cooling table centrifuge	Heraeus Fresco 17	Heraeus
Tabel top centrifuge	Centrifuge 5415C	Eppendorf

## 2.2 Miscellaneous materials

### 2.2.1 Disposables

The disposable materials listed in Table 2.4 were used in this work.

**Table 2.4:** Product, type and supplier of used disposable materials.

Materials	Type	Supplier
Aliquoting pipette tips	Combitips	Greiner bio-one
Bacterial culture tubes	14 ml PP Tube	Greiner bio-one
Capillary tubes	0.2 mm	World Precision Lab
Cell culture dishes	10 cm	Greiner bio-one
Cell culture plates	24 and 6 Well Plates	Greiner bio-one
Cell scraper	Cell Scraper	Greiner bio-one
Coverslips	24x50 mm	Menzel Gläser
Coverslips	12 mm diameter	Menzel Gläser
Filter paper	Chromatography (3 mm)	Whatman
Injekt	1ml	Braun
Latex gloves	Satin plus	Kimtech
Microscope slides	Mattrand, geschliffen 76x26 mm	Knittel Glaser
Microscope slides	Super frost ultra plus	Menzel Gläser
Nitril gloves	Activ Aloe	Blossom
Nitrocellulose transfer membrane	Protran Nitrocellulose	Whatman
PCR tubes	0.5 ml	Eppendorf
Pipette filter tips	FT10; FT100; FT200; FT1000	Greiner bio-one
Pipette tips	10 µl; 200 µl; 1000 µl	Greiner bio-one
Plastic pipettes	2 ml; 5 ml; 10 ml; 50 ml cell star	Greiner bio-one
PAGE	NuPAGE 4-12% Bis-Tris Gel 1.0 mm X 12 well	Invitrogen
PAGE	NuPAGE 4-12% Bis-Tris Gel 1.5 mm X 10 well	Invitrogen
Reaction tubes 1,5ml; 2ml	Safe Lock Tubes	Eppendorf
Reaction tubes 15ml; 50mL	Cell Star TUBES	Greiner bio-one
Thin pipette tips for kapillary filling	20 µL Physio Care Concept	Eppendorf

Materials	Type	Supplier
Tissue culture flasks	T75	Greiner bio-one
Tissue culture flasks	T25	Greiner bio-one
Transfer pipettes	Transfer Pipettes	Sarstedt

### 2.2.2 Non-disposables

The reusable materials listed in Table 2.5 were used in this work.

**Table 2.5:** Product, type and supplier of used non-disposable materials.

Materials	Type/Purpose	Supplier
Glass beaker	DURAN	Schott
Forceps	Inox.4	Dumont
Glass bottles	DURAN	Schott
Glass erlenmeyer flasks	DURAN	Schott
Glass measuring cylinder	DURAN	Hirschmann
Glass pipettes	2 mL; 5 mL; 10 mL; 25 mL	Brand
Micro scale	019.96843 1 mm in 100	Novex
Hemocytometer	0.1 mm depth; 0.0025 mm <sup>2</sup>	Marienfeld
Optical dishes	Glass bottom culture dishes (35 mm)	MatTek
Forceps	No 4 and No5	Neolab
Brush	Vibratomy	Nova
Brush	Microtomy	Roth
ImmEdge pen	Immunostaining	Vector Lab

### 2.3 Chemicals

Product and supplier of the chemicals that were used in this work are listed in Table 2.6.

**Table 2.6:** Product and supplier of used chemicals.

Product	Supplier	Product	Supplier
Agarose	Roth	Agar	Roth
Agaroes (low melting)	Molekula	Ampicillin	Calbiochem



Product	Supplier	Product	Supplier
Blocking reagent (B Block)	Roche	Bromophenol blue	Merck
BSA	Roth	Bicine	Fluka
BM purple AP substrate	Roche	CHAPS	Sigma
Chloroform	Roth	Collagenase Type II	Gibco
DTT	Roth	D-Glucose	Sigma
DNA ladder	Bioline	DEPC	Roth
Ethidium bromide	Fisher Scientific	Ethanol	Roth
Eosin	Chroma	Formamide	Roth
Formaldehyde (10% without methanol)	Polyscience	Formalin (37% with 10% methanol)	Sigma
FBS gold	PAA Lab	Glycine	Roth
Glycerol	Sigma	Hydrochloric acid	Roth
Hemalum	Chroma	Hydrogen peroxide	Sigma
Heparin	Fluka	HEPES Na	Sigma
HRP-Substrate	Thermo Scientific	IPTG	Sigma
Kanamycin	Serva	KCl	Roth
KH <sub>2</sub> PO <sub>4</sub>	Roth	Levamisole	Fluka
LB agar	Roth	LB medium	Roth
Lysis buffer (10x)	Cell Signaling	MOPS buffer (20x)	NuPage
MgCl <sub>2</sub> , 6H <sub>2</sub> O	Roth	Methanol	Roche
Mounting medium (Entellan/Xylol-based)	Merck	Mounting medium (Kaiser's glycerol gelatin/water-based)	Merck
Nonidet P40	Sigma	NaN <sub>3</sub>	Sigma
Na <sub>2</sub> HPO <sub>4</sub>	Roth	NaOH	Roth

Product	Supplier	Product	Supplier
Nitrocellulose membrane	Whatman	dNTPs	Invitrogen
N-phenylthiourea	Alfa aesar	Oligo dT	Invitrogen
PIPES	Roche	Para-formaldehyde	Sigma
Precision Plus Protein Standard	BioRad	Polyacrylamide precast gel	Invitrogen
Propanol	Roche	PMSF	Sigma
Paraffin	Sigma	PEG-3500	Sigma
Phenol red	Sigma	2-Propanol	Roche
Protease inhibitor cocktail	Thermo Scientific	Reverse transcriptase (MMLV)	Invitrogen
RNase inhibitor	Roche	Rhodamine phalloidin	Invitrogen
Sodium chloride	Roth	Sodium citrate	Roth
SDS	Fluka	Stripping buffer	NuPage
Sodium acetate	Roth	Superscript II (RT)	Invitrogen
Tween 20	Sigma	Triton X100	Sigma
Tris base	Roth	Tricane	MP Biomed
Tris base	Roth	Trizol	Invitrogen
Whatman filter paper	Whatman	X-gal	Fluka
Xylol	Roth	Yeast tRNA	Roche

## 2.4 Enzymes

The enzymes listed in Table 2.7 were used in this work. Compatible 10x buffers for different enzymes were supplied with the enzymes.

**Table 2.7:** Product and supplier of used enzymes.

Product	Supplier	Product	Supplier
MMLV reverse transcriptase	Invitrogen	EcoRI	NEB
Superscript II	Invitrogen	NotI	NEB

Product	Supplier	Product	Supplier
Taq DNA polymerase		SacII	NEB
Top-Taq DNA polymerase	Quiagen	SpeI	NEB
T4 DNA ligase	Promega	Apel	NEB
SP6 RNA polymerase	Roche	SacI	NEB
T7 RNA polymerase	Roche	NdeI	NEB
T3 RNA polymerase	Roche	XbaI	NEB
DNase I	Roche	XhoI	NEB
DNase II	Roche		

## 2.5 Oligonucleotides

The oligos listed in Table 2.8 were used in this work. All primers were purchased from Sigma-Aldrich GmbH.

**Table 2.8:** Oligonucleotides used in this study.

Oligo name	Primer sequence (5'-3')	Gene accession
Npnt fwd1_rat	CACAGTGCAAACACGGAGAG	XM_001075443.1 XM_001075423.1
Npnt rev1_rat	GCATCAGCATGTATCCGTTG	XM_001075443.1 XM_001075423.1
Npnt fwd2_rat	CTGGGGACAGTGTCAACCTT	XM_001075443.1
Npnt rev2_rat	GCATCAGCATGTATCCGTTG	XM_001075443.1
Npnt fwd1_mouse	AATCGGCCTATGTCGCTATG	NM_001029836.1 & NM_033525.2
Npnt rev1_mouse	GCAGCATGTATCCGTTGAGA	NM_001029836.1 & NM_033525.2
Primer F1_dr	CATTCGGGAGCTTCAAGTGT	NM_001145580
Primer F2_dr	ATGTGGATCATAAAGTTCATGTTGA	NM_001145580
Primer R_dr	CTGAAGGTCAAAGCCGTCAT	NM_001145580

Oligo name	Primer sequence (5'-3')	Gene accession
Npnt full fwd_dr	CACCATGTGGATCATAAAGTTCATG TTGA	NM_001145580
Npnt full rev_dr	TCATCCTACCGCACTCTGTTG	NM_001145580
Npnt fwd_dr	CAATGGTCTGTGTCGGTACG	NM_001145580
Gapdh fwd_mammal	CAGAAGACTGTGGATGGCCC	NM_017008.3 & NM_008084.2
Gapdh rev_mammal	AGTGTAGCCCAGGATGCCCT	NM_017008.3 & NM_008084.2
Gapdh fwd_dr	TGGGTGTCAACCATGAGAAA	NM_001115114.1
Gapdh rev_dr	AACCTGGTGCTCCGTGTATC	NM_001115114.1
Itga fwd	GAAAAGCCCACGGTTTACAA	NM_001114911.1
Itga rev	TCCCCTGTGAACTCTCCAAC	NM_001114911.1
egfra fwd	ACCGTCTGGGAGTTGATGAC	NM_194424.1
egfra rev	TGTGTGGGACGTGTTTCAGAT	NM_194424.1

## 2.6 Antibodies

The primary and secondary antibodies used in this study are listed in Table 2.9 including additional information.

**Table 2.9:** Antibodies used in this study.

Primary antibody			
Antigen	Purpose/Dilution	Isotype	Supplier
Zn8 (Alcam)	IHC 1:10	Mouse IgG1	Developmental Studies Hybridoma Bank
Acetylated Tubulin	WB 1:1000	Rabbit polyclonal	Sigma
DsRED	IHC 1:200	Rabbit polyclonal	Clontech
Pan-Actin	WB 1:1000	Rabbit polyclonal	Cell Signaling

Primary antibody			
Antigen	Purpose/Dilution	Isotype	Supplier
Nephronectin	WB 1:250	Rabbit polyclonal	Cosmo bio lab
Nephronectin	IHC 1:100	Rabbit polyclonal	Gift from Louis F. Reichardt, USA
Phospho-Smad1/5/8	WB 1:1000	Rabbit polyclonal	Cell Signalling
S46 (atrial myosin heavy chain)	IHC 1:10	Mouse IgG1	Developmental Studies Hybridoma Bank
Anti Digoxigenin-AP conjugated	in situ 1:5000	Fab fragments	Roche
Anti Fluorescin-POD	in situ 1:50	Fab fragments	Roche

Secondary antibody			
Antigen	Purpose/Dilution	Isotype	Supplier
Alexa Fluor 488 Anti-Rabbit	ICC 1:200	goat IgG	Invitrogen
Alexa Fluor 594 Anti-Rabbit	ICC 1:200	goat IgG	Invitrogen
Alexa Fluor 488 Anti-Mouse	ICC 1:200	goat IgG	Invitrogen
Alexa Fluor 594 Anti-Mouse	ICC 1:200	goat IgG	Invitrogen
Alexa Fluor 646 Anti-Mouse	ICC 1:200	goat IgG	Invitrogen
Anti-Rabbit IgG HRP-linked	WB 1:10000	donkey IgG	GE Health care UK limited
Anti-Mouse IgG HRP-linked	WB 1:10000	sheep IgG	GE Health care UK limited

## 2.7 Fish food

Brine shrimp cysts, substitute of the brine shrimp cysts (SDS) and flakes that were used to feed zebrafish are listed in Table 2.10. All food was purchased from “Special diets services”.

**Table 2.10:** List of fish food for different developmental stages of zebrafish.

Fish age	Food
≥ 5 dpf to < 12 dpf	SDS 100 twice/day
≥ 12 dpf to < 1 month	SDS 100 once and artemia (brine shrimp cysts) twice/day
≥ 1 month to < 2 months	SDS 200 once and artemia twice/day
≥ 2 month to < 3 months	SDS 300 once and artemia twice/day
Adult fish (≥ 3 months)	Mixture of flakes (Topical breeder mix) and SDS400 (1:1) once and artemia twice/day

## 2.8 Buffer and solutions

The buffer and solutions used in this work are listed in Table 2.11. Unless specified otherwise the solutions were prepared in distilled and autoclaved water. Freshly prepared solutions for an application were not autoclaved.

**Table 2.11:** Compositions of buffers and solutions.

Buffer/Medium/Solution	Compositions
Agarose gel loading buffer	0.25% bromophenol blue [w/v] 0.25% xylene cyanol FF [w/v] 15% Ficoll 400 [v/v] in dH <sub>2</sub> O
Alkaline phosphatase (NTMT) buffer	1 ml NaCl (5 M) 510 mg MgCl <sub>2</sub> , 6H <sub>2</sub> O 50 µl Tween 20 5 ml Tris (1 M; pH 9.5) 100 µl 1 M levamisole, dH <sub>2</sub> O q.s. to 50 ml
Antigen retrieval buffer	0.1 M Tris/HCl buffer (pH 9.0)
AEC stock	1 tablet AEC (20 mg) dissolve in 7.5 ml N,N dimethyl formamide store at -20°C

Buffer/Medium/Solution	Compositions
AEC working solution	50 $\mu$ l AEC stock 900 $\mu$ l dH <sub>2</sub> O 100 $\mu$ l 0.5 M acetate buffer (pH 4.9) 1 $\mu$ l H <sub>2</sub> O <sub>2</sub> (30%)
Acetate buffer (pH 4.9)	85 g CH <sub>3</sub> COONa, 3H <sub>2</sub> O 900 ml dH <sub>2</sub> O adjust pH with glacial acetic acid dH <sub>2</sub> O q.s. to 1 l
Blocking buffer (for <i>in situ</i> )	5% goat serum in PBS [v/v]
B-Block	2% blocking reagent [w/v] 10% goat serum in PBST [v/v] 0.1% Tween 20 [v/v] store at -20°C
Conditioned water	75 g NaHCO <sub>3</sub> 18 g sea salt 8.4 g CaSO <sub>4</sub> dH <sub>2</sub> O water q.s. to 1000 l pH: $\approx$ 6.8-7.5, conductivity: 180-350 $\mu$ S
DEPC-Water	0.01% DEPC [v/v] in dH <sub>2</sub> O incubate overnight at RT and then autoclave for 60 min.
DNase I solution	100 mg DNase I dissolve in 10 ml 10 $\mu$ M MgCl <sub>2</sub> solution, filter and store at -20°C
Digestion buffer (heart tissue)	180 ml SADO mix 90 mg pancreatin 29 mg collagenase type II (240 U/mg) stir for $\approx$ 10 min and filter using a 0.22 $\mu$ m sterile filter. 540 $\mu$ l DNase I (10 mg/ml in 10 $\mu$ M MgCl <sub>2</sub> solution)

Buffer/Medium/Solution	Compositions
Deyolking buffer	55 mM NaCl 1.8 mM KCl 1.25 mM NaHCO <sub>3</sub> dissolve in dH <sub>2</sub> O
E3 medium	5 mM NaCl 0.17 mM KCl 0.33 mM CaCl <sub>2</sub> 0.33 mM MgSO <sub>4</sub> 0.6 μM methylene blue
Levamisole (1 M)	241 mg levamisole in 1 ml TBST
MOPS Buffer (10x, 1000 ml)	4.18 g 3-[N-morpholino] propanesulfonic acid 680 mg sodium acetate 2 ml 0.5 M EDTA dissolve in 1 l dH <sub>2</sub> O and store at 4 °C in the dark without autoclavation (MOPS gets degraded)
PBS (1x)	8 g NaCl 0.2 g KCl 1.44 g Na <sub>2</sub> HPO <sub>4</sub> 0.24 g KH <sub>2</sub> PO <sub>4</sub> dissolve in 800 ml of dH <sub>2</sub> O, adjust pH to 7.4 and add H <sub>2</sub> O q.s. to 1 l
PCR buffer (10x) without MgCl <sub>2</sub>	20ml KCl (1 M) 4ml TrisHCl (1 M), pH 9 0.4ml Triton X100 sterile distilled water q.s. to 40 ml
PFA in PBS (4%)	4 g PFA dissolve in 100 ml PBS (add few drops of NaOH). Heat at 55 °C until PFA is dissolved. Cool and adjust the pH to 6-7
PBT	0.1% Tween in PBS [v/v]



Buffer/Medium/Solution	Compositions
PBT/glycine	0.2% glycine in PBT [w/v]
PT	0.3% Triton X100 in PBS [v/v]
PBA	5% BSA [w/v] 0.02% NaN <sub>3</sub> [w/v] dissolve in PBS
PBAT	0.3% Triton X100 in PBA [v/v]
PBDT	0.1% DMSO and 0.1% Triton X100 in PBS
PEM	0.1 M PIPES 1 mM MgSO <sub>4</sub> , 7H <sub>2</sub> O 2 mM EGTA adjust pH to 7
Pre-hybridization Mixture	50 ml Formamide 25 ml 20x SSC 1 g blocking reagent 10.9 ml RNase free water dissolve at 65°C and cool to RT 1 ml 0.5 M EDTA 100 µl Tween 20 1 ml 10% CHAPS 2 ml Heparin solution (5 mg/ml) 10 ml Yeast tRNA (10 mg/ml) store at -20°C
RIPA buffer	2.5 ml 10% SDS in water 15 ml NaCl (5 M) 5 ml NP40 25 ml 10% deoxycholate in water [w/v] 1 ml EDTA (0.5 M) 25 ml Tris (1M, pH 8.0) dissolve in DEPC-treated water q.s. to 500 ml. Don't autoclave afterwards

Buffer/Medium/Solution	Compositions
SADO mix	50 ml HEPES Na (200 mM; pH 7.6) 50 ml NaCl (1.3 M) 5 ml KCl (300 mM) 5 ml NaH <sub>2</sub> PO <sub>4</sub> (100 mM) 1 ml glucose (2 M) dissolve in 390 ml dH <sub>2</sub> O
SSC (20x)	17.53 g NaCl 8.82 g Na citrate dissolve in 80 ml DEPC-treated water and adjust the pH to 7. DEPC-treated water q.s. to 100 ml
SSC/Formamide/Tween	5 ml SSC (20x) 25 ml formamide 50 µl Tween 20 DEPC-treated water q.s. to 100 ml
TBST (10x)	8 g NaCl 0.2 g KCl 25 ml Tris (1 M; pH 7.5) 1 ml Tween 20 dH <sub>2</sub> O q.s. to 100 ml
TAE running buffer (1x)	0.04 M Tris base 0.002 M glacial acetic acid 0.002 M EDTA, 2H <sub>2</sub> O dissolve in dH <sub>2</sub> O
TBS	40 g NaCl 1.8 g tris base dissolve in 4.5 l dH <sub>2</sub> O adjust the pH 7.6 dH <sub>2</sub> O q.s. to 5 l
TBST	0.1% Tween 20 in TBS [v/v]

Buffer/Medium/Solution	Compositions
Transformation buffer (KCM buffer)	500 mM KCl 150 mM CaCl <sub>2</sub> 250 mM MgCl <sub>2</sub>
Transfer buffer (20x)	163.2 g bicine 209.3 g bis Tris 12 g EDTA dH <sub>2</sub> O q.s. to 2 l
Transfer buffer (1x)	250 ml 20x transfer buffer 1 l methanol dH <sub>2</sub> O q.s. to 5 l
TSB buffer	10 g PEG-3500 5 ml DMSO 1 ml 1 M MgCl <sub>2</sub> 1 ml 1 M MgSO <sub>4</sub> LB medium (pH 6.1) q.s. to 100 ml sterilize by passing through 0.45 µm filter and store at 4 °C
Wash buffer	110 mM NaCl 3.5 mM KCl 2.7 mM CaCl <sub>2</sub> 500 µl 1 M Tris HCl (pH 8.5) dH <sub>2</sub> O q.s. to 50 ml

## 2.9 Kits

The kits that were used in this work are listed in Table 2.12.

**Table 2.12:** List of kits used in this study.

Kit	Purpose	Supplier
Agarose gel extraction kit	cDNA isolation	QIAGEN
Avidin/Biotin Blocking kit	Block nonspecific binding of Biotin/Avidin for enzymatic immunostaining	Vector Lab

Kit	Purpose	Supplier
ABC solution kit	Enzymatic immunostaining	Vector Lab
PCR purification kit	PCR product cleanup	QIAGEN
QIAprep spin Miniprep	Plasmid extraction	QIAGEN
QIAprep spin Midiprep	Plasmid extraction	QIAGEN
RNA easy	RNA isolation	QIAGEN
mMessage Machine	<i>In vitro</i> capped mRNA synthesis	Ambion
DIG RNA labeling kit (SP6/T7)	<i>In situ</i> probe synthesis	Roche
Bio-Rad Dc protein assay kit	Protein concentration	BIO-RAD
SuperSignal West Femto substrate	Chemiluminescence	Thermo Scientific

## 2.10 Antibiotics

Antibiotics that were used in this study are listed in Table 2.13. Ampicilin and kanamycin were stored at 4°C. Chloramphenicol and tetracyclin were stored at -20°C and Gentamycin was stored at RT.

**Table 2.13:** Antibiotics and their working concentrations.

Antibiotics	Working concentration	
	Liquid culture	Agar plates
Ampicilin	100 µg/ml	100 µg/ml
Chloramphenicol	15 µg/ml	30 µg/ml
Kanamycin	20 µg/ml	20 µg/ml
Gentamycin	10 µg/ml	7 µg/ml
Tetracycline	10 µg/ml	10 µg/ml

## 2.11 Zebrafish lines

Different zebrafish lines used in this work are listed in Table 2.14.

**Table 2.14:** List of zebrafish lines and their specification.

Fish line	Reference	Specification
AB line		Wild type
<i>Tg(myI7:EGFP-HsHRAS)<sup>s883</sup></i>	(95)	EGFP is localized in the plasma membrane of cardiomyocytes.
<i>Tg(kdrl:EGFP)<sup>s843</sup></i>	(96)	EGFP is expressed in endothelial cells.
<i>Tg(-5.1myI7:nDsRed2)f2</i>	(97)	DsRed is localized in the nuclei of cardiomyocytes.
<i>Tg(TOP:GFP)<sup>w25</sup></i>	(98)	EGFP is expressed under control of the promoter region containing 4 consensus LEF binding sites.
<i>Tg(hsp70l:dkk1-GFP)<sup>w32</sup></i>	(99)	dkk1 is expressed under the control of the heat shock protein 70 promoter.

## 2.12 Plasmids

Different constructs were used for *in situ* probe synthesis in this work. Gene name, construct backbone and restriction enzymes are listed in Table 2.15.

**Table 2.15:** List of plasmids for *in situ* probe synthesis, restriction enzymes and respective RNA polymerases.

Gene name	Vector	Resistance to	Enzyme	RNA polymerase	Type of probe
<i>amhc</i>	pSPORT1	Ampicillin	EcoRI	SP6	Antisense
<i>amhc</i>	pSPORT1	Ampicillin	BamHI	T7	Sense
<i>fbln1</i>	Unknown	Ampicillin	XhoI	T7	Antisense
<i>bmp4</i>	pCS2+	Ampicillin	BamHI	T3	Antisense
<i>vmhc</i>	pGEMT- Easy	Ampicillin	NotI	T7	Antisense
<i>vmhc</i>	pGEMT- Easy	Ampicillin	SacII	SP6	Sense

Gene name	Vector	Resistance to	Enzyme	RNA polymerase	Type of probe
<i>cspg2</i>	pBluescript II SK(+)	Ampicillin	NotI	T7	Antisense
<i>npnt</i>	pGEMT-Easy	Ampicillin	SacII	SP6	Antisense
<i>npnt</i>	pGEMT-Easy	Ampicillin	SpeI	T7	Sense
<i>notch1b</i>	pBluescript SK(+)	Ampicillin	BamHI	T3	Antisense
<i>notch1b</i>	pBluescript SK(+)	Ampicillin	SacII	T7	Sense
<i>nppa</i>	Unknown	Ampicillin	NotI	SP6	Antisense
<i>has2</i>	pBSK	Ampicillin	XbaI	T7	Antisense
<i>tbx2b</i>	pBS II SK	Ampicillin	BamHI	T7	Antisense
<i>eGFP</i>	pCS2+	Ampicillin	EcoRI	T7	Antisense
<i>eGFP</i>	pCS2+	Ampicillin	XhoI	SP6	Sense

### 2.13 Morpholino oligonucleotides

Morpholinos were purchased from Gene Tools and dissolved in sterile water as 1 mM stock solution (Table 2.16).

**Table 2.16:** List of morpholinos, their target sites and sequences.

Morpholino	Target	Sequence (5'-3')
MO1	Translation inhibitory morpholino against <i>npnt</i>	CATGAACTTTATGATCCACA TCTCC
MO2	Splicing inhibitory morpholino against <i>npnt</i>	TGTGAAACGGCAGACGGAA CTCACT
MO3	Splicing inhibitory morpholino against <i>npnt</i>	GAATAGGCTAAGTGCCGTC TCACCT
Has2-MO	Translation inhibitory morpholino against <i>has2</i>	AGCAGCTCTTTGGAGATGT CCCGTT

## 2.14 Growth media

Different media used for bacterial, cardiomyocyte and non-myocyte culture in this work are listed in Table 2.17.

**Table 2.17:** Name, purpose and formulation of used media.

Media	Purpose	Formulation
Neonetal medium	Cardiomyocyte isolation from neonatal rat heart	DMEM/F-12 medium supplemented with: Na-pyruvate (3 mM) L-glutamin (2 mM) ascorbic acid (0.1 mM) insulin/transferin/Na selenite (1:100) BSA (0.2%) penicillin (100 U/ml) streptomycin (100 mg/ml)
Preplating medium	Non-myocyte separation from harvested cells from neonatal rat heart	DMEM/F-12 medium supplimented with FBS (10%) L-glutamin (2 mM) penicillin (100 U/ml) streptomycin (100 mg/ml)
LB agar	Propagation of bacteria	35 g in 1 l H <sub>2</sub> O
LB medium	Propagation of bacteria	20 g in 1 l H <sub>2</sub> O
SOC medium	Bacterial transformation	Ready made from Sigma

## 2.15 Competent cells

Different competent bacterial strains were used for transformation (Table 2.18).

**Table 2.18:** Bacteria used as competent cells for plasmid propagation.

Bacterial Strain	Specification
XL1-Blue	Competent cells
Dh5 $\alpha$	Competent cells

## 2.16 Software

Software used for data analysis in this study is listed in Table 2.19.

**Table 2.19:** Software used in this study and its application.

Software	Application
Microsoft Office Excel, Word, Powerpoint	Data analysis and Documentation
Adobe Photoshop, Illustrator, Reader	Figure preparation
Image J	Image analysis
LSM Image Browser	Confocal Image analysis
GraphPad Prism	Graphical representation and statistical analysis



### 3. Methods

#### 3.1 Zebrafish maintenance

Wild type AB and transgenic zebrafish (*Danio rerio*) are in general maintained at 28 °C as described (100). For this study zebrafish were maintained in a state-of-the-art zebrafish housing system by Tecniplast (Tecniplast Deutschland GmbH) using conditioned water (Figure 3.1).

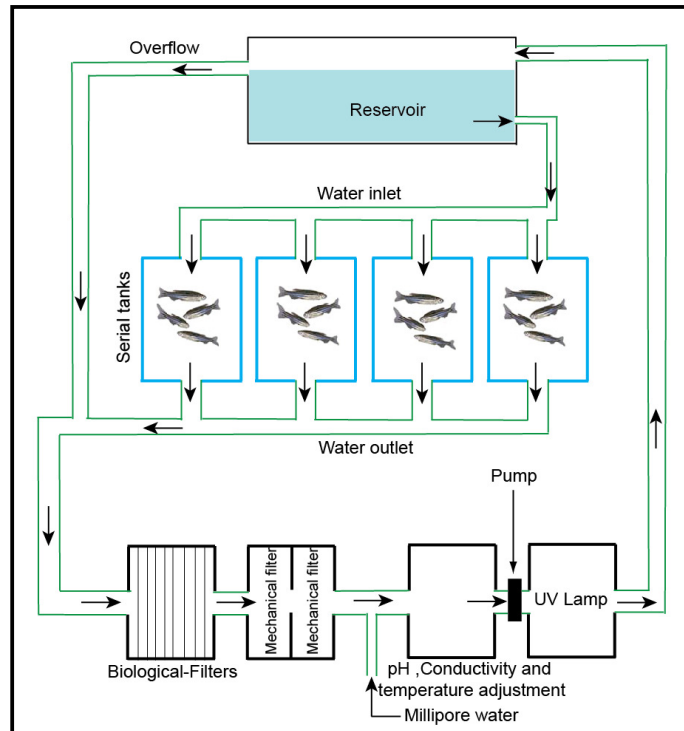


**Figure 3.1: Scheme of the used zebrafish housing system.** Arrows indicate direction of water flow.

Water temperature was maintained at 26-28 °C and air temperature at 27-29 °C. In this system 10-20% of the water in each fish tank is exchanged per day as zebrafish waste contains ammonium compounds, which are highly toxic. In addition, biological filters were used to detoxify the water. The biological filters provide a large surface area to grow denitrifying aerobic bacteria like *Nitrosomonas* and *Nitrobacter*, which degrade ammonium compounds to nitrite. Other mechanical filters plus pH adjustment, conductivity adjustment, and a sterilization unit were connected in a series to maintain the properties of the conditioned water.

### **3.2 RNA isolation and reverse transcription (RT)**

RNA was extracted from zebrafish embryos (30 to 50) and from rat or mouse heart ventricles (fetal: >20; postnatal: 3 to 5) at different developmental stages using Trizol reagent according to manufacturer's instructions with minor modifications. To homogenize  $\leq 1$  g of tissue 1 ml of Trizol reagent was used. Isolated RNA was dissolved in 30 to 50  $\mu$ l RNase free water and stored at  $-80^{\circ}\text{C}$ .

cDNA was prepared from isolated RNA using MMLV or superscript II reverse transcriptase. For MMLV-mediated reverse transcription 1  $\mu$ g RNA was incubated with 1  $\mu$ l dNTP mix (10 mM), 0.5  $\mu$ g oligo dT and RNase free water q.s. to 10  $\mu$ l at  $65^{\circ}\text{C}$  for 5 min. Then this reaction mixture was incubated with 2  $\mu$ l MMLV reverse transcriptase buffer (10x), 7  $\mu$ l RNase free water and 1  $\mu$ l MMLV reverse transcriptase at  $37^{\circ}\text{C}$  for 50 min. After 50 min the incubation reaction was inactivated by incubation at  $80^{\circ}\text{C}$  for 10 min and RNase free water was added q.s. to 100  $\mu$ l. Synthesized cDNA was stored at  $-80^{\circ}\text{C}$  for further use.

### **3.3 cDNA amplification by PCR**

For PCR-mediated cDNA amplification, a standard PCR reaction was set up. As a template for the reaction 1  $\mu$ l cDNA was used. A master mix was prepared by adding 10 pmol forward and reverse primers, 10 nmol dNTPs, 40 nmol  $\text{MgCl}_2$ , 0.5 U Taq polymerase and 1x PCR amplification buffer ( $\text{MgCl}_2$  free). The amplification was carried out in a GeneAmp PCR System 9700 thermocycler from Applied Biosystems under the following conditions: initial denaturation for 2-5 min at  $94^{\circ}\text{C}$ ; 24-35 cycles of 30 sec at  $94^{\circ}\text{C}$ , annealing at  $58^{\circ}\text{C}$  to  $60^{\circ}\text{C}$  and extension of 1 min per 1 kb of product size at  $72^{\circ}\text{C}$ . After the last cycle the reaction was held for 7 min at the extension temperature to allow the completion of amplification of all products. Subsequently, the temperature was lowered to  $4^{\circ}\text{C}$  to stop the reaction.

### **3.4 Agarose gel electrophoresis**

The cDNA was resolved on 1.5-2% agarose gels prepared in TAE buffer containing EtBr. The electrophoresis was run for 30 to 60 min in TAE

depending upon PCR product size. cDNA was visualized under UV light,  $\lambda=260$  nm.

### 3.5 cDNA elution from agarose gel

Resolved PCR products were purified from agarose gel using the QIAquick gel extraction kit according to manufacturer's instructions (QIAGEN) and eluted with 30  $\mu$ l nuclease free water.

### 3.6 Cloning

To generate different constructs cDNA was synthesized from mRNA extracted from 52 hpf embryos. cDNA was amplified with the help of PCR using appropriate primer pairs and TopTaq DNA polymerase (Qiagen). To clone the full length coding sequence of *npnt* containing its partial 3'UTR region, a 1945 bp fragment of zebrafish *npnt* cDNA (NM\_001145580) was amplified with the primer pair Npnt full fwd\_dr and Npnt full rev\_dr. To make a construct for *in situ* probe generation against *npnt*, *integrin  $\alpha 8$  (itga8)* and EGF receptor a (*egfra*) mRNA, a 517 bp (primer pair: Npnt fwd\_dr, Primer R), a 713 bp (primer pair: *Itga fwd and Itga rev*) and a 729 bp cDNA fragment (primer pair: *egfra fwd and egfra rev*) was amplified. All amplified cDNAs were resolved by agarose gel electrophoresis and eluted from the gel.

TopTaq has 5'–3' exonuclease activity but no 3'–5' exonuclease activity and this enzyme leaves an "A" overhang at the 3' end. To make sticky end ligation pGEMT easy vector (Promega) was used which carries a complementary "T" overhang.

Purified cDNA was ligated into the pGEMT easy vector by incubating a mixture of 5  $\mu$ l rapid ligation buffer (2x), 3  $\mu$ l eluted cDNA, 1  $\mu$ l pGEMT easy vector and 1  $\mu$ l T4 DNA ligase (joins between the 5'-phosphate and the 3'-hydroxyl groups) at 4°C overnight. Full length *npnt* cDNA was subcloned into the pCS2+ vector after EcoR1 double digestion, with the help of T4 DNA ligase (RZPD, pCS2+-Fnpnt), and was subsequently sequenced.

### 3.7 Preparation of competent *E.coli* cells

A single colony of *E. coli* strain (DH5 $\alpha$  or XL1Blue) was inoculated in 5-6 ml LB medium and cultured overnight at 37°C with shaking. 4 ml of grown culture was

added into fresh 250 ml LB and grown to early logarithmic phase ( $OD_{600}=0.3-0.6$ ). The culture was centrifuged for 5 min at 2500 rpm at 4°C in a table top centrifuge. The bacterial pellet was resuspended in 25 ml cold TSB buffer (1/10<sup>th</sup> volume of the bacterial suspension) and incubated on ice for 10 min. Competent cell suspension was aliquoted into cold eppendorf tubes (100 µl and 200 µl) and snap frozen in liquid nitrogen. Aliquoted frozen competent bacterial cells were stored at -80°C.

### **3.8 Transformation of *E. coli* competent cells**

Part of a ligation reaction mixture (5 µl) or 1-10 ng of plasmid DNA was added to 20 µl of 5 × KCM buffer; water was added q.s. to 100 µl in a 1.5 ml eppendorf tube. An equal volume of thawed competent cells was added to the reaction mixture and mixed by flicking. The reaction mixture was incubated on ice for 20 min followed by incubation at RT for 10 min. Then 1 ml of LB medium (without any antibiotic) was added to the mixture and incubated for 1h at 37°C with vigorous shaking. Finally cells were plated on LB Agar plates containing appropriate antibiotic. Plates were incubated at 37°C overnight.

### **3.9 Plasmid DNA isolation**

The “mini-prep” method is useful for preparing partially purified plasmid DNA in small quantities from a number of transformants. It is based on the alkaline lysis method using SDS (101). A single colony was selected and inoculated in 3 to 5 ml of LB medium containing the appropriate antibiotic with a sterile pipette tip. Bacterial cells were cultured overnight at 37°C with vigorous shaking. The cells were harvested by centrifugation for 4 min at 4000 rpm in a table top centrifuge (Eppendorf 5415C). Plasmid DNA was isolated using the QIAGEN miniprep kit following the manufacturer’s instructions. At last plasmid DNA was extracted from the affinity column with 30 µl sterile water. Large amount of plasmid DNA was prepared using the QIAGEN Plasmid Midi Kit according to the manufacturer’s instructions.

### **3.10 Determination of the concentration of nucleic acids**

The DNA and RNA concentrations in solution were estimated using a spectrophotometer (Nanodrop 2000c-Peqlab). The absorbance of the solution

was measured at 260 nm and the concentration of nucleic acids was calculated by the manufacturers software based on the Beer-Lambert Law ( $A_\lambda = \epsilon bc$ ). Where  $A_\lambda$  is the absorbance ( $A_\lambda = \log_{10} P_0 / P$ ),  $\epsilon$  is the molar absorptivity (molar extinction coefficient),  $b$  is the path length of the sample and  $c$  is the concentration of the compound in solution.

The molar absorptivity of double stranded DNA is  $\epsilon = 50 \text{ cm}^{-1} \text{ M}^{-1}$ , for single stranded DNA is  $\epsilon = 33 \text{ cm}^{-1} \text{ M}^{-1}$ , and for RNA is  $\epsilon = 40 \text{ cm}^{-1} \text{ M}^{-1}$ .

### 3.11 *In situ* hybridization

#### 3.11.1 Probe synthesis

*In situ* constructs were linearized with proper restriction enzymes (Table 2.10) and used as template for probe synthesis. Reaction mixtures containing 1  $\mu\text{g}$  linearized plasmid (13  $\mu\text{l}$  final volume), 2  $\mu\text{l}$  10x NTP labeling mixture, 2  $\mu\text{l}$  10x transcription buffer, 1  $\mu\text{l}$  protector RNase inhibitor and 2  $\mu\text{l}$  RNA polymerase (SP6/T7/T3) were incubated at 37°C for 2 h (Table 2.10). After probe synthesis the DNA template was digested by incubation for 30 min at 37°C after adding 2.5  $\mu\text{l}$  DNase buffer (10x) and 2.5  $\mu\text{l}$  DNase I. The synthesized probe was precipitated by adding 2.5  $\mu\text{l}$  0.2 M EDTA, 2.5  $\mu\text{l}$  5 M LiCl and 93  $\mu\text{l}$  ethanol and incubation at -80°C for 40 min. After centrifugation at 17000 x  $g$  for 10 min at 4°C the supernatant was removed and the pelleted probe was washed with 200  $\mu\text{l}$  70% ethanol (kept at -20°C for 15 min) and again centrifuged (10 min, 17000 x  $g$ , 4°C). Subsequently, the supernatant was removed and the probe was air dried. Finally, the probe was dissolved in 40  $\mu\text{l}$  water and 1  $\mu\text{l}$  RNase inhibitor (final con. 1 U/ $\mu\text{l}$ ) and stored at -80°C for further use.

#### 3.11.2 Fixation and storage of embryos

Embryos were fixed with 4% PFA (paraformaldehyde) overnight or up to 3 days at 4°C. Embryos younger than 24 hpf were fixed with chorion and decorinated after fixation. Older embryos were fixed after dechorination. Fixed embryos were washed twice with PBST for 30 min at RT. Washed embryos were dehydrated with a series of methanol:PBT solutions (25:75, 50:50, 75:25) and twice with 100% methanol (10 min each step at 4°C). Then embryos were used directly for *in situ* or stored in methanol at -20°C for later use.

### 3.11.3 1<sup>st</sup> day-hybridization

Embryos were rehydrated through a series of methanol:PBT solutions (75:25, 50:50, 25:75), and washed twice with PBT (10 min each step at 4°C). Older than 40 hpf embryos were bleached with 6% hydrogen peroxide in PBT for 30 min at 4°C and washed thrice with PBT for 5 min. Washed embryos were treated with proteinase K (10 µg/ml) as follows:

- Up to 26+ somite stage (22 hpf) 30 sec to 1 min digestion at RT
- Prim 5 to prim 15 (24 hpf to 30 hpf) 10 min digestion at RT
- Prim 15 to Pec fin (36 hpf to 60 hpf) 25 min digestion at RT
- Protruding mouth (>72 hpf) 30 min digestion in RT

Proteinase K was inactivated by washing twice with PBT buffer containing glycine (2 mg/ml) and thrice with PBT. Embryos older than 20 hpf were washed twice with RIPA buffer and then washed thrice with PBT. Embryos of all stages were fixed for 20 min at RT with PBT containing 4% PFA and 0.2% glutaraldehyde. Fixed embryos were washed thrice with PBT, with prehybridization buffer for 10 min and then incubated in prehybridization buffer for 2 h at 70°C. DIG-labeled probes were diluted in hybridization buffer (1 µg/ml) and denatured by heating at 100°C on a heating block for 5 min. After 2 h incubation in prehybridization buffer embryos were incubated overnight at 70°C in hybridization buffer having denatured probe.

### 3.11.4 2<sup>nd</sup> day-unbound probe removal

Hybridized embryos were washed twice with prehybridization buffer (30 min each, 65°C), once with a mixture of prehybridization buffer:SSC/Formamide/Tween 20 (1:1) (10 min, 65°C), five times with SSC/Formamide/Tween 20 (20 min each, 65°C), with the mixture of TBST:SSC/Formamide/Tween 20 (1:1) (10 min, RT), and then washed thrice with TBST at RT. Embryos were incubated in blocking solution for 1 h at RT. At the same time anti-DIG antibody was incubated in blocking solution (antibody dilution-1:5000) at RT. After blocking embryos were incubated with antibody solution at 4°C for overnight.

### 3.11.5 3<sup>rd</sup> day-unbound antibody removal and staining

Antibody solution was removed and embryos were washed with TBST at RT twice for 5 min, twice for 15 min and thrice for 30 min. Subsequently, embryos were washed thrice with NTM-T buffer (alkaline phosphatase buffer) at RT for 20 min and incubated in staining solution (BM purple, Roche) in the dark at RT. The incubation time depended on the probe and took a few hours up to several days. For longer incubation embryos were incubated at 4°C on a belly dancer shaker. Staining was stopped by washing in dH<sub>2</sub>O or dH<sub>2</sub>O containing 0.1% Tween 20. For cleaning the embryos were washed twice with 100% ethanol for 15 min, then washed with 50% ethanol and at last with PBT. For whole-mount photography embryos were washed in ddH<sub>2</sub>O and stored in 50% glycerol.

### 3.12 Embedding and documentation

Cleaned whole-mount embryos were fixed in 4% PFA in PBS overnight at 4°C and then embedded in 17% gelatin in PBS. Gelatin was dissolved in PBS by boiling and solution temperature was adjusted to 50-60°C before embedding. Embedding was done on plastic moulds. and Gelatin polymerization was achieved by incubation on ice. Polymerized gelatin blocks were fixed by incubating in 4% PFA overnight at RT. 100 µm thick sections were made by vibratome at RT and mounted on glass slides using water based mounting medium (Kaiser's glycerol gelatin, Merck) for microscopy.

### 3.13 Capped *npnt* mRNA synthesis

#### 3.13.1 Linearized template generation

Capped *npnt* mRNA was generated using a "mMESSAGE mMACHINE SP6" *in vitro* transcription kit. pCS2+-Fnpnt plasmid was linearized by overnight restriction digestion with *SacII* at 37°C [reaction mixture: 5 µg plasmid + 5 µl 10x BSA + 5 µl 10x buffer 2 + 8 U *SacII* + nuclease free water q.s. to 50 µl]. Restriction digestion was stopped by adding 5 µl (1/10th volume) ammonium acetate reaction stop buffer, 2.5 µl 0.5 M EDTA (1/20th volume) and 100 µl (2 volume) ethanol to the digestion mixture and incubation at -20°C for 15 min. This mixture was then centrifuged at 17000 x *g* for 15 min at 4°C and the pelleted linearized plasmid was resuspended in 10 µl RNase free water.

### 3.13.2 *In vitro* capped RNA synthesis

To synthesize capped *npnt* mRNA, 1 µg of linearized template DNA was incubated in the mixture of 10 µl 2x NTP/CAP mix, 2 µl enzyme mix, 2 µl 10x reaction buffer and nuclease free water q.s. to 20 µl at 37°C for 2 h. Later on template DNA was denatured by incubating the reaction mixture with 1 µl Turbo DNase at 37°C for 15 min. Synthesized capped *npnt* mRNA was purified by LiCl precipitation. For this, reaction mixture was mixed with 30 µl LiCl precipitation solution and 30 µl nuclease free water and incubated for 30 min at -20°C, followed by centrifugation at 17000 x *g* for 15 min at 4°C. Capped *npnt* mRNA pellet was washed with 1 ml 70% nuclease free ethanol and centrifuged at 17000 x *g* for 15 min at 4°C. After removing the supernatant the pellet was air-dried and dissolved in 20 µl nuclease free water. To inhibit RNA degradation a RNase inhibitor was added to the capped RNA solution (1 U/µl final concentration) and stored at -80°C for further use.

### 3.14 Manipulation of gene expression

Gene expression was manipulated by injection of morpholino oligonucleotides or capped mRNA with the help of a microinjector. For knockdown studies single cell stage embryos were injected with different amounts of morpholino oligonucleotides ( $\leq 4$  nl). Four different morpholino oligonucleotides (MOs) were used for this study (Table 2.16). For rescue experiments single cell stage embryos were injected with different amounts of capped *npnt* mRNA alone (control) or together with MO2. The total volume of injected solution was  $\leq 4$  nl. Capped *npnt* mRNA was dissolved in sterile and RNase free 0.1M KCl solution. Phenol red was added (0.05%) to injected solutions.

### 3.15 BMP signaling inhibition

Dorsomorphin, a chemical antagonist of BMP receptors, was used to inhibit BMP signaling (102). Different concentrations of dorsomorphin (2 µM, 5 µM, 10 µM or 50 µM) were added to MO2-injected or wild type embryos at 25 hpf in E3 medium to inhibit BMP signaling. Dorsomorphin has shown its maximum inhibitory effect on Smad phosphorylation and a concentration of 10 µM and this concentration was used for BMP signaling inhibition studies. Cardiac morphology and expression patterns of different genes of these embryo hearts



were analysed by immunostaining and *in situ* hybridization techniques at 52 hpf.

### **3.16 Protein extraction from whole zebrafish embryos**

Protein was extracted from 50 to 60 pooled embryos at 52 hpf for Npnt knock down and at 48 hpf for BMP signaling inhibition study. At first the yolk was removed by shearing (pipetting) and shaking in de yolking buffer (2 x 3 min, 1100 rpm) and then washed by shaking (3 min, 1100 rpm, on a MHL20 shaker) with washing buffer. Washed embryos were pelleted by centrifugation (300 x g, 1 min at 4°C) and supernatant was removed. Pelleted embryos were homogenized with Precellys 24-Dual homogenizer (Peqlab) in a lysis mixture containing lysis buffer from Cell Signaling, protease inhibitor mix (Thermo Scientific) and 1 mM PMSF. Homogenized tissue was centrifuged for 10 min at 10000 x g and 4°C. Supernatants were collected in 1.5 ml Eppendorf tubes and stored at -80°C for further experiments.

### **3.17 Determination of protein concentration**

Protein concentration was estimated using the BioRad D<sub>C</sub> Protein Assay Kit which is based on the Lowry method (103). Five µl protein extract was mixed with 5 µl water, 20 µl reagent A and 200 µl reagent B and incubated for 15 min at RT. Absorbance of the solution was measured by a microplate reader (spectrophotometer from Tecan) at λ=720 nm. Protein sample concentration was calculated by the manufacturer's software based on a standard curve that was determined using BSA standards.

### **3.18 Western blot analysis**

Cell lysates or tissue extracts were resolved by a gradient (4-12%) SDS-polyacrylamide gel (104). Lysates or extracts were mixed with reducing reagent and NuPage loading dye from Invitrogen and were incubated at 95°C for 5 min. Samples containing 15-25 µg protein were loaded on NuPAGE 4-12% Novex Bis-Tris Gels (Invitrogen) and resolved by electrophoresis for 30 min at 75 V followed by 1.30 to 2 h at 150 V at 4°C. Resolved protein samples were transferred to a nitrocellulose membrane by electrophoresis at 20 W for 1 h at 4°C. Afterwards the membrane (protein blot) was blocked by incubation in

blocking solution (5% bovine albumine or 5% skimmed milk in TBST) for 1 h at RT. The blots were then incubated with rabbit polyclonal anti-Npnt antibody (1:250 in 5% skimmed milk/TBST), mouse anti-pan-Actin antibody (1:1000 in 5% bovine albumin/TBST), rabbit anti phospho-Smad 1/5/8 antibody (1:1000 in 5% bovine albumin/TBST), or rabbit monoclonal anti-acetylated tubulin antibody (1:1000 in 5% Bovine albumin/TBST) at 4°C overnight under shaking. After overnight incubation blots were washed thrice with TBST for 5 min at RT and then incubated for 1 h with HRP conjugated secondary antibody in blocking buffer (1: 6000) at RT. After incubation blots were washed thrice with TBST for 5 min at RT. The bound antibodies were detected by incubating the membrane with a 1:1 mixture of a chemiluminescent substrate and an enhancer solution from Thermo Scientific (Super signal) and chemiluminescence was documented by a blot developing system from FujiFilm, which can detect chemiluminescence.

### **3.19 Histological analysis**

Hematoxylin/eosin staining was performed for morphometric analyses. Zebrafish, mouse or rat embryos were fixed in 4% PFA/PBS at 4°C overnight. Fixed embryos were dehydrated by incubating them in series of ethanol:water mixtures (50:50, 70:30, 80:20, 90:10, 96:04) and twice with 100% ethanol (for zebrafish: 1 h each step at RT and for mouse/rat 2 h each step at RT). Dehydrated embryos were washed with butanol overnight at RT and then twice with paraffin (at least 2-3 h each step at 65°C). Washed embryos were embedded in paraffin and sectioned with a microtome (7 µm thick) and mounted on glass slides after stretching them by putting them in a 55°C water bath. After mounting, glass slides were incubated at 37°C overnight and stored at RT for further experiments. Mounted sections were deparaffinised by washing thrice with xylol (7 min each step), twice with 100% ethanol (2min each step) and then series of ethanol: water mixtures (96:4, 90:10, 70:30, 50:50) for 1 min each step. At last sections were washed with tap water at least for 5 min. For staining rehydrated mounted sections were incubated in Hemalum for 10 min and washed with warm running tap water until sections became blue. Sections were rinsed with distilled water for 1-2 min. After Hemalum staining sections were incubated with eosin solution for 6 min and

shortly washed once with 95% ethanol and once with 100% ethanol. At last sections were put into xylol and mounted with xylol-based mounting medium (Entellan, Merck). Mounted samples were analysed by bright field microscopy.

### 3.20 Immunohistochemistry

Zebrafish immunohistochemistry was performed as previously described (81). Around 30 embryos were washed shortly (not > 30 sec) with PT. For Alcam staining embryos were fixed for 4 h in 4% methanol-free formaldehyde (Polyscience) in PEM at RT. Samples were washed thrice with PBS and incubated in PBA for 1h at RT. After blocking, embryos were incubated with mouse monoclonal anti-Alcam (zn8) antibody (1:10 in PBA) for overnight at 4°C. Subsequently, samples were washed thrice with PBS and incubated with anti-mouse antibody conjugated with ALEXA fluochrome for 2 h at RT. For atrial myosin heavy chain and DsRed staining embryos were fixed for overnight in 1% methanol-free formaldehyde (Polyscience) in PEM at 4°C. Samples were washed thrice with PBS and incubated in PBA for 1h at 4°C. After blocking, embryos were incubated with mouse monoclonal anti-atrial myosin heavy chain (s46) (1:10 in PBA) and/or rabbit polyclonal anti-DsRed antibody (1:200 in PBA) for overnight at 4°C. Subsequently, samples were washed thrice with PBS and incubated with anti-mouse and/or anti-rabbit antibody conjugated with different ALEXA fluochrome overnight at 4°C. After staining samples were washed thrice with PBS and incubated in 4% PFA for 1-2 h at RT. For F-Actin staining samples were incubated with rhodamine-labeled phalloidin (1:75, 1 h, RT) in PBDT. Whole mount embryos were used for confocal microscopy after embedding in 1.5% (w/v) low melting agarose gel in PBS.

For immunohistochemistry of rat tissue, rat embryos (E14) were processed for paraffin sectioning and 6 µm thick sections were mounted on slides. Sections were deparaffinised by washing thrice with Xylol for 7 min, with 100% ethanol for 2 min, 96%, 90%, 70% and 50% ethanol for 1 min and at last with warm tap water (at least for 5 min). Before immunostaining antigen retrieval was performed by incubating the slides in 0.1M Tris/HCl buffer (pH 9.0) overnight at 80°C. After cooling down the slides were rinsed thrice with PBS for 5 min. Each tissue section was circumscribed with an ImmEdge pen. Endogenous avidin was blocked by incubating the tissue sections with avidin

solution for 15 min at RT and washed once with PBS. Subsequently endogenous biotin was blocked by incubating the tissue sections with biotin solution for 15 min at RT and washed once with PBS. Tissue sections were blocked by incubating with 5% goat serum in PBS for 1 h at RT. Blocked sections were incubated in blocking buffer containing rabbit polyclonal Npnt antibody (1:100) and for negative control sections were incubated with blocking buffer overnight at 4°C in a humidified chamber. Samples were washed thrice with PBS and subsequently incubated in 0.1% H<sub>2</sub>O<sub>2</sub> in PBS for 10 min at dark to block endogenous peroxidase. To stop the H<sub>2</sub>O<sub>2</sub> reaction samples were washed thrice with PBS. Subsequently, samples were incubated with biotin conjugated antirabbit antibody (secondary antibody) in PBS (1:100) for 45 min at RT. ABC solution mixture was prepared by adding 1 µl of each solution from ABC kit in 100 µl PBS and incubated for 30 min before adding on sections. Secondary antibody was washed away by rinsing thrice with PBS. Subsequently sections were incubated with ABC solution for 30 min at RT and washed thrice with PBS. AEC substrate was prepared according to the manufacturer instructions and sections were incubated with AEC substrate for 15 min at RT. After these slides were rinsed with dH<sub>2</sub>O for three times they were incubated in Hematoxylin for 30 sec. Excess Hematoxylin was removed by rinsing the slides with running tap water for 3 min and washed sections were mounted with Kaisers glycerin (water based mounting medium). All washing steps lasted 5 min. Washing and Hematoxylin incubation was done using glass slide holder.

### **3.21 Isolation of neonatal rat heart cells**

Neonatal rats (P3) were decapitated, the chest was opened and hearts were removed with a curved forcep. Isolated hearts (10 to 20) were placed in a petridish 20 ml PBS without Ca<sup>2+</sup> and Mg<sup>2+</sup> containing 5 mM glucose in on ice. Using a scalpel blade, the aorta and the atria were removed. The remaining ventricles were gently squeezed with forceps to remove the blood and washed with PBS without Ca<sup>2+</sup> and Mg<sup>2+</sup> containing 5 mM glucose.

The ventricles were placed on a dry petridish and were minced as small as possible using a scalpel blade. The minced heart tissue was transferred to a Corex glass tube, containing 10 ml of digestion buffer and one magnetic stir

bar, in a 37°C water bath on a magnetic stirrer (200 to 300 rpm). After 3 min the corex glass tube was removed that the tissue could settle on the bottom (3 min tissue sedimentation). Subsequently the supernatant was discarded. This wash step was followed by a series of digestion steps each with 10 ml digestion buffer. The first two digestion steps involved 10 minutes of digestion followed by 5 min sedimentation. This procedure was continued with 8 min digestion and 5 min sedimentation for 5 steps more. After each sedimentation step, the supernatant containing the cells was collected and transferred to 50 ml falcon tube containing 4 ml ice-cold horse serum (each tube to collect 40 ml supernatant) and kept on ice. The tubes containing the cell suspension in horse serum were centrifuged at 330 x *g* for 3 minutes at 4°C. Subsequently the supernatant was discarded and the cell pellets were resuspended in preheated preplating medium (37°C, 10 ml per 5 hearts). The cell suspension was preplated on 10 cm cell culture dishes (10 ml cell suspension/dish) and incubated for 1h 30 min at 37°C at 5% CO<sub>2</sub> level. During this preplating, non-myocytes attach to the cell culture dish whereas cardiomyocytes get enriched in the medium.

The supernatant from the preplating step was collected in 50 ml falcon tubes. Cells were pelleted at 330 x *g* for 3 min at 4°C and RNA was isolated from the cell pellet (cardiomyocytes) or from the attached non-myocytes after washing twice with PBS using the QIAGEN RNA easy kit according to manufacturer's instructions.

### **3.22 Microscopy and morphological analysis**

For the Nomarski (Zeiss) and confocal imaging of live fish hearts, embryos were anesthetized with 0.02% tricane in E3 medium and mounted with 1.5% low melting agarose in E3 medium. For immunohistochemistry fixed whole-mount embryos were mounted with 1.5% low melting agarose in PBS. Confocal sections (1.3 μm) were taken with a Zeiss LSM710 confocal microscope covering the entire heart. Images were processed with the software LSM Image Browser to obtain projections (Zeiss). Mounted tissue sections were used for brightfield microscopy. Cell counting experiments were done with the help of ImageJ software.

### **3.23 Statistical analysis**

Data are expressed as mean  $\pm$  SEM of at least three independent experiments. Statistical significance of differences was evaluated by One-way ANOVA followed by Bonferroni's post-hoc test (GraphPad Prism).  $p < 0.05$  was considered statistically significant.

## 4. Results

### 4.1 *npnt* is transiently expressed during mammalian heart development

One aim of our laboratory is the identification of novel regulators of heart development. For this purpose we performed a large scale temporal RNA expression analysis based on microarray technology. This analysis revealed the expression profile of over 28000 genes from E11 to P10.5 (unpublished data). From this study we have identified the gene *npnt*, encoding the protein Nephronectin, as transiently expressed in the rat heart at the time of valve initiation, valve formation and trabeculation (E11 to E17) (Figure 4.1A) (105). These results were confirmed by RT-PCR for both known variants of rat *npnt* using independent sets of mRNA (Figure 4.1B).

RT-PCR data using mRNA isolated from mouse hearts showed that also both known mouse *npnt* variants are transiently expressed exhibiting a comparable cardiac expression profile as the rat variants (Figure 4.1C). To determine whether Npnt is also expressed on protein level in the heart and to assess its spatial expression pattern in the rat heart we performed enzymatic immunostaining on paraffin tissue sections of E14 rat embryos (Figure 4.1D-G). Immunostaining data suggest that around this stage Npnt expression is confined to the myocardium, whereas endocardial and epicardial layers did not express detectable levels of nephronectin (Figure 4.1E-G).

The myocardial layer consists of cardiomyocytes and non-myocytes, like fibroblasts as well as smooth muscle cells and endothelial cells from vessels and microvessels. To assess which cell type expresses nephronectin we have isolated cardiomyocytes and non-myocytes from postnatal day P1 heart ventricles and isolated RNA from both cell fractions. RT-PCR data revealed that both the cardiomyocyte and the non-myocyte cell fraction express *npnt* (Figure 4.1H).

Taken together, our data demonstrate that *npnt* is transiently expressed in cardiomyocytes and non-myocytes of the myocardial layer during mammalian heart development at the time of cardiac valve formation and trabeculation.

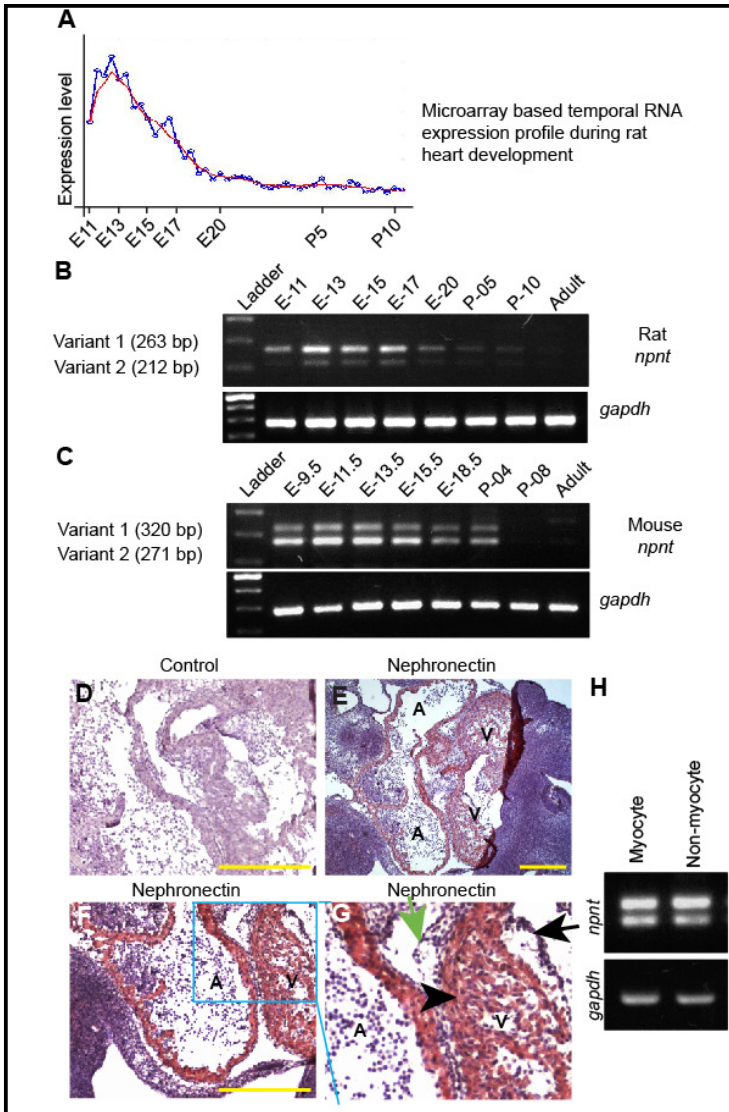


**Figure 4.1: *npnt* is transiently expressed during rat and mouse heart development.** (A) *npnt* expression levels in rat heart tissue from embryonic day E11 to postnatal day P10.5 in 12 hours intervals according to a microarray analysis using Affymetrix GeneChip Rat Expression Set 230. (B) RT-PCR analysis of *npnt* mRNA expression during rat heart development. mRNA was isolated from rat heart tissue collected at sequential developmental stages as indicated. Equal amounts were loaded as verified by using *gapdh* as a loading control. (C) RT-PCR analysis of *npnt* mRNA expression during mouse heart development. mRNA was isolated from mouse whole heart tissue collected at sequential developmental stages as indicated. Equal amounts were loaded as verified by using *gapdh* as a loading control. (D-G) *Npnt* expression in the rat heart was determined by enzymatic immunostaining on the paraffin sections from E14.5 rat embryos. (D) Brightfield image of the negative control. (E-G) Brightfield images showing *Npnt* expression in the myocardium (black arrowhead) whereas epicardium (green arrow) and endocardium (black arrow) are devoid of *Npnt* expression. (H) RT-PCR analysis of *npnt* mRNA expression in the cardiomyocyte and non-myocyte fraction isolated from P3 hearts. Equal amounts were loaded as verified by using *gapdh* as a loading control. A: atrium; V: ventricle; E: embryonic day; P: postnatal day. Scale bars: 50  $\mu$ m.

mRNA was isolated from mouse whole heart tissue collected at sequential developmental stages as indicated. Equal amounts were loaded as verified by using *gapdh* as a loading control. (D-G) *Npnt* expression in the rat heart was determined by enzymatic immunostaining on the paraffin sections from E14.5 rat embryos. (D) Brightfield image of the negative control. (E-G) Brightfield images showing *Npnt* expression in the myocardium (black arrowhead) whereas epicardium (green arrow) and endocardium (black arrow) are devoid of *Npnt* expression. (H) RT-PCR analysis of *npnt* mRNA expression in the cardiomyocyte and non-myocyte fraction isolated from P3 hearts. Equal amounts were loaded as verified by using *gapdh* as a loading control. A: atrium; V: ventricle; E: embryonic day; P: postnatal day. Scale bars: 50  $\mu$ m.

## 4.2 Cloning for *in situ* probe and full length *npnt* synthesis

We have cloned 521 bp of the coding sequence of *npnt* to synthesize an *in situ* probe against *npnt*. In addition we have cloned full length *npnt* to synthesize *in*



*in vitro* capped mRNA for rescue experiments. We have sequenced all cloned *npnt* cDNAs. Interestingly, they were not fully identical to the *npnt* sequence published by NCBI (NM\_001145580.1) on 23<sup>rd</sup> of November 2010. As per NCBI data *npnt* contains 13 exons and the last exon contains a stop codon. Our sequencing report indicates that all of our clones lacked exon E3 (51 bp) and part of exon E13 including the stop codon. Instead, our data suggest that *npnt* contains one extra exon (E14) containing part of the coding sequence, a stop codon and part of the 3' UTR (Figure 4.2).

```

E1 TTCCAGTCTGACCACTGACGGATTTAAATCTCATCATCATTCCCATTCACAGACCGGACACAGCCCGGACGCTCGGATAATA
E1 TTCCAGTCTGACCACTGACGGATTTAAATCTCATCATCATTCCCATTCACAGACCGGACACAGCCCGGACGCTCGGATAATA
CGCCCACTGCACGCGCCCGGACATGTCGGATCATAAAGTTCATGTTGATGTGGACCTGCTGGATCGCAGTGGACCGCGACTTCGATG
CGCCCACTGCACGCGCCCGGACATGTCGGATCATAAAGTTCATGTTGATGTGGACCTGCTGGATCGCAGTGGACCGCGACTTCGATG
CGAAGTG E2 GTCCCGACAGATGTCCTCATCCAATGGTCTGTGTCGGTACGGCGCCGCAATTGACTGCTGTGGGCTGGACGAG
CGAAGTG E2 GTCCCGACAGATGTCCTCATCCAATGGTCTGTGTCGGTACGGCGCCGCAATTGACTGCTGTGGGCTGGACGAG
AGTCTCTCGGCCAGTGCACCC E3 ----- E4 GCT
AGTCTCTCGGCCAGTGCACCC E3 CCTCTACGCTTAAACCCGACAGTAATCGGATAAGGTGTCAGCCCAAAG E4 GCT
ATGTACGCAACGATCCAAACGCGAGAAATGCGTGGACCCAAACAAATGCAAGTGCATCCAGGTTATACAGGAAAAACATGCCAAC
ATGTACGCAACGATCCAAACGCGAGAAATGCGTGGACCCAAACAAATGCAAGTGCATCCAGGTTATACAGGAAAAACATGCCAAC
AAG E5 ACCTGAACGACTGTGGCCTGAAGCCTCTCTCTGTAAGCACCCTGCATGAACACATTCGGGAGCTTCAAGTGTACTG
AAG E5 ACCTGAACGACTGTGGCCTGAAGCCTCTCTCTGTAAGCACCCTGCATGAACACATTCGGGAGCTTCAAGTGTACTG
TCTGAATGGCTTCATGCTGCTGCCGGATGGGAGCTGGCCCA E6 ATGCCGAACTTGCAGCATGGGAACTGCCCATATGCGTGT
TCTGAATGGCTTCATGCTGCTGCCGGATGGGAGCTGGCCCA E6 ATGCCGAACTTGCAGCATGGGAACTGCCCATATGCGTGT
GAGGTAATGAAAGGAGAGGTTGCTGCCAGTGCCTCCAGCTTCCAGCTCTACAGCTGGCTCCAGATGGCAGGACCTGTGTGG E7 ATG
GAGGTAATGAAAGGAGAGGTTGCTGCCAGTGCCTCCAGCTTCCAGCTCTACAGCTGGCTCCAGATGGCAGGACCTGTGTGG E7 ATG
TGGATGAATGTGCCGAGGTTTGGTCTTTGTCGCCCTTTCGGGAACTGCATCAACACATTTGGGAGTTACATCTGCAAGTGCCAT
TGGATGAATGTGCCGAGGTTTGGTCTTTGTCGCCCTTTCGGGAACTGCATCAACACATTTGGGAGTTACATCTGCAAGTGCCAT
GACCGCTTTGACCTTCAGTACCTCAATGGGAAATATCACTGTACAG E8 ATGTCAATGAATGCCCTTTGGTGCAGCACCAGTGTG
GACCGCTTTGACCTTCAGTACCTCAATGGGAAATATCACTGTACAG E8 ATGTCAATGAATGCCCTTTGGTGCAGCACCAGTGTG
GTCCATACGCCACCTGTTATAACACACCTGGTTTATACAACTGCAAGTGTAAAGAGAGACTACAGAGGCTGGGCTACGACTGCCAAA
GTCCATACGCCACCTGTTATAACACACCTGGTTTATACAACTGCAAGTGTAAAGAGAGACTACAGAGGCTGGGCTACGACTGCCAAA
C E9 CCATCCCAGAGTGTAAATGACCTCCACGACCTGGAAAGACCACACCAGCAGCAATAAACAAGAGCCGGCAACAAA
C E9 CCATCCCAGAGTGTAAATGACCTCCACGACCTGGAAAGACCACACCAGCAGCAATAAACAAGAGCCGGCAACAAA
ATTCCAGGATCAGACCCAAAAGAGGACCCACAACTAAGACTCCAGTAACGGCCAAAGCATCTCACCTACAATCACCACCAC
ATTCCAGGATCAGACCCAAAAGAGGACCCACAACTAAGACTCCAGTAACGGCCAAAGCATCTCACCTACAATCACCACCAC
CACCCTACCCAAACCTCTTCCAACAAAAAATCACCCTCCAGCAAGAGTCCCGGTGACCAACCCTTAAGCCATTCATCC
CACCCTACCCAAACCTCTTCCAACAAAAAATCACCCTCCAGCAAGAGTCCCGGTGACCAACCCTTAAGCCATTCATCC
CAACAAAGAGCCCTGTGCTGGTGCAGAACCAAACTAAGCTCCGACTCACAGCACACCACCAAAAAGTCCCACTGCTTACA
CAACAAAGAGCCCTGTGCTGGTGCAGAACCAAACTAAGCTCCGACTCACAGCACACCACCAAAAAGTCCCACTGCTTACA
CGAGTGGTTCCTTTTATCCCAACACCGAGACCTTTCACCATCCGTTTGTGACACCAATTGATAACAGCATCAAAGACATCACCCA
CGAGTGGTTCCTTTTATCCCAACACCGAGACCTTTCACCATCCGTTTGTGACACCAATTGATAACAGCATCAAAGACATCACCCA
GAAAACAAGAGCCGATCTTACA E10 TACCACGAAATCATGGGAAGAACAATGTTCTGGTATCCGATTTAGACATTGAACTGGG
GAAAACAAGAGCCGATCTTACA E10 TACCACGAAATCATGGGAAGAACAATGTTCTGGTATCCGATTTAGACATTGAACTGGG
CAACACCGAAGAGGAGCTGAAGGATGACCCAG E11 AGTCTGCCTATCTGAGCTGCCATTTGATCACGGTTTGTGTGGATGGAT
CAACACCGAAGAGGAGCTGAAGGATGACCCAG E11 AGTCTGCCTATCTGAGCTGCCATTTGATCACGGTTTGTGTGGATGGAT
CCAGCCAGAGAGGGAGACCTTCATGGGAGACATCGGAAGATCCTTCGGT E12 GGAGGTACC TAACCATCTCTGAGGCCGG
CCAGCCAGAGAGGGAGACCTTCATGGGAGACATCGGAAGATCCTTCGGT E12 GGAGGTACC TAACCATCTCTGAGGCCGG
GGAGAAGCCTGCTGGCGTGTGCTCAGCTGATCCTCCCTGAAAACCCCTGGAACGAGGGGAACTGTGCTTGCCTTCAGAC
GGAGAAGCCTGCTGGCGTGTGCTCAGCTGATCCTCCCTGAAAACCCCTGGAACGAGGGGAACTGTGCTTGCCTTCAGAC
ACAACATGCCAGTCAACATCTGCGAATCTTCAGCTGTTCTACAGAAAAGCTCGGACACACTCCCCTGCTCTGGGACCAACA
ACAACATGCCAGTCAACATCTGCGAATCTTCAGCTGTTCTACAGAAAAGCTCGGACACACTCCCCTGCTCTGGGACCAACA
GGAGAAAAGCCTCGAGCTCCACACAGATCACCCTTTGGGCAATGGCTAGAAAAGTGT E13 CATCTGAAGGCCGAGCGCCG
GGAGAAAAGCCTCGAGCTCCACACAGATCACCCTTTGGGCAATGGCTAGAAAAGTGT E13 CATCTGAAGGCCGAGCGCCG
GAGAGCCCGAAGGCCGAAATGCTCTGGATGACATGAGTCTCAAACGAGGTTCTGTGAGGAGGACAACTGAGGAGACTT
GAGAGCCCGAAGGCCGAAATGCTCTGGATGACATGAGTCTCAAACGAGGTTCTGTGAGGAGGACAACTGAGGAGACTT
--- E14 AGGATTCGAGAAAGATGGACCTTATGGAAAGGAGCTGGCCTTCTGTCACTCCGATATGGTAATGCTGCACTTTT
TAA E14 -----
TACCGCCGTCAACTGCATGCTCCAGCTCAACAGACTGGCTACGATGACCTATTCTTGTAGAACAAACAGGAAAGTATTTAGT

```

**Figure 4.2:** Comparison of the sequence results (red) to the published NCBI sequence (black). **ATG:** start codon. **TAA** or **TGA:** stop codons.

We assume that the cloned cDNA represents the *npnt* mRNA. Our full length clone contains part of the 5' UTR, full coding sequence and part of the 3' UTR.

### 4.3 *npnt* is transiently expressed in the heart during zebrafish development

To determine the expression pattern of *npnt* in zebrafish we performed whole-mount *in situ* hybridization analyses using sense and antisense riboprobes against *npnt* (Figure 4.3). At 24 hpf *npnt* is markedly expressed at the tail bud, head, in the posterior part of the gut and in the pharyngeal endoderm (Figures 4.3B,C).

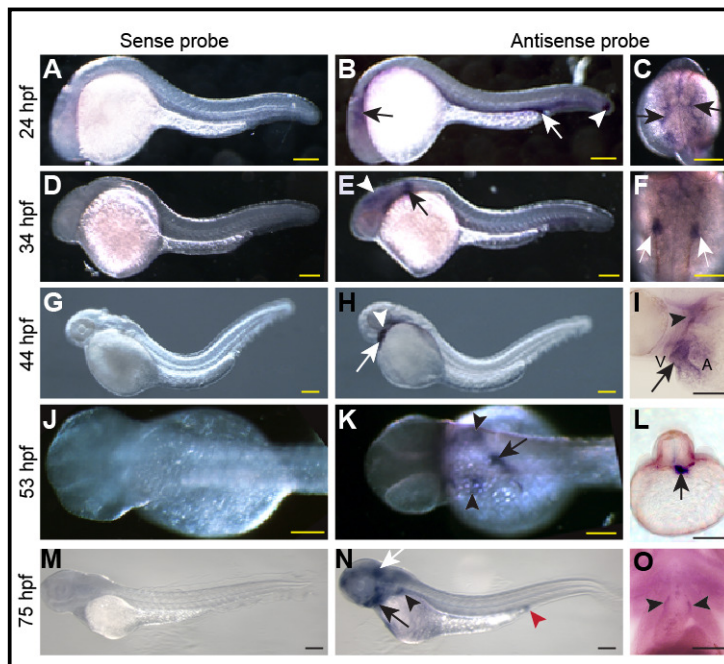


**Figure 4.3: *npnt* is transiently expressed during zebrafish heart development.** (A-O)

Zebrafish *npnt* expression was determined by whole-mount *in situ* hybridization using antisense probe (B,C,E,F,H,I,K,L,N,O) and sense probe (A,D,G,J,M) as a negative control. (B) Lateral view of a 24 hpf embryo showing *npnt* expression in tailbud (white arrowhead), head (black arrow) and posterior part of

the gut (white arrow). (C) Dorsal view of the anterior part of the trunk is demonstrating *npnt* expression in pharyngeal endoderm (black arrows). (E,F) Lateral and dorsal view at 34 hpf showing *npnt* expression in the pronephric region (arrows) and head (E, arrowhead). (H,I) Ventrolateral view (H) and parasagittal section (I) at 44 hpf demonstrating *npnt* expression in heart (arrow) and jaw (arrowhead). (K) Dorsal view showing *npnt* expression at 53 hpf in pharynx, esophagus (arrow) and pharyngeal endoderm (arrowheads). (L) Cross-section through the trunk confirming *npnt* expression in the endodermal cells of the anterior gut (arrow). (N) Lateral view of a 75 hpf embryo demonstrating *npnt* expression in head (white arrow), pectoral fin (black arrowhead), pharyngeal arches (black arrow) and cloaca (red arrowhead) (O) Ventral view of a embryo is demonstrating *npnt* is expressed in the bulbus (black arrows) at 75 hpf. A: atrium; V: ventricle; Scale bars: 100  $\mu$ m.

At 34 hpf highest expression of *npnt* was observed in the pronephric region, with persistent expression in the head (Figures 4.3E,F). *npnt* expression in the heart was first detected at 44 hpf (Figure 4.3H) when it was also expressed in pharyngeal pouch and mandibular cartilage (Figure 4.3H). Parasagittal sections of the 44 hpf embryonic heart demonstrated that *npnt* is expressed throughout the heart (Figure 4.3I). Cardiac *npnt* expression was still observed at 48 hpf but was undetectable at 53 hpf when *npnt* expression was most prominent in the pharynx, esophagus and the pharyngeal endoderm (Figures 4.3K,L). At 75 hpf *npnt* is markedly expressed at the head, pectoral fin cloaca, cardiac bulbus, and pharyngeal arches but was undetectable in the cardiac chambers (Figures 4.3N,O). Taken together, our data demonstrate that *npnt* is transiently expressed in the heart during zebrafish development.

#### 4.4 *Npnt* knockdown utilizing different morpholinos

To assess the role of *Npnt* in zebrafish heart development morpholinos were used to knock down *Npnt* protein levels. Three different morpholinos were designed: one translation inhibitory morpholino (MO1), binding at the start codon and part of 5' UTR, and two splicing inhibitory morpholinos (MO2 and MO3), targeting the splice donor site of exon E4 (MO2) or the splice donor site of exon E1 (MO3) (Figures 4.4A,B). Our data indicate that both MO2 injection (1.4 to 2.0 pmol) and MO3 injection (1.4 to 2.4 pmol) were effective in disrupting correct splicing of *npnt* pre-mRNA resulting in a marked decrease of mature *npnt* mRNA (Figures 4.4C,D). RT-PCR analyses with the primer pair F2/R demonstrated that MO2 injection resulted in exon E4 deletion (Figure 4.4C). cDNA sequencing revealed that MO2 injection resulted not in a frame shift but in the deletion of 120 bp encoding one EGF domain. To determine whether a shortened *Npnt* protein is produced we performed Western blot analyses utilizing a polyclonal anti-*Npnt* antibody. Injection of MO1 (3.5 pmol), MO2 (1.4 pmol) and MO3 (2.4 pmol) resulted in a marked decrease of *Npnt* protein level and no truncated *Npnt* protein was detected (Figure 4.4E). Therefore, all subsequent studies were performed using these amounts of morpholinos. Taken together, our results demonstrate that injection of MO2 and MO3 efficiently knocked down the expression of *npnt* on mature mRNA and for MO1, MO2 and MO3 also on protein level.

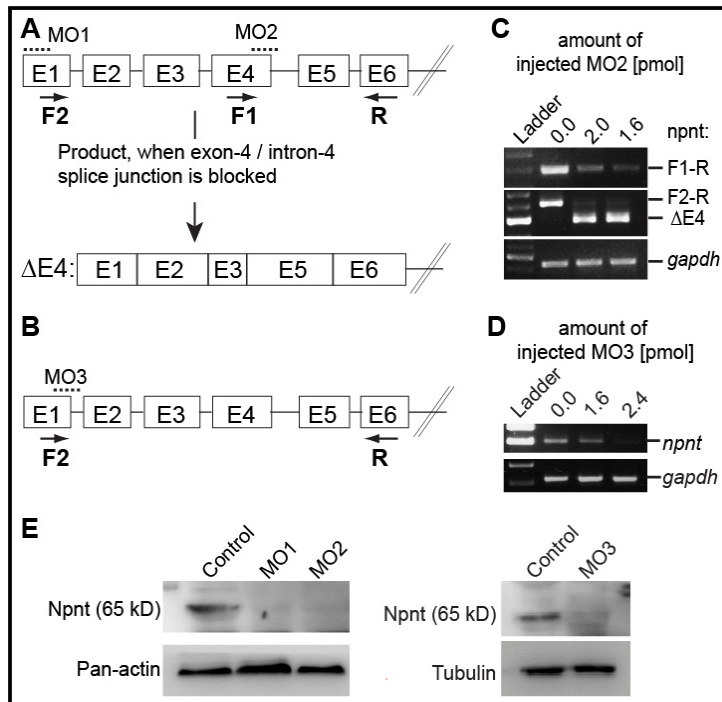


**Figure 4.4: Morpholino-mediated *Npnt* knock-down.** (A,B) Scheme of the effect of the *npnt* splice inhibitory morpholino MO2 and MO3. Exons are represented by boxes with numbers and introns by lines. Dotted lines indicate the region targeted by MO1 (translation inhibitory morpholino) or MO2 and MO3. Arrows indicate RT-PCR primer positions in the *npnt* gene. (C) RT-PCR analysis of mRNAs from control and MO2-injected

embryos at 52 hpf using the *npnt* primers as indicated in (A) and *gapdh* primers (loading control). MO2 inhibited *npnt* pre-mRNA splicing resulting in exon E4 deletion (n=3). (D) RT-PCR analysis of mRNAs from control and MO3-injected embryos at 52 hpf using the *npnt* primers as indicated in (B) and *gapdh* primers (loading control). MO3 inhibited *npnt* pre-mRNA splicing resulting in downregulation of mature *npnt* mRNA production (n=3). (E) Western blot analysis of protein extracts from control and either MO1-, MO2- or MO3-injected embryos at 52 hpf (n=3). All three morpholinos efficiently knocked down Npnt protein level.

#### 4.5 *Npnt* knockdown disrupts heart development and is lethal

To determine the effect of Npnt knockdown on zebrafish heart development we injected morpholinos in embryos of transgenic zebrafish *Tg(myf17:EGFP-HsHRAS)<sup>s883</sup>* (n > 200, 4 independent experiments). In these zebrafish GFP is localized at the cardiomyocyte plasma membrane facilitating the analysis of heart morphology in living zebrafish. MO1, MO2 or MO3 injection did not show any obvious effect on zebrafish development until 40 hpf. However, Npnt knockdown resulted in 89%  $\pm$  7.9% lethality at 7 dpf (Figure 4.5A). The first obvious phenotype observed was pericardial edema at 75 hpf indicating a cardiac defect (Figure 4.5B). A closer analysis of the morphant hearts revealed that valve leaflet formation at 110 hpf is perturbed in 86%  $\pm$  3.9% of the morphants, resulting in > 30% of those in the lack of valve leaflets (Figures 4.5C,D). The morphants are also characterized by swelling of the cardiac jelly

separating the endocardium and myocardium throughout the heart (Figure 4.5D). Taken together, our data indicate that *Npnt* is essential for cardiac development in zebrafish.

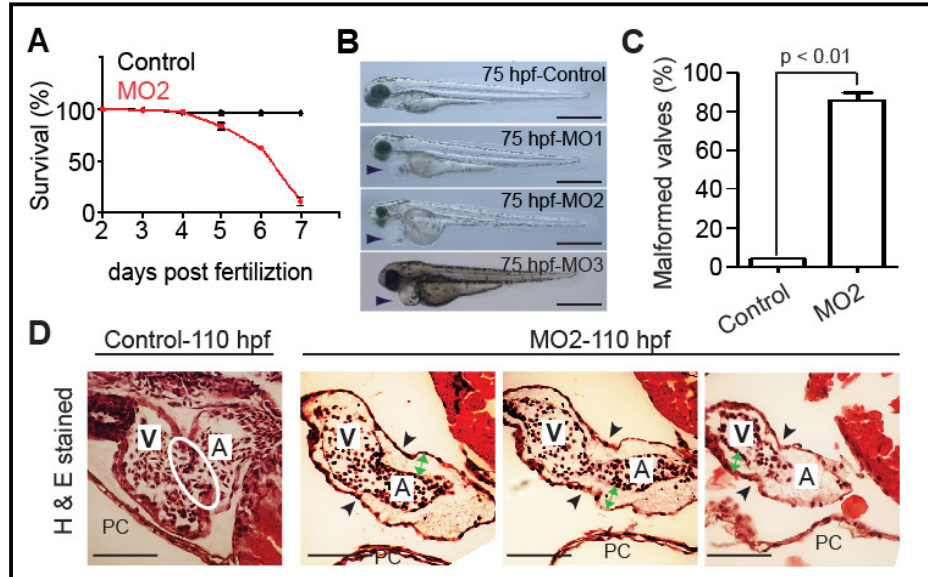
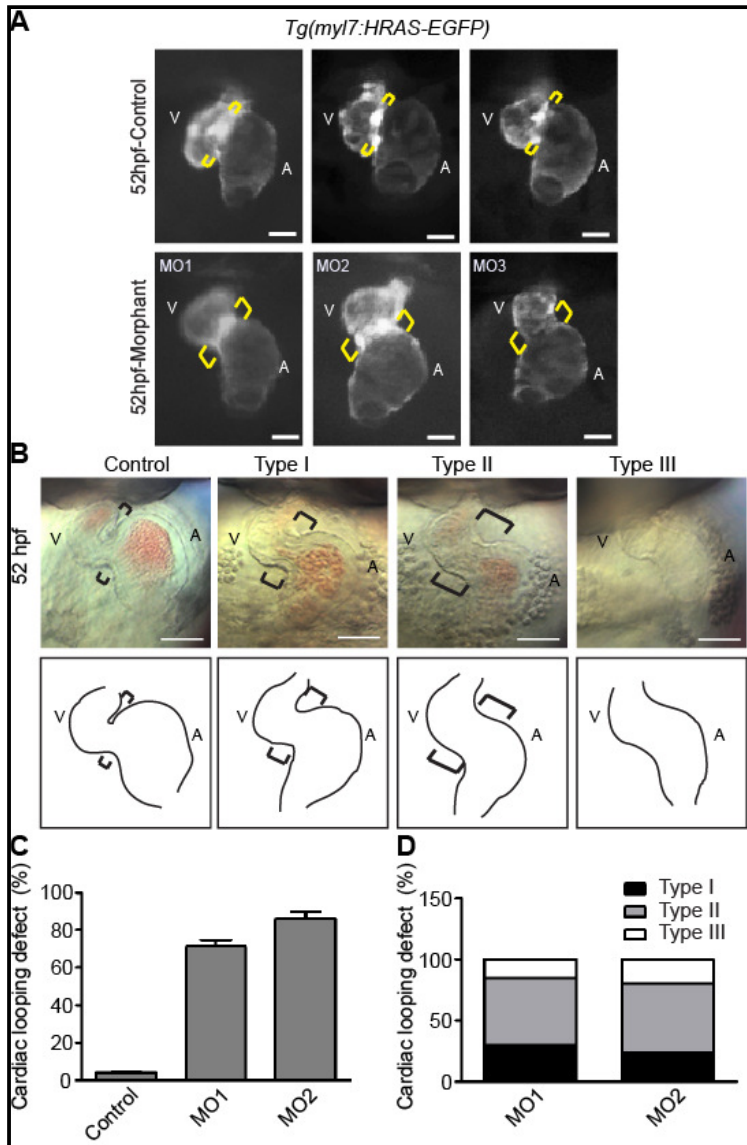


**Figure 4.5: Morpholino-mediated *Npnt* knockdown disrupts heart development and is lethal.** (A) *Npnt* knockdown resulted in  $89\% \pm 7.9\%$  lethality at 7 dpf. (B) Lateral view of control, MO1-, MO2- or MO3-injected embryos at 75 hpf. MO1-, MO2- or MO3-mediated *Npnt* knockdown resulted in pericardial edema (arrowheads). Scale bars: 500  $\mu$ m. (C) Quantitative analysis is indicating that valve formation is perturbed in  $86\% \pm 3.9\%$  morphant hearts at 110 hpf. (D) H & E stained sagittal sections of hearts from control and MO2-injected embryos at 110 hpf are showing morphant hearts that failed to form proper valve leaflets at the AV boundary. White circle highlights properly formed AV valve leaflets in control embryos. Black arrowheads indicate AV boundary and green double arrows indicate expanded cardiac jelly. A: atrium; V: ventricle; PC: pericardium. Scale bars: 50  $\mu$ m.

#### 4.6 *Npnt* knockdown causes an extended AV canal

To determine the earliest effect of *Npnt* knockdown on the morphology of the heart either MO1, MO2 or MO3 was injected in embryos of transgenic zebrafish *Tg(myI7:EGFP-HsHRAS)<sup>s883</sup>* ( $n > 200$ , 4 independent experiments). Compared to control hearts from non-injected or phenol red-injected embryos, hearts from morpholino (either MO1 or MO2 or MO3)-injected embryos exhibited an extended tube like structure at the AV boundary at 52 hpf (Figure 4.6A).





Quantitative analysis of embryos regarding AV canal expansion in total ( $n > 150$  from 3 independent experiments, mean  $\pm$  SEM). (D) Quantitative analysis regarding type I, type II and type III AV canal expansion. Note that type II was the most common phenotype (over 50%) in both MO1- and MO2-injected embryos. A: atrium; V: ventricle. Scale bars: 50  $\mu$ m.

Based on the severity of the cardiac defect at 52 hpf morphants were categorized into three classes: type I (mild extension of the AV canal), type II (clear extension of the AV canal), type III (straight heart) (Figure 4.6B). MO1 injection caused heart defects in  $71\% \pm 4.0\%$  (type I:  $29\% \pm 2.6\%$ , type II:  $54\% \pm 5.3\%$ , type III:  $17\% \pm 8.3\%$ ) and MO2 injection in  $86\% \pm 4.4\%$  (type I:  $21\% \pm 3.2\%$ , type II:  $56\% \pm 4.0\%$ , type III:  $23\% \pm 3.9\%$ ) of injected embryos (Figures 4.6C,D). All three morpholinos resulted in *Npnt* knockdown and in similar phenotypes suggesting that the observed phenotypes are a functional

**Figure 4.6: Depletion of *Npnt* by three different morpholinos causes an extended AV canal (A)**

Morpholino-injected embryos from transgenic zebrafish *Tg(myf7:EGFP-HsHRAS)<sup>s883</sup>* showed an expansion of the AV canal at 52 hpf compared to control embryos. (B) Nomarski (DIC) images of hearts from control and morpholino-injected embryos at 52 hpf representing AV canal expansion defects. Depending on severity of heart defects phenotypes were classified into type I (mild extension of the AV canal), type II (clear extension of the AV canal) and type III (straight heart). Brackets indicate the AV boundary. (C)

consequence of *Npnt* depletion and earliest morphological phenotype is an extension of the AV canal.

#### 4.7 Microinjection of *npnt* mRNA rescues AV canal extension

To prove that the observed cardiac phenotypes are specific to the depletion of *Npnt*, rescue experiments were performed by co-injecting *in vitro* transcribed capped *npnt* mRNA and MO2. Efficiency of *in vitro* transcription and the correct size of the *in vitro* synthesized capped *npnt* mRNA (2100 kb) were confirmed by denaturing agarose gel electrophoresis (Figure 4.7A). Note that, MO2 is a splice inhibitory morpholino that does not affect translation of injected *npnt* mRNA.

The sequence of all cloned *npnt* cDNAs were identical but in part different from the published *npnt* sequence by NCBI on 23<sup>rd</sup> of November 2010 (see 4.2 and Figure 4.2). Assuming that the cloned cDNA represents the *npnt* mRNA at 52 hpf, we used linearized pCS2+-*Fnnt* plasmid as template to generate capped *npnt* mRNA for rescue experiments. Injection of 30 pg of capped *npnt* mRNA had no effect on cardiac development and did not rescue the MO2-induced AV canal extension defects. In contrast, injection of 50 pg of capped *npnt* mRNA rescued the AV canal extension defect in a subset of MO2-injected embryos (Figure 4.7B) and had only a minor effect on cardiac development when injected alone (88%  $\pm$  1.46% normal hearts at 52 hpf, Figure 4.7C). Importantly, 40%  $\pm$  2.33% of embryos had normal AV canal length after co-injection of mRNA and MO2 compared to 11%  $\pm$  2.0% after only MO2-injection (Figure 4.7C). In addition, injection of 50 pg capped *npnt* mRNA markedly reduced the severity of the cardiac extension defect in the remaining embryos with defective hearts resulting in an increased amount of type I defects (23.6%  $\pm$  1.21% to 48.7%  $\pm$  2.38%) and a decrease in type II defects (60%  $\pm$  1.09% to 26.5%  $\pm$  2.6%) (Figure 4.7D). The slight increase in the type III phenotype (16.4%  $\pm$  2.38% to 24.8%  $\pm$  2.41%) might be due to the *npnt* overexpression phenotype. Rescued embryos did not form cardiac edema at 75 hpf (Figure 4.7E). Injection of 80 pg capped *npnt* mRNA caused severe defects in zebrafish development including cyclopia and heart defects (Figure 4.7F). In summary, our data show that the MO-mediated phenotypes are due to

Npnt protein depletion and demonstrate that Npnt is required for heart development in zebrafish.

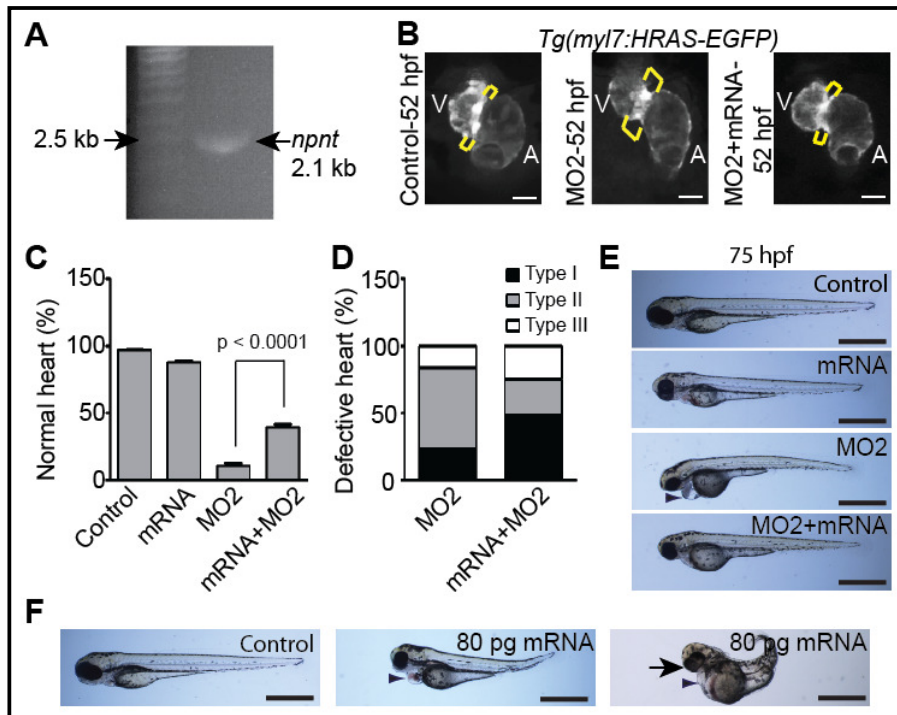


**Figure 4.7: Extended AV canal of Npnt morphant hearts could be rescued by *in vitro* synthesized capped *npnt* mRNA injection.** (A) Denatured agarose gel picture demonstrating the size of the *in vitro* synthesized capped *npnt* mRNA after electrophoresis. (B) Representative images of hearts from control, MO2- and MO2+*npnt* mRNA-injected embryos from transgenic zebrafish *Tg(myI7:EGFP-HsHRAS)<sup>s883</sup>* at 52 hpf (scale bars: 50  $\mu$ m). Brackets indicate the AV boundary. (C) Quantitative analysis of the rescue experiment scoring for normal hearts ( $n > 160$  from three independent experiments, mean  $\pm$  SEM). (D) Quantitative analysis of the rescue experiment scoring type I, type II and type III AV canal defects. (E) Lateral view of control, *npnt* mRNA, MO2- or MO2 + *npnt* mRNA-injected embryos at 75 hpf (scale bars: 500  $\mu$ m). Note that injection of *npnt* mRNA rescued the Npnt-depleted AV canal extension defect and pericardial edema (arrowhead). (F) Lateral view of control, or 80 pg capped *npnt* mRNA-injected embryos at 75 hpf. Note that, >50% embryos carry pericardial edema (black arrowhead) and >25% embryos carry cycloopia (black arrow) as an overexpression phenotype (scale bars: 500  $\mu$ m). A: atrium; V: ventricle.



#### 4.8 Npnt depletion does not affect the total number of cardiomyocytes

To better characterize the functional consequence of Npnt depletion for heart development the transgenic zebrafish lines *Tg(myI7:EGFP-HsHRAS)<sup>s883</sup>* expressing GFP at the cardiomyocyte plasma membrane and *Tg(-5.1myI7:nDsRed2)f2* expressing RFP in cardiomyocyte nuclei were used. Projections of cardiac optical sections from *Tg(myI7:EGFP-HsHRAS)<sup>s883</sup>* control and Npnt morphant embryos at 52 hpf showed no obvious differences in the morphology of chamber cardiomyocytes (Figures 4.8A,B). In contrast, the morphology of the AV boundary was affected by Npnt knockdown. Npnt morphants exhibited an extended tube like structure at the AV boundary (Figures 4.8B,D) compared to the control hearts (Figures 4.8A,C).

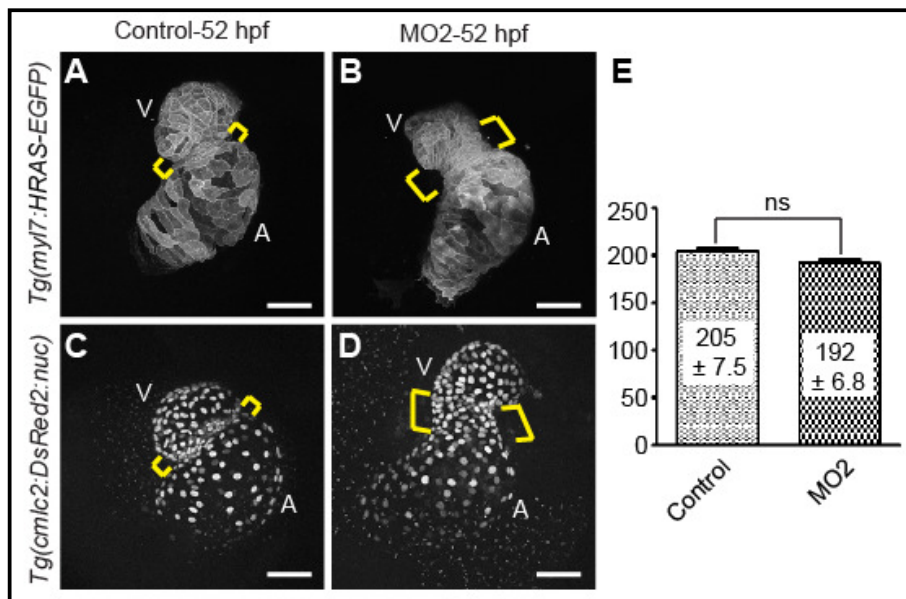


**Figure 4.8: The AV canal of Npnt morphants is expanded, without affecting cardiomyocyte number.** (A-D) Projections of confocal images of hearts from control (A,C) and MO2-injected (B,D) embryos from transgenic zebrafish *Tg(myI7:EGFP-HsHRAS)<sup>s883</sup>* (A,B) and *Tg(-5.1myI7:nDsRed2)f2* (C,D) at 52 hpf suggesting an extension of the AV canal (brackets) in Npnt morphants. (E) Quantitative analysis scoring total number of cardiomyocytes in hearts from control and Npnt depleted embryos. A: atrium; V: ventricle. Scale bars: 50  $\mu$ m. (n = 5, mean  $\pm$  SEM).

An extension of the AV canal could either be due to an increase in proliferation of AV cells or a patterning defect, meaning that more cells differentiate into AV cells at the expense of chamber cells. Cell count

experiments using *Tg(-5.1myl7:nDsRed2)f2* embryos at 52 hpf revealed that the overall number of cardiomyocytes (chambers + AV boundary) was not significantly different between control and morphant hearts ( $205 \pm 7.5$  vs.  $192 \pm 6.8$ ,  $n = 5$ ) (Figure 4.8E). These data indicate that the extension of the AV canal was due to an increase in cells differentiating into AV canal cells at the expense of chamber cells, without affecting cardiomyocyte proliferation.

To evaluate which chamber cells contribute to the additional AV canal cells we performed immunostaining against atrial myosin heavy chain on embryos from double transgenic animals (*Tg(-5.1myl7:nDsRed2)f2* x *Tg(myI7:EGFP-HsHRAS)<sup>s883</sup>*) (Figure 4.9).

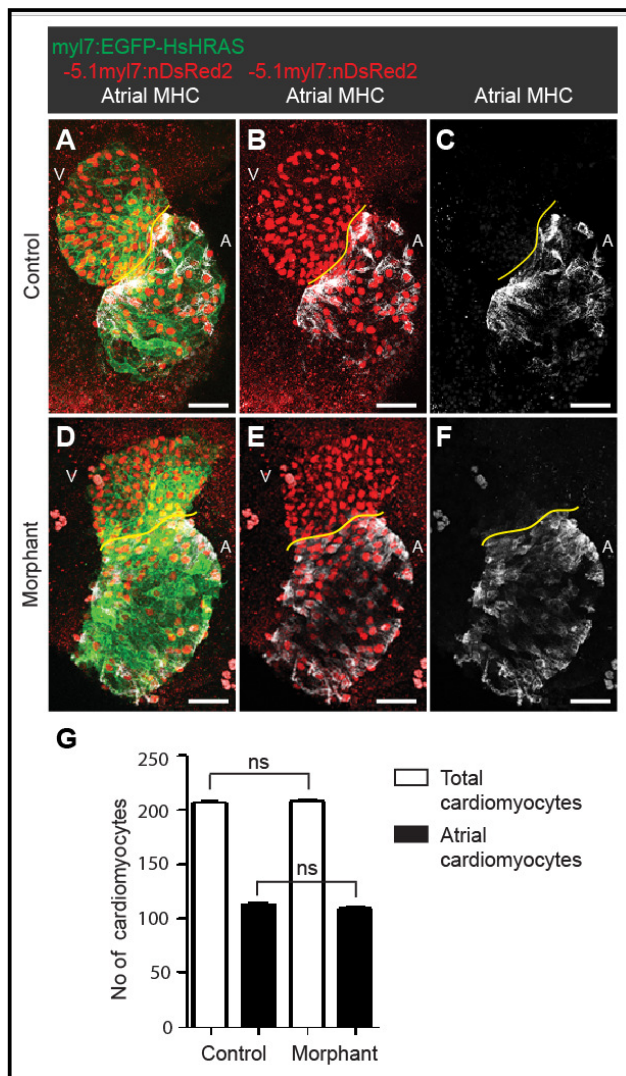


**Figure 4.9. Additional AV canal cells might be at the expense of ventricular cells.** (A-F) Projections of confocal images of hearts from whole-mount atrial myosin heavy chain- (white) and DsRed-stained (red) control (A-C) and MO2-injected (D-F) embryos from double transgenic animals (*Tg(-5.1myl7:nDsRed2)f2* x *Tg(myI7:EGFP-HsHRAS)<sup>s883</sup>*). (G) Quantitative analysis of the overall number of cardiomyocytes (chambers + AV boundary) and the number of atrial cardiomyocytes. A: atrium; V: ventricle. Scale bars: 50  $\mu$ m. ( $n=5$ , mean  $\pm$  SEM).

Atrial myosin heavy chain staining marks only cardiomyocytes from atrial origin, thus it helps to identify the origin of the additional cardiomyocytes in the extended AV canal. As in the previous experiment (Figure 4.8E) the overall number of cardiomyocytes (chambers + AV boundary) was not significantly different between control and morphant hearts (Figure 4.9G). Counting of cardiomyocytes in hearts stained for atrial myosin heavy chain revealed that also the number of atrial cardiomyocytes was not significantly different between control and morphants hearts (Figure 4.9). These data suggest that the extension of the AV canal is due to an increase in cells differentiating into AV canal cells at the expense of ventricular cells in *Npnt* morphants.

#### **4.9 *Npnt* depletion causes an expansion of myocardial AV canal gene expression**

To determine how *Npnt* knockdown affects cardiac AV canal differentiation, we assessed the expression of early differentiation markers of the AV canal myocardium like *cspg2* (zebrafish *versican* homolog) and *bone morphogenetic protein 4* (*bmp4*). During early cardiac development *bmp4* and *cspg2* are expressed throughout the heart in the myocardium and then later at 37 hpf *cspg2* expression becomes restricted to the AV canal region and *bmp4* expression restricted to non-chamber myocardium (OFT, AV canal and IFT) (37). The expression of another ECM gene, *fibulin1* (106), is restricted to the AV myocardium at 2 dpf. To assess the effect of *Npnt* knockdown on the expression of these AV canal specific myocardial genes at 52 hpf whole-mount *in situ* hybridization analyses were performed. Compared to control hearts (Figures 4.10A,C,E) expression of all these genes was expanded in *Npnt* morphant hearts at the AV boundary at 52 hpf (Figures 4.10B,D,F). In addition, ectopic expression of *cspg2* was detected at the IFT (Figure 4.10D).

The expression of the ventricular cardiomyocyte specific gene *vmhc* and the atrial cardiomyocyte specific gene *amhc* is first evident at the 19 somite stage (16 hpf) (65). To assess the affect of *Npnt* knockdown on chamber specific expression of the marker genes *vmhc* and *amhc* *in situ* hybridization was performed. Expression of the chamber specific marker genes was unaffected in *Npnt* morphant hearts (Figures 4.10G,H,I,J). Our data indicate

that the extended tube like structure represents an extended AV canal on a molecular level.

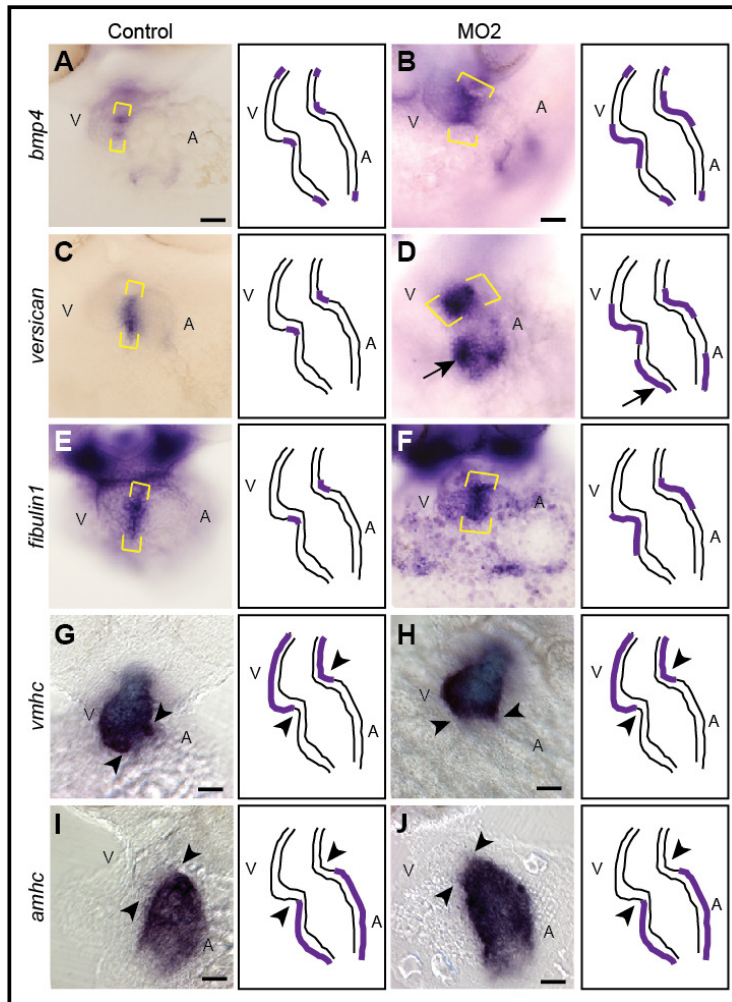


**Figure 4.10: Npnt morphant hearts have an extended AV canal at the molecular level in the myocardium.** (A-F)

Sections of 52 hpf control and MO2-injected embryos after whole-mount *in situ* hybridization with probes against *bmp4* (A,B) and the ECM genes *cspg2* (C,D) and *fibulin1* (E,F). The expression pattern of these genes was expanded in the myocardium of Npnt morphants (brackets). (G-J) Sections of 52 hpf control (G,I) and MO2-injected (H,J) embryos after whole-mount *in situ* hybridization with probes against the chamber-specific marker genes

*amhc* and *vmhc*. Npnt knockdown does not affect the expression pattern of the chamber-specific genes. Arrowheads indicate AV canal. A: atrium; V: ventricle. Scale bars: 50  $\mu$ m.

#### 4.10 Npnt morphant hearts have an extended AV canal endocardium

Our data regarding myocardial cells suggest that the extension of the AV canal is due to a defect in Npnt morphants to restrict AV canal differentiation. Initially *notch1b* is expressed throughout the anteroposterior extent of the cardiac endocardium but at 45 hpf expression is restricted to the AV valve-forming region (107). To determine how Npnt knockdown affects endocardial differentiation at the AV canal, we assessed the expression of early differentiation markers of the valve forming AV canal endocardium. In accordance with an expanded AV canal endocardial expression of *notch1b* was

expanded in *Npnt* morphant hearts at the AV boundary at 52 hpf compared to control hearts (Figures 4.11A,B). Another AV canal marker is Alcam, a cell surface adhesion molecule (108), which is localized to the lateral side of myocardial cells and differentiated AV canal endocardial cells (81). During early cardiac development endocardial cells are squamous and Alcam-negative, but at 36 hpf a single tier of cells at the border between the atrium and the ventricle differentiates into a cuboidal shaped Alcam-positive cell (81). This change in shape and the initiation of Alcam expression are the earliest manifestations of endocardial differentiation in the AV canal.

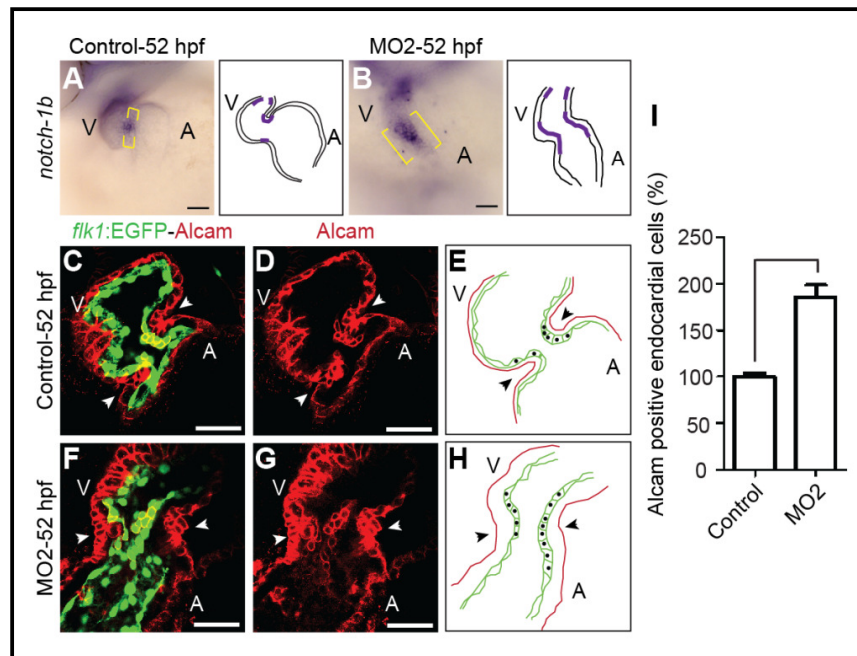


**Figure 4.11: The AV canal endocardium of *Npnt* morphants is expanded.** (A,B) Sections of 52 hpf control and MO2-injected embryos after whole-mount *in situ* hybridization with a probe against *notch1b*. Expression was expanded in *Npnt* morphants (brackets). Confocal sections of whole-mount Alcam-stained (red: myocardium and differentiated endocardial cells) control (C,D) and MO2-injected (F,G) embryos from transgenic zebrafish *Tg(kdrl:EGFP)<sup>s843</sup>* at 52 hpf. Morpholino-mediated knockdown of *Npnt* caused an increase of differentiated endocardial cells (cuboidal-shaped, Alcam- and EGFP-positive) from < 6 tiers to at least 8 - 12 tiers of cells at the AV boundary. Arrowheads indicate AV boundary. (E,H) Schematic drawings of D and G respectively (red line: myocardium; green: endocardial cells; black dots: Alcam-positive endocardial cells). (I) Quantitative analysis: The AV canal endocardium in *Npnt* morphants is extended by  $86\% \pm 13.1\%$  (mean  $\pm$  SEM) in comparison to control hearts. Arrowheads: AV boundary; A: atrium; V: ventricle. Scale bars: 50  $\mu$ m.

To examine endocardial cell differentiation in more detail embryos from the transgenic zebrafish line *Tg(kdrl:EGFP)<sup>s843</sup>* expressing GFP in all



endothelial cells were used and counter stained with an anti-Alcam antibody. At the AV boundary 5 to 6 tiers of endocardial cells expressed Alcam in control hearts at 52 hpf (Figures 4.11C,D,E). In contrast, in the *Npnt* morphants 8 to 12 tiers of cells at the AV canal region were Alcam-positive (Figures 4.11F,G,H). Taken together, these data indicate that *Npnt* knockdown caused a patterning defect resulting in an increased number of differentiated AV myocardial and endocardial cells and thus an extended AV canal.

#### 4.11 *Npnt* knockdown causes abnormal expansion of the cardiac jelly

Myocardium and endocardium are separated by ECM that is termed cardiac jelly. One characteristic of the AV cells is an increased expression of ECM components at the onset of looping (37, 49), which facilitates endocardial cell migration. Around 30 hpf, visibly distinct ventricular and atrial chambers form and by 36 hpf the heart undergoes looping morphogenesis (81).

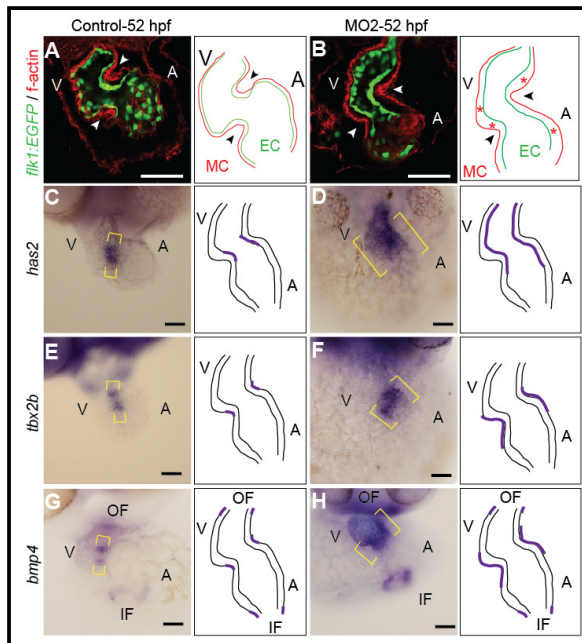


**Figure 4.12: *Npnt* knockdown causes cardiac jelly expansion and expanded expression of *has2*, *tbx2b* and *bmp4*.**

(A,B) Confocal sections from whole-mount F-actin-stained (red) control (A) and MO2-injected (B) embryos heart from transgenic zebrafish *Tg(kdrl:EGFP)<sup>s843</sup>* at 52 hpf. The space between endocardium and myocardium (cardiac jelly) was increased in the AV boundary (arrowheads) as well as throughout the chambers (red asterisks) in *Npnt* morphants. (C-H) Sections of 52 hpf control and MO2-injected embryos after whole-mount *in situ* hybridization showing *has2*, *tbx2b* and *bmp4* expression at the AV boundary (brackets). Note that expression of all analyzed genes is expanded in *Npnt* morphants. A: atrium; V: ventricle. Scale bar: 50  $\mu$ m.

To determine whether the extended AV canal is producing normal amounts of cardiac jelly, embryos from the transgenic zebrafish line *Tg(kdrl:EGFP)<sup>s843</sup>* were used. Embryos were counter stained with rhodamine phalloidin (detects F-actin) to visualize the myocardium.

Analysis of confocal sections of hearts from control and *Npnt* morphant hearts at 52 hpf showed that the space between endocardium and myocardium is markedly increased in the morphants at the AV region as well as chambers (Figures 4.12A,B). This suggests that *Npnt* knockdown caused an abnormal expansion of the cardiac jelly. A major constituent of the cardiac jelly is glycosaminoglycan hyaluronan (HA) which is synthesized by the enzyme hyaluronan synthase 2 (*has2*) (53). It has multiple functions during AV canal morphogenesis: First, HA is required to form expanded cardiac jelly that facilitates endocardial cell migration. Second, it promotes Ras-dependent transformation into pre-valvular mesenchyme and provides a migratory substrate for these invasive cells (53). *has2* is a downstream target of *tbx2* (109). Both of these genes are known to be regulated by BMP signaling (53, 109, 110). In wild type zebrafish the expression of *has2* is restricted to the AV boundary endocardium (49), whereas *bmp4* and *tbx2* expression is restricted to the AV boundary myocardium at 2 dpf (37, 49, 111) (Figures 4.12C,E,G). *bmp4* is in addition expressed at the OFT and IFT (Figure 4.12G) (37). In contrast, expression of *has2*, *tbx2b* and *bmp4* are expanded in *Npnt* morphants at the AV boundary (Figures 4.12D,F,H). Taken together, these results suggest that *Npnt* is an inhibitory upstream regulator of *bmp4*, *tbx2b*, and *has2* expression controlling cardiac jelly formation.

#### 4.12 *Npnt* knockdown causes abnormal trabeculation

It has been reported that ventricular trabeculation is initiated at around 72 hpf by protrusion of cardiomyocytes out of the monolayered ventricular myocardium, generating small clusters of cells (74, 112). To evaluate whether trabeculation is affected in *Npnt* morphant hearts we examined confocal optical sections of the hearts from 80 hpf *Tg(myI7:EGFP-HsHRAS)<sup>s883</sup>* control and MO2-injected embryos. Consistent with published data control embryos exhibit around 80 hpf highly trabeculated ventricles (Figures 4.13A,B). In contrast, the *Npnt* morphant hearts were devoid of trabeculation (Figures 4.13C,D). Saggital confocal sections revealed that myocardial cells are disorganized in *Npnt* morphants at 80 hpf (Figures 4.13C,D). H&E stained cardiac sections of 110 hpf embryos showed finger like projections (trabeculae) extended into the ventricular lumen from monolayered compact myocardium. In contrast, in *Npnt*

morphant hearts the monolayered ventricular myocardium remains devoid of trabeculae. In addition endocardium and myocardium in control hearts are separated by a thin layer of cardiac jelly whereas in *Npnt* morphant hearts extensive cardiac jelly is present (Figures 4.13E,F). Thus, *Npnt* knockdown causes not only an extension of the AV canal but also perturbed trabeculation.

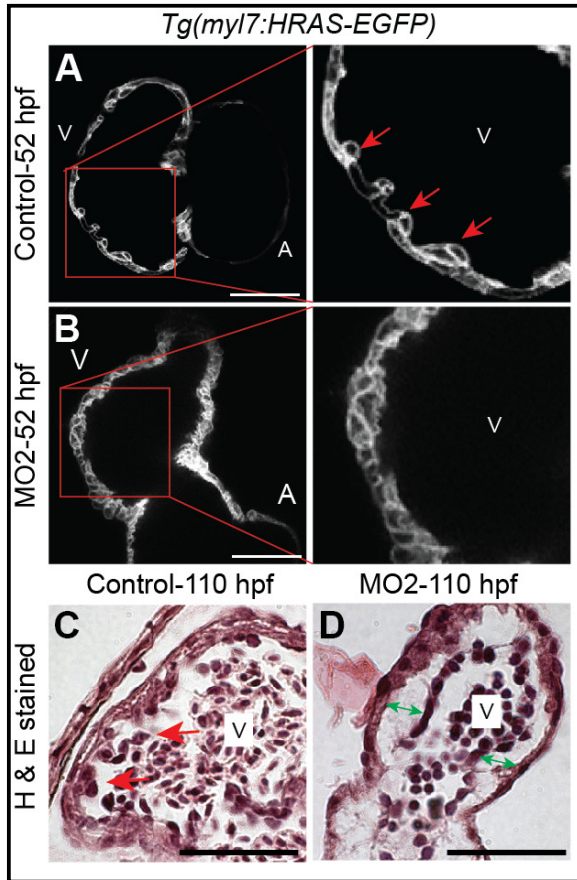


**Figure 4.13: *Npnt* depletion perturbed ventricular trabeculation.** (A,B)

Confocal images of hearts from control (A) and MO2-injected (B) embryos from transgenic zebrafish *Tg(myl7:EGFP-HsHRAS)<sup>s883</sup>* at 80 hpf suggesting initiation of trabeculation of the ventricular myocardial layer is perturbed in *Npnt* morphants. Red arrows: trabeculae. (C,D) H & E stained sagittal sections of hearts from control (C) and MO2-injected (D) embryos at 110 hpf. Control embryos develop in contrast to morphant embryos proper trabeculae on the ventricular myocardial wall (red arrows). Black arrowhead: AV boundary; green arrows: expanded cardiac jelly; A: atrium; V: ventricle. Scale bars: 50  $\mu$ m.

### 4.13 *Has2* knockdown reduces the number of AV endocardial cells

The transformation of endothelium to mesenchyme is a prerequisite for valve leaflet formation (113). Both the mechanism behind the stimulation of the myocardium to release activation signals and the acquisition of the signal by the endocardium are poorly understood (114). One important molecule to enable EMT is *Has2*. Studies using *has2<sup>-/-</sup>* embryonic heart explants have shown that cardiac endothelial cells failed to transform into mesenchyme, an essential developmental event for valvogenesis (53). To determine whether the observed expanded expression of *has2* caused the increased number of AV endocardial cells we performed *Has2* knockdown experiments (Figure 4.14).



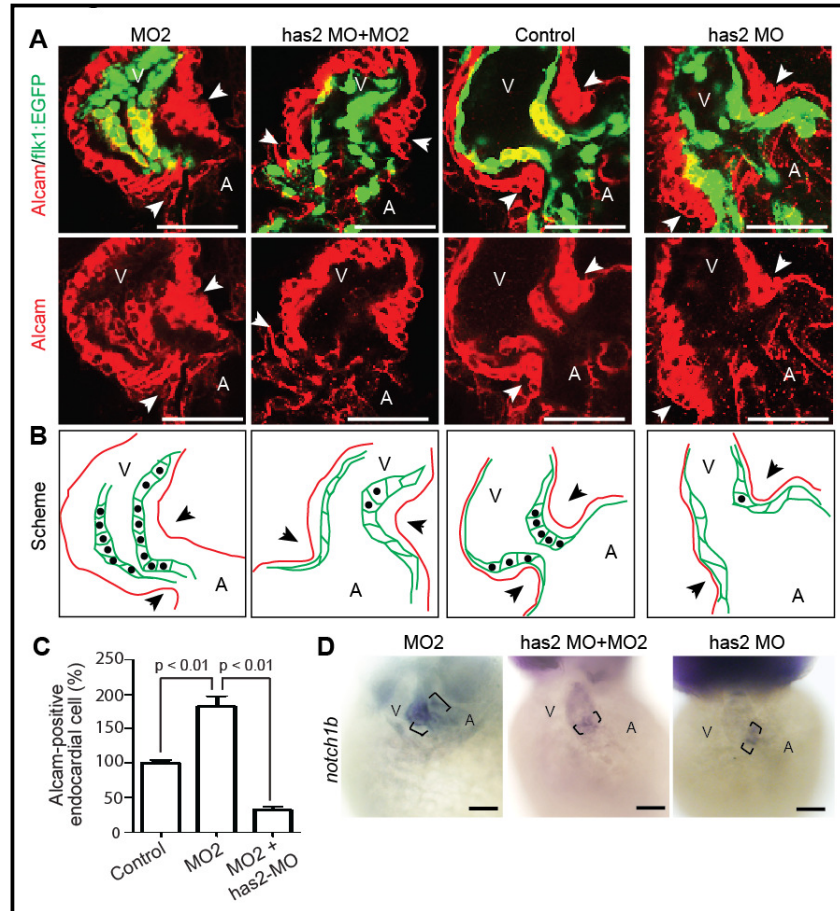


**Figure 4.14: Morpholino-mediated *has2* knockdown rescues the endocardial phenotype in *Npnt* morphants.** (A) Confocal sections of whole-mount Alcam-stained (red: myocardium and differentiated endocardial cells) MO2-, MO2/*has2* morpholino-co-, *has2*-MO- and control injected embryos from transgenic zebrafish *Tg(kdrl:EGFP)<sup>s843</sup>* at 52 hpf. (B) Schematic drawings of A (red line: myocardium; green: endocardial cells; black dots: Alcam-positive endocardial cells). Morpholino-mediated knockdown of *Npnt* caused an increase of differentiated AV endocardial cells (cuboidal-shaped, Alcam- and EGFP-positive) from  $\leq 6$  tiers of cells in the wild type to at least 8 - 12 tiers of cells at the AV boundary. Knockdown of *has2* in *Npnt* morphants reduced the number to 1 - 2 tiers of Alcam-positive endocardial cells at the AV boundary. Arrowheads indicate AV boundary. (C) Quantitative analysis. *has2* knockdown in *Npnt* morphants rescued the AV canal endocardium extension (mean  $\pm$  SEM). (D) Brightfield images of 52 hpf MO2-, MO2/*has2* morpholino-co- and *has2* morpholino-injected embryos after whole-mount *in situ* hybridization showing *notch1b* expression (brackets). Note that *has2* knockdown reduced the expanded expression of *notch1b* in *Npnt* morphants (brackets). A: atrium; V: ventricle. Scale bars: 50  $\mu$ m.

Single cell stage embryos were injected with translation blocking *has2* (gift from J. Bakkers) and/or *npnt* morpholinos and were subsequently analysed for the expression of AV endocardial specific genes like Alcam and *notch1b* at

52 hpf. *has2* knockdown reduced the increased number of Alcam-positive AV endocardial cells from  $\geq 8$  tiers of cells ( $183\% \pm 32.2\%$  compared to control) in the *Npnt* morphants to  $\leq 3$  tiers of cells ( $31\% \pm 11.9\%$  compared to control) at the AV canal region (Figures 4.14A,B,C). *has2* knockdown in control embryos resulted also in reduced numbers of Alcam-positive AV endocardial cells from  $\geq 5$  tiers of cells to  $\leq 2$  tiers of cells at the AV canal region (Figures 4.14A,B). Moreover, *has2* knockdown in *Npnt* morphant or control embryos resulted in the reduction or abolishment of *notch1b* expression (Figures 4.14C). Taken together our data suggest that the increased number of AV endocardial cells in *Npnt* morphants is at least in part due to the expanded expression of *has2*.

#### **4.14 *bmp4* and *cspg2* misexpression is not dependent on expanded *has2* misexpression**

To better understand the function of *Npnt* we were interested to elucidate how other regulators of valve development are linked to the downstream signaling cascade of *Npnt*. Whole-mount *in situ* hybridization analyses have shown that AV canal myocardium specific expression of *bmp4* and *cspg2* were expanded in *Npnt* morphant hearts at the AV boundary at 52 hpf compared to control hearts (Figures 4.15A-D). To determine whether the expanded expression of *has2* caused the myocardial phenotype or not, we determined by *in situ* hybridization analysis the expression of *cspg2* and *bmp4* after *has2* knockdown in control and *Npnt* morphant embryos and uninjected control embryos. Our data revealed that the expression of *bmp4* in *Npnt* morphant hearts remained unchanged after *has2* knockdown (Figures 4.15C,E) and *has2* morphant hearts showed similar *bmp4* expression as uninjected control embryo hearts (Figures 4.15A,G). *has2* knockdown in *Npnt* morphants could also not rescue the expanded expression of *cspg2* (Figures 4.15D,F). In addition, *has2* knockdown in control embryos resulted in expanded expression of *cspg2* in comparison to uninjected controls (Figures 4.15B,H). These data indicate that *has2* is not an upstream regulator of *cspg2* and *bmp4*.

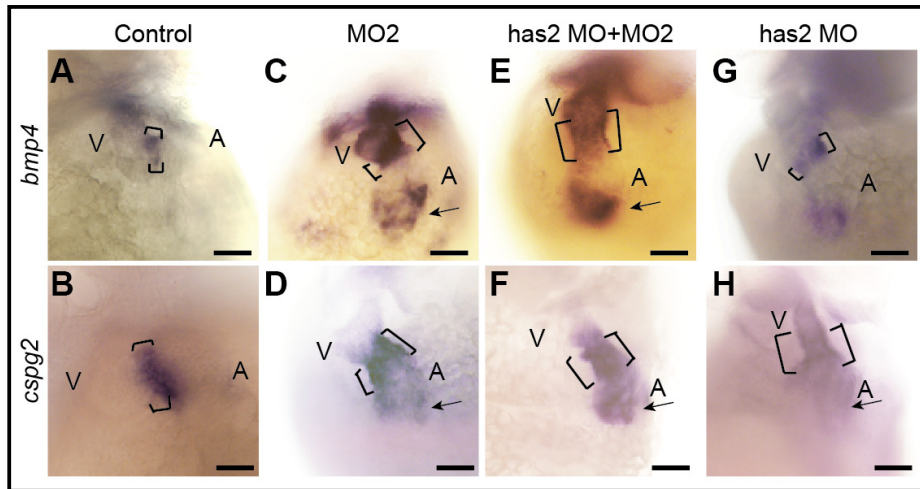
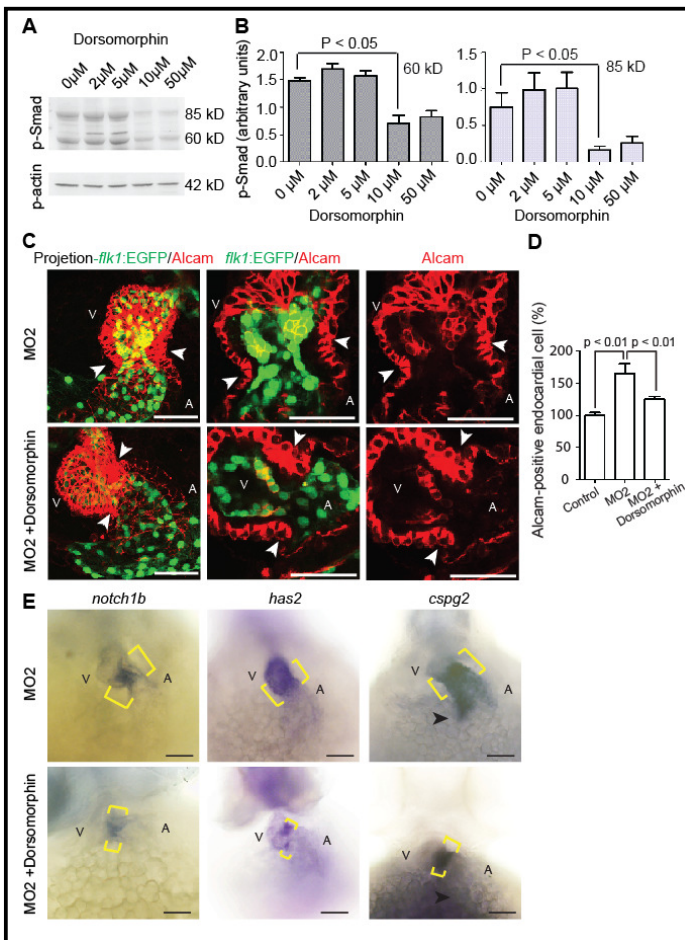


**Figure 4.15: Morpholino-mediated *has2* knockdown failed to rescue the myocardial phenotype.** (A-H) Brightfield images of 52 hpf control, MO2-injected and MO2/*has2* morpholino-co-injected and *has2* morpholino injected embryos after whole-mount *in situ* hybridization showing *bmp4* (A,C,E,G) and *cspg2* expression (brackets). Note that *has2* knockdown failed to rescue the expanded expression of *cspg2* and *bmp4* in Npnt morphants (brackets and arrows). *has2* knockdown in wild type embryos cause up-regulation of *cspg2* (B,H). A: atrium; V: ventricle. Scale bars: 50  $\mu$ m.

#### 4.15 Diminished BMP signaling reduces AV canal expansion via inhibition of ectopic expression of *has2* and *cspg2*

BMP4 is a member of the TGF $\beta$  superfamily of cytokines, which is important for numerous developmental processes (115, 116). BMP4 acts via activating heterodimeric complexes of type I and type II serine/threonine kinase receptors (116). Previous *in vitro* explant studies and *in vivo* studies suggested that BMP4 is a key regulator for the initiation of cushion formation as well as for proper AV septation (107, 117). However, there is a debate whether BMP4 is an upstream regulator of *has2* expression. Using explant cultures of late gastrula anterior lateral endoderm from chicken it has been shown that inhibition of BMP signaling does not affect *has2* expression (118). An established downstream target of BMP-Smad pathway is *tbx2* (109, 119). Interestingly, a recent study has shown that ventricular *tbx2* misexpression in a mouse model exhibited increased *has2* expression (109). To determine if BMP signaling acts downstream of Npnt we inhibited BMP-Smad signaling in Npnt morphants at 25 hpf with dorsomorphin, a pharmacological antagonist of type I BMP receptors (102, 120), and analysed the embryos at 52 hpf regarding phosphorylation of Smad. The amount of phosphorylated Smad (p-Smad) was

quantified by Western blot analysis, using protein isolated from 52 hpf control and dorsomorphin treated embryos (Figure 4.16A). Our p-Smad antibody detected two bands, one at 65 kD and another at 80 kD (Figure 4.16A). The amount of p-Smad was normalized to pan-Actin expression (Figure 4.16B). Western blot analysis revealed that dorsomorphin exhibits its maximum inhibitory effect at a concentration of 10  $\mu$ M (Figure 4.16B). Thus, we used 10  $\mu$ M dorsomorphin for all of our experiments.



treatment stained for Alcam (red: myocardium and differentiated endocardial cells). Inhibition of BMP signaling in Npnt morphants decreased the number of Alcam-positive from from  $\geq 8$  tiers of cells to  $\leq 6$  tiers of cells at AV canal region (basal level). (D) Quantitative analysis. Inhibition of BMPs signaling in the Npnt morphants rescued the AV canal endocardium extension (mean  $\pm$  SEM). (E) Brightfield images of 52 hpf untreated and dorsomorphin-treated Npnt morphants after whole-mount *in situ* hybridization showing *notch1b*, *cspg2* and *has2* expression (brackets). Data shows that *notch1b* and *has2* expression is reduced at the AV boundary after dorsomorphin treatment. Moreover, ectopic expression of *cspg2* at the inflow tract in Npnt morphants is abolished (arrowheads) and *cspg2* expression at the AV boundary is partially rescued. A: atrium; V: ventricle. Scale bar: 50  $\mu$ m.

Dorsomorphin treatment reduced the number of Alcam-positive AV endocardial cells from  $\geq 8$  tiers of cells ( $166\% \pm 32.7\%$  compared to control) in the *Npnt* morphants to  $\leq 6$  tiers of cells ( $125.3\% \pm 10.7\%$  compared to control) at the AV canal region (Figures 4.16C,D). BMP receptor I inhibition also rescued the expanded expression of *notch1b* expression (Figures 4.16E).

To assess whether ectopic expression of *has2* and *cspg2* is dependent on BMP signaling, we performed *in situ* hybridization analyses for *has2* and *cspg2* expression on 52 hpf *Npnt* morphants and dorsomorphin-treated *Npnt* morphants. Dorsomorphin partially rescued the expanded expression of these genes at the AV region in *Npnt* morphants (Figure 4.16E) and interestingly abolished ectopic expression of *cspg2* in the IFT (arrowheads). Taken together, our data suggest that knockdown of *Npnt* causes ectopic expression of *bmp4*, which is mainly responsible for the phenotype of *Npnt* morphants and suggest that BMP is an upstream regulator of *has2* and *cspg2* in zebrafish heart.

#### **4.16 Chemical inhibition of BMP signaling has no obvious effect on wild type zebrafish embryos hearts**

To assess whether under physiological conditions *has2* is a downstream target of BMP or not, we treated wild type embryos at 25 hpf with dorsomorphin and performed *in situ* hybridization analyses for *has2*, *cspg2* and *notch1b* expression at 52 hpf. In addition we performed immunostaining against Alcam to determine changes in endocardial cell differentiation at the AV canal utilizing *Tg(kdrl:EGFP)<sup>s843</sup>* transgenic embryos. In control embryos (wild type) inhibition of BMP signaling did not affect basal expression of AV canal marker genes like *notch1b*, *has2* and *cspg2* (Figure 4.17A) and had no effect on the number of Alcam-positive cells (Figures 4.17B,C). Taken together, our data identify *Npnt* as an upstream regulator of BMP signaling. Moreover, these findings suggest that ectopic BMP signaling regulates *has2* and *cspg2*.



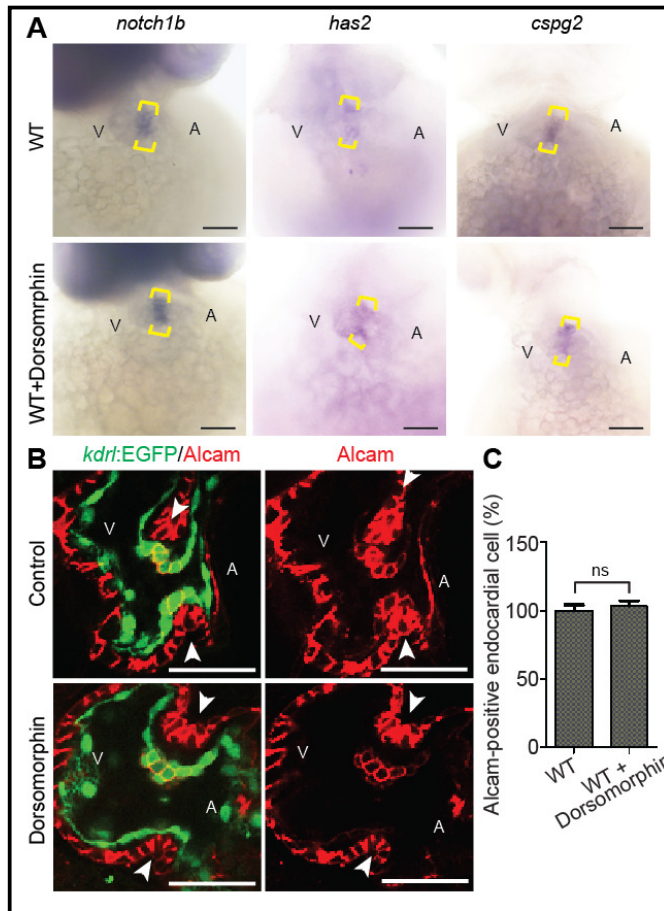


**Figure 4.17: Dorsomorphin-mediated inhibition of BMP signaling does not interfere with the basal level of AV specific gene expression at 52 hpf.** (A) Brightfield images of 52 hpf WT and 10  $\mu$ M dorsomorphin-treated embryos after whole-mount *in situ* hybridization with probes against *notch1b*, *has2* and *cspg2*. Expression of these genes at the AV canal region remained unaffected in dorsomorphin-treated embryos (brackets). (B) Confocal sections of whole-mount Alcam-stained (red) WT and 10  $\mu$ M dorsomorphin-treated embryos from transgenic zebrafish *Tg(kdrl:EGFP)<sup>S843</sup>* at 52 hpf. The number of differentiated endocardial cells (cuboidal-

shaped, Alcam- and EGFP-positive) remained unchanged (5 - 6 tiers of cells at the AV canal region) in dorsomorphin-treated animals. Arrowheads indicate AV boundary. (C) Quantitative analysis. Inhibition of BMPs signaling in the WT embryos does not affect the basal no of Alcam-positive cells at the AV canal region (mean  $\pm$  SEM). A: atrium; V: ventricle. Scale bar: 50 $\mu$ m.

#### 4.17 Wnt/ $\beta$ -catenin signaling is not the downstream target of Npnt

Several *in vitro* studies have shown that in colorectal cancer cells and embryonic stem-cells the genes *bmp4*, *cspg2* and *has2* are transcriptional targets of the Wnt/ $\beta$ -catenin pathway (121, 122). It has also been suggested that AV endocardial differentiation is mediated through Wnt/ $\beta$ -catenin signaling (49). To determine whether Wnt signaling is affected in Npnt morphants, MO2 was injected into embryos transgenic for *Tg(TOP:GFP)<sup>w25</sup>*, a reporter for Wnt/ $\beta$ -catenin signaling. Activation of GFP expression was determined by *in situ* hybridization on 52 hpf old embryos. However, GFP signal was neither detected in the heart of Npnt morphants nor in control embryos at 52 hpf.

However, we could detect a signal in the head, eyes, jaw and trunk (Figure 4.18). These data suggested that Npnt does not signal through Wnt signaling pathway around 52 hpf in the zebrafish heart.

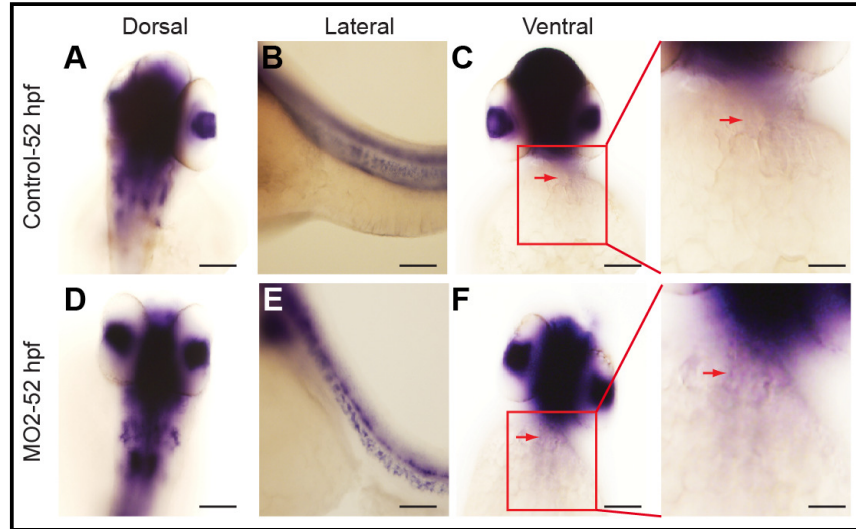


**Figure 4.18: Npnt knockdown does not result in ectopic activation of Wnt/ $\beta$ -catenin signaling at 52 hpf in the heart.** (A-F) Activation of Wnt/ $\beta$ -catenin signaling was determined by whole-mount *in situ* hybridization against GFP on control and MO2-injected embryos from the reporter line *Tg(TOP:GFP)<sup>w25</sup>*, where activation of Wnt/ $\beta$ -catenin signaling results in GFP expression. Dorsal, lateral and ventral views are showing activation of Wnt/ $\beta$ -catenin signaling in the head, trunk, eye lens and jaw for both the control as well as MO2-injected embryos. Note that expression of *GFP* could not be detected in the heart (arrows). Scale bars: 50  $\mu$ m.

#### 4.18 Npnt does not signal through integrin $\alpha$ 8

Recently it has been shown that Npnt acts during kidney development as a ligand of integrin  $\alpha$ 8 $\beta$ 1 regulating cell migration (85, 87). To determine whether integrin  $\alpha$ 8 $\beta$ 1 might act also during heart development as a receptor for Npnt, we determined *integrin  $\alpha$ 8* expression by *in situ* hybridization in the zebrafish heart. *integrin  $\alpha$ 8* was strongly expressed in jaw, pectoral fin, eye lens and other tissues but not detectable in the heart (Figure 4.19). These data indicate that Npnt does not signal through integrin  $\alpha$ 8 during zebrafish heart development.

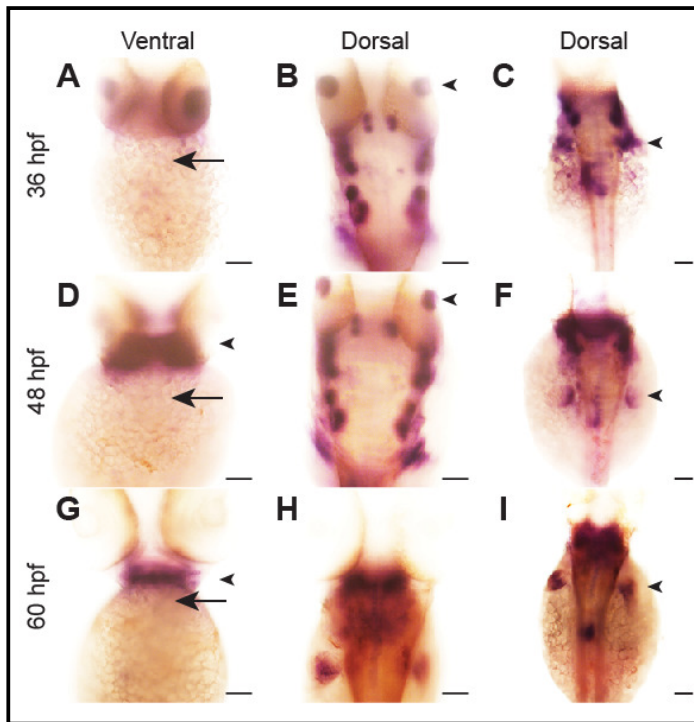


**Figure 4.19: *itga8* is not expressed during early heart development.** (A-I) Brightfield images of 52 hpf WT embryos after whole-mount *in situ* hybridization with probes against *itga8*. Ventral and dorsal views of 36 hpf, 48 hpf and 60 hpf embryos are showing expression of *itga8* in several tissues like jaw, pectoral fin and eye lens (arrowheads). Expression of *itga8* could not be detected in the heart (arrows). Scale bars: 50  $\mu$ m.



## 5. Discussion and outlook

Our data identify Npnt as a novel regulator of early heart development. Several lines of evidence support this conclusion. First, Npnt knockdown in zebrafish causes  $\approx 90\%$  lethality at 7 dpf. Second, Npnt morphant hearts were characterized by an expanded AV canal, increased cardiac jelly, impaired trabeculation and failure of proper valve leaflet formation at the AV boundary. Third, Has2 knockdown rescued the endocardial phenotype in Npnt morphants. Fourth, chemical inhibition of BMP signaling rescued AV canal extension in Npnt morphants in respect to myocardium as well as endocardium. In summary, our data indicate that Npnt regulates the differentiation of the AV segment via the BMP4-Has2 signaling cascade.

### 5.1 The ECM is critical for valve development

Previously, it has been shown that regionally specific interactions of the myocardium and endocardium are required to initiate the formation of prevalvular cell differentiation (23, 123, 124). Changes in the composition or amount of the ECM can interfere with valve formation. *cspg2* and *has2* knockout mice exhibit reduced amount of cardiac jelly and fail to form endocardial cushions (53, 60). However, AV cushion development appeared normal in *fibulin1* knockout mice (125). Here, we discovered Npnt as a novel component of the cardiac ECM during early development. Surprisingly, the knockdown of Npnt caused in contrast to the above-mentioned studies an increase in cardiac jelly throughout the anteroposterior extent of the heart.

The increase in cardiac jelly and possibly the change in the composition of the cardiac jelly might be responsible for the failure of Npnt morphants to form proper valves. The expanded cardiac jelly in Npnt morphant hearts might act as an inhibitor of signaling as the ECM modulates the activity, bioavailability, or presentation of growth factors to cell surface receptors (114). It has for example been shown that increased expression of versican and associated proteins results in an increase in the pericellular matrix of cells, an expansion of the ECM and a change of the viscoelastic nature of the ECM. Such mechanical changes are known to have dramatic effects on the tension exerted on cells and the traction forces generated by the cell. These forces are known to impact signaling influencing for example migration (114-116). Thus,

Npnt knockdown might cause a change of the viscoelastic nature of the ECM that hinders AV endocardial cells to migrate into the ECM at the AV boundary preventing proper valve leaflet formation. In the future it will be important to analyze the composition of the cardiac jelly in Npnt morphants.

## 5.2 Npnt does not regulate Wnt signaling

Npnt appears in general to act both as a structural protein as well as a ligand that induces signaling. First, it is known that Npnt acts as a ligand for integrin  $\alpha 8 \beta 1$  regulating migration during kidney development (87). Second, Npnt contains EGF domains that have been shown to be required for Npnt-induced osteoblast differentiation (126). Similarly, it has been suggested that the EGF domains of Versican can bind and activate growth factor receptors (127, 128). The concept that Npnt acts as a ligand during heart development could also explain why Npnt knockdown affects only the AV boundary although it is expressed throughout the myocardium.

One way to gain insight into how Npnt regulates valve development is to compare the phenotype of Npnt morphants with existing phenotypes of other morphants or mutants. Interestingly, the Npnt morphant phenotype shares some characteristics with the zebrafish *apc* mutant in which the Wnt signaling pathway is constitutively activated. *apc* mutant and Npnt morphant hearts appear normal at 36 hpf. Between 37 and 45 hpf several genes including *bmp4*, *has2*, *cspg2* and *notch1b* become restricted to the AV canal. This restriction is in both morphants impaired. Moreover, compared to wild type embryos *apc* mutant and Npnt morphant embryos form excessive cardiac jelly and fail to loop. As *bmp4*, *versican* and *has2* are purportedly transcriptional targets of the Wnt/ $\beta$ -catenin signaling pathway (121, 122), Npnt could be a target of this cascade or may signal through the Wnt signaling cascade. Thus, it is important to determine the activity of the Wnt signaling pathway at 2 dpf when Npnt exhibits its function. Hurlstone *et al.* have shown that in wild type embryos Wnt/ $\beta$ -catenin signaling is restricted at the AV boundary at 72 hpf. In contrast, in *apc* mutant this signaling becomes activated throughout the anteroposterior extent of the heart (49). Unfortunately, they do not report data regarding Wnt/ $\beta$ -catenin signaling at 2 dpf. Our analysis revealed that there is no activation of Wnt expression in the heart of *Tg(TOP:GFP)<sup>w25</sup>* embryos at 2

dpf. In addition, *Npnt* knockdown did not induce ectopic activation of Wnt in *Tg(TOP:GFP)<sup>w25</sup>* embryos in the heart at 2 dpf. These findings indicate that the observed earliest cardiac phenotype of *Npnt* morphants at 52 hpf is not due to the ectopic activation of Wnt/ $\beta$ -catenin signaling.

### 5.3 *Npnt* signals through the BMP4-Has2 axis

Our experimental outcomes suggest that *Npnt* is required to restrict the expression of *cspg2* and *has2*. Previously, it has been shown that *has2* plays an essential role in the formation of cardiac jelly and initiation of cardiac valve development via hyaluronan synthesis (53). Our *has2* knockdown experiments in wild type embryos confirmed the role of *has2* in the formation of cardiac jelly and prevalvular AV endocardial cell differentiation in zebrafish. Importantly, *has2* knockdown in *Npnt* morphants rescued the observed endocardial phenotype and demonstrates that *Npnt* controls AV endocardial cell differentiation by regulating *has2* expression.

*has2* knockdown in *Npnt* morphants neither rescued ectopic expression of *bmp4* nor *cspg2*. Thus, there appears to be no cross talk between BMP4 and Has2 or BMP4 is an upstream regulator of *has2* expression and the endocardial phenotype is a consequence of the ectopic myocardial expression of *bmp4*. Previously, BMP signaling has been shown to regulate *has2* expression (109) but the data are controversial (118). Inhibition of BMP signaling in *Npnt* morphants reverted the endocardial phenotype to normal, partially rescued the AV canal extension defect and reduced *has2* and *cspg2* gene expression. Our data indicate that *Npnt* is required to restrict the expression of BMP4 and that expanded *bmp4* expression in *Npnt* morphants causes increased expression of *cspg2* and *has2* which explains the expansion of the AV canal as well as the increase in cardiac jelly. Thus, it appears likely that BMP4 is an upstream regulator of *has2* expression and that the endocardial phenotype is a consequence of the ectopic myocardial expression of *bmp4*.

In wild type embryos dorsomorphin did not affect basal expression of the genes important for AV canal differentiation. This might be due to the fact that dorsomorphin treatment resulted only in partial inhibition of BMP-Smad signaling and that complete inhibition could not be achieved even at higher

dorsomorphin concentrations (Figure 4.16). Another possible explanation is that endogenous BMP signaling is redundant at the AV canal. To further substantiate the importance of BMP4 one could utilize the transgenic zebrafish line *tg(hsp70:noggin3)* that expresses the specific BMP inhibitor *noggin3* under the control of *hsp70* promoter and allows efficient inhibition at distinct time points (129). This transgenic line could also be used to rescue the cardiac phenotype of the *Npnt* morphant. Taken together, our data demonstrate that *Npnt* is an upstream regulator of BMP signaling. Moreover, these findings suggest that ectopic BMP signaling regulates *has2* and *cspg2* expression.

Our data have identified Nephronectin as an upstream regulator of BMP4 signaling, however, the underlying mechanism remains unclear. For example, one would assume for an inhibitor of BMP4 expression or signaling to be expressed only in the chambers but not in the AV canal itself. Based on our experimental outcomes and others published reports we hypothesize two regulatory mechanisms for how *Npnt* regulates BMP4 signaling: 1) *Npnt* binds to a chamber-specific receptor inhibiting *bmp4* expression. 2) *Npnt* prevents the diffusion and thus the bioavailability to BMP4.

### 5.3.1 Receptor-mediated inhibition of *bmp4* expression

One possible regulation of BMP signaling in the chambers is a receptor-mediated inhibition by *Npnt* (Figure 5.1).

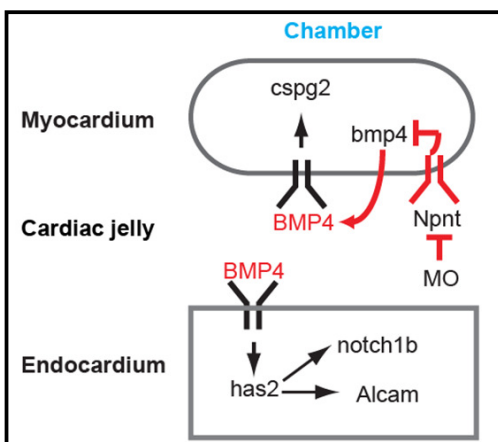


**Figure 5.1: Proposed model of the regulatory role of *Npnt* via its potential receptor.** *Npnt* activates a receptor expressed only in the chamber myocardium repressing BMP4 signaling.

Recently it has been shown that *Npnt* acts during kidney development as a ligand of integrin  $\alpha 8\beta 1$  regulating cell migration (85, 87). However, during the time of *npnt* expression in the zebrafish heart we did not detect integrin  $\alpha 8$

expression by *in situ* hybridization in the zebrafish heart whereas strong expression was detected in jaw, pectoral fin, eye lens and other tissues. These data indicate that Npnt does not signal through integrin  $\alpha 8$  during zebrafish heart development. However, Nephronectin can bind also other integrins like integrin  $\alpha V$  (vitronectin receptor) (85). Interestingly, integrin  $\alpha V$  is expressed in the heart during early zebrafish development (130). Thus integrin  $\alpha V$  could be a potential receptor for Npnt signaling. To validate this hypothesis it will be important to determine the spatiotemporal expression pattern of integrin  $\alpha V$  around the time of *npnt* expression as well as to investigate the consequences of integrin  $\alpha V$  knockdown for zebrafish heart development. If Npnt indeed signals through integrin  $\alpha V$  to inhibit BMP signaling it will be important to identify which subtype of  $\beta$  integrins is utilized, to elucidate the downstream signaling and whether this mechanism plays a role in other developing organs.

### 5.3.2 Npnt controls BMP4 bioavailability by limiting its diffusion

Npnt might exert its functions via modulating the bioavailability of BMP4. We hypothesize that Npnt is required for the establishment of an ECM that limits the diffusion rate of BMP4 (Figure 5.3).

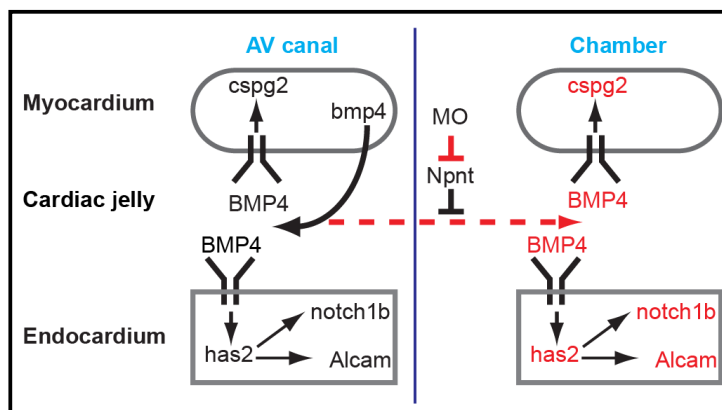


**Figure 5.3: Proposed model of the regulatory role of Nephronectin by inhibiting its diffusion.** BMP4 can bind with the glycosylated anionic domain of Npnt and thus might prevent its diffusion towards the chambers.

A limited diffusion rate would cause an increased concentration of BMP4 at the proximity of the expressing cell limiting BMP4 to signal in an autocrine fashion. Depletion of Npnt would prevent BMP4 retention resulting in the diffusion of BMP4 towards the chambers switching from autocrine to paracrine signaling. As the chambers also express BMP receptors (131) BMP4 might

reprogram chamber cells into AV canal cells. Ectopic expression of BMP4 might be due to an autoregulation of BMP4 gene transcription (132).

Osteoblast differentiation and valve formation share some regulatory mechanisms (133). Thus, the osteoblast differentiation system might provide arguments to support our hypothesis of BMP4 diffusion control. Importantly, it has been shown that *Npnt* is highly expressed during early osteoblast differentiation and *Npnt* overexpression promotes osteoblast differentiation (94). In addition, BMPs signaling plays an important role in early osteoblast differentiation (40). Interestingly, osteoblast differentiation is dependent on ECM deposition, which sequesters BMPs to facilitate BMP receptor activation to induce differentiation (134).

So far it has only been shown that *Npnt* expression correlates with BMP4 signaling. However, the fact that *Npnt* contains a mucin-like repeat domain indicating glycosylation (87) suggests that *Npnt* can bind and sequester cytokines, growth factors and morphogens regulating their bioavailability to their cell surface receptors as shown previously for several other proteoglycans (135). The data by Sato *et al.* further substantiate that *Npnt* is glycosylated as they have shown that the size of the secreted *Npnt* on a reducing polyacrylamide gel is around 120 kDa instead of the predicted size of 61 kDa (85).

Osteoblast differentiation can be studied *in vitro* utilizing the M3TC3 cell line. In future experiments it will be important to confirm the accumulation of BMP4 on the cell surface and to manipulate the expression of *Npnt*. Knockdown experiments should reveal whether BMP4 accumulation and signaling depends on *Npnt*. Overexpression experiment will show whether *Npnt* is sufficient to retain BMP4 on the cell surface. In addition, it is possible to determine the role of *Npnt* regarding BMP signaling in the heart also by utilizing the well-established mouse AV canal explant culture system (48).

#### **5.4 *Npnt* signals through growth factor receptors**

*Npnt* has several  $\text{Ca}^{2+}$  dependent EGF-like repeat domains and it has been suggested that *Npnt* can induce signaling through its EGF-like repeats that are required for *Npnt*-induced osteoblast differentiation (94). Thus, *Npnt* might activate or modulate growth factor receptor signaling during heart development.

We hypothesize that *Npnt* affects ErbB receptor signaling. Several lines of evidence support this hypothesis: First, signaling via ErbB receptors is important for cardiac valve development and ventricular trabeculation (28, 136, 137). Second, Ca<sup>2+</sup> dependent EGF-like repeats of several proteins like EGF, TGF- $\alpha$ , heparin binding EGF, amphiregulin, epiregulin, and neuregulin (heregulin-1) bind to the extracellular domain of ErbB receptors and activate its downstream signaling (138). Similarly, the EGF-like repeats of Versican can bind and activate ErbB receptors (127, 128).

The ErbB receptor family consists of four different type-I tyrosine kinase receptors (ErbB1 to ErbB4 also known as HER1 to HER4). For activation of downstream signaling ErbB receptor homodimerise or heterodimerise with other ErbB family members in the presence of a ligand (138). In mice myocardial, endocardial as well as invading mesenchymal cells express ErbB2 during cardiac development. Invading mesenchymal cells and a subpopulation of endocardial cells are predominantly ErbB3-positive but ErbB4-negative (28, 137). In contrast, the myocardium is ErbB4-positive (around E9.5-E11) (28, 136). Using AV canal explant cultures it has been demonstrated that cushion mesenchyme transformation in the AV canal of ErbB2<sup>-/-</sup> and ErbB3<sup>-/-</sup> mice embryos is significantly reduced. In contrast, EMT was not affected in ErbB4<sup>-/-</sup> mice. However these mice exhibit myocardial differentiation and trabeculation problems (28, 136). These data suggest that signaling via ErbB2/ErbB3 heterodimers is important for cardiac valve development and via ErbB2/ErbB4s for ventricular trabeculation.

The phenotype of *Npnt* morphants is very similar to the phenotypes of ErbB2<sup>-/-</sup> and ErbB3<sup>-/-</sup> mice. Thus, it will be important to determine in the future the spatiotemporal expression pattern of ErbB2-4 during early heart development in wild type and *Npnt* morphant zebrafish (30 to 80 hpf). In addition, it will be interesting to perform overexpression experiments *in vitro* and *in vivo* to determine the affect of *Npnt* on downstream signaling of ErbBs (activation of ERK1/2 and PI3 kinase cascade).

## 5.5 *Npnt* depletion does not affect cardiomyocyte number

Our data demonstrate on a molecular and cellular level that the AV canal in *Npnt* morphants contains around double as many cells as the AV canal in wild

type embryos. Where do these cells come from? There are two possible explanations. One is that *Npnt* depletion triggers increased proliferation of AV canal cells or that *Npnt* depletion results in more cells differentiating into AV canal cells. In case that *Npnt* regulates AV canal cell proliferation the total number of cardiomyocytes should increase. However, our data suggest that the total number of cardiomyocytes as well as the number of atrial cardiomyocytes is unaffected. Based on these data, one may conclude that *Npnt* depletion results in an increased number of cells differentiating into AV canal cells on the expense of chamber cells. This suggests that *Npnt* morphants exhibit a patterning phenotype. However, it will be important in future experiments to further substantiate this conclusion as the applied technique to determine cell numbers has limitations. First, the addition of cell numbers is relatively small to the total number of cardiomyocytes in the heart. Second, the variation in the cardiomyocyte number of individual hearts is relatively high compared to the increase in AV canal cells in *Npnt* morphants. Third, AV canal cells in wild type embryos are difficult to count, as their cell density is very high. In contrast, the cell density of AV canal cells in the elongated and less looped *Npnt* morphant hearts is lower. This difference might result in a miscalculation of the cell numbers. Therefore, a detailed cell cycle analysis should be performed in the future.

## 5.6 Conclusion

Our data establish Nephronectin as a novel regulator of heart development. Our data suggest that *Npnt* is required as a regulator of BMP4-Has2 signaling to restrict AV canal differentiation and cardiac jelly swelling at the preavalvular stage. Furthermore, our data indicate that *Npnt* is also involved in trabeculation.

In the future it will be important to determine how *Npnt* regulates BMP4 signaling and whether it affects additional signaling pathways. We hypothesize that *Npnt* regulates heart development on several levels by modulating the bioavailability of growth factors and by acting as a ligand for integrin receptors as well as for growth factor receptors. It might also be possible that *Npnt* modulates receptor signaling by bringing via EGF-like repeats and RGD domain ErbB receptors and integrins in close proximity.

The finding that nephronectin is required for proper heart development is



---

important for several reasons. To our knowledge, this is the first evidence that Nephronectin is transiently expressed in the heart. Second, this is the first evidence that Nephronectin regulates valve formation and trabeculation. Third, our data establish Nephronectin as a novel regulator of BMP4 and adds novel data on the dispute whether BMP4 is an upstream regulator of Has2. Fourth, we demonstrate that Has2 plays a major role in the differentiation of endocardial cells in the AV canal. Finally, the information provided by this study may be of medical relevance. Defects in cardiac valves and associated structures account for 25% to 30% of all cardiovascular anomalies and their underlying cause is often unknown.

## 6. Summary

It has been estimated that about 1% of live births carry severe congenital heart defects and 20-30% among them have valve malformations (3). Despite its medical importance the underlying cause of many valvular diseases remains undiscovered. Thus, it is important to identify genes that play a crucial role in cardiac valve formation and maturation.

A temporal RNA expression analysis of heart development suggested that the extracellular matrix protein Nephronectin might be a novel regulator of valve development and/or trabeculation. Nephronectin is transiently expressed during rat heart development at the time of heart valve morphogenesis and trabeculation. Moreover, the extracellular matrix is known to be crucial for organogenesis. It is a complex, dynamic and critical component that regulates cell behavior by modulating the activity, bioavailability, or presentation of growth factors to cell surface receptors.

In order to verify the hypothesis that Nephronectin is a novel regulator of valve formation and/or trabeculation the zebrafish was chosen as model system. Females are able to spawn at intervals of 5 days laying hundreds of eggs in each clutch. Development progresses rapidly with precursors to all major organs appearing within 36 hours post fertilization. Zebrafish embryos develop externally, are translucent and continue to grow for several days despite developing severely malformed, non functional hearts. In addition, gene expression can be easily modulated.

During the present study it has been shown that Nephronectin expression is correlated to valve development and trabeculation. Morpholino-mediated knockdown of Nephronectin in zebrafish caused failure of valve formation and trabeculation resulting in > 85% lethality at 7 days post fertilization.

Cardiac valve formation is initiated at the junction of atrium and ventricle and is characterized by extracellular matrix deposition and endocardial cell differentiation. In accordance with the above-described phenotype the earliest observed abnormality in Nephronectin morphants was an extended tube like structure at the atrio-ventricular boundary. In addition, the expression of myocardial genes involved in cardiac valve formation (*cspg2*, *fibulin1*, *tbx2b*, *bmp4*) was expanded and endocardial cells along the extended tube like

structure exhibited characteristics of atrio-ventricular cells (*has2*, *notch1b* and Alcam expression, cuboidal cell shape). Inhibition of *has2* in Nephronectin morphants rescued the endocardial but not the myocardial expansion. In contrast, diminishment of BMP signaling in *npnt* morphants resulted in reduced ectopic expression of myocardial and endocardial atrio-ventricular markers. Taken together, these results identify Nephronectin as a novel upstream regulator of BMP4-HAS2 signaling playing a crucial role in atrio-ventricular canal differentiation.

## 7. References

1. Hoffman JI & Kaplan S (2002) The incidence of congenital heart disease. *J Am Coll Cardiol* 39(12):1890-1900.
2. Bruneau BG (2008) The developmental genetics of congenital heart disease. *Nature* 451(7181):943-948.
3. Hoffman JI (1995) Incidence of congenital heart disease: II. Prenatal incidence. *Pediatr Cardiol* 16(4):155-165.
4. Pierpont ME, *et al.* (2007) Genetic basis for congenital heart defects: current knowledge: a scientific statement from the American Heart Association Congenital Cardiac Defects Committee, Council on Cardiovascular Disease in the Young: endorsed by the American Academy of Pediatrics. *Circulation* 115(23):3015-3038.
5. Weismann CG & Gelb BD (2007) The genetics of congenital heart disease: a review of recent developments. *Curr Opin Cardiol* 22(3):200-206.
6. Basson CT, *et al.* (1997) Mutations in human TBX5 [corrected] cause limb and cardiac malformation in Holt-Oram syndrome. *Nat Genet* 15(1):30-35.
7. Robinson PN, *et al.* (2002) Mutations of FBN1 and genotype-phenotype correlations in Marfan syndrome and related fibrillinopathies. *Hum Mutat* 20(3):153-161.
8. Tartaglia M, *et al.* (2001) Mutations in PTPN11, encoding the protein tyrosine phosphatase SHP-2, cause Noonan syndrome. *Nat Genet* 29(4):465-468.
9. Martens MA, Wilson SJ, & Reutens DC (2008) Research Review: Williams syndrome: a critical review of the cognitive, behavioral, and neuroanatomical phenotype. *J Child Psychol Psychiatry* 49(6):576-608.
10. Garg V, *et al.* (2005) Mutations in NOTCH1 cause aortic valve disease. *Nature* 437(7056):270-274.
11. Kirk EP, *et al.* (2007) Mutations in cardiac T-box factor gene TBX20 are associated with diverse cardiac pathologies, including defects of septation and valvulogenesis and cardiomyopathy. *Am J Hum Genet* 81(2):280-291.
12. de Lange FJ, *et al.* (2004) Lineage and morphogenetic analysis of the cardiac valves. *Circ Res* 95(6):645-654.
13. Lincoln J, Alfieri CM, & Yutzey KE (2004) Development of heart valve leaflets and supporting apparatus in chicken and mouse embryos. *Dev Dyn* 230(2):239-250.
14. Pennisi DJ & Mikawa T (2009) FGFR-1 is required by epicardium-derived cells for myocardial invasion and correct coronary vascular lineage differentiation. *Dev Biol* 328(1):148-159.
15. Brand T (2003) Heart development: molecular insights into cardiac specification and early morphogenesis. *Dev Biol* 258(1):1-19.
16. Armstrong EJ & Bischoff J (2004) Heart valve development: endothelial cell signaling and differentiation. *Circ Res* 95(5):459-470.
17. Person AD, Klewer SE, & Runyan RB (2005) Cell biology of cardiac cushion development. *Int Rev Cytol* 243:287-335.
18. DeRuiter MC, Poelmann RE, VanderPlas-de Vries I, Mentink MM, & Gittenberger-de Groot AC (1992) The development of the myocardium and endocardium in mouse embryos. Fusion of two heart tubes? *Anat Embryol (Berl)* 185(5):461-473.
19. Martinsen BJ (2005) Reference guide to the stages of chick heart embryology. *Dev Dyn* 233(4):1217-1237.

20. Fishman MC & Chien KR (1997) Fashioning the vertebrate heart: earliest embryonic decisions. *Development* 124(11):2099-2117.
21. Moorman A, Webb S, Brown NA, Lamers W, & Anderson RH (2003) Development of the heart: (1) formation of the cardiac chambers and arterial trunks. *Heart* 89(7):806-814.
22. Camenisch TD, *et al.* (2002) Temporal and distinct TGFbeta ligand requirements during mouse and avian endocardial cushion morphogenesis. *Dev Biol* 248(1):170-181.
23. Krug EL, Runyan RB, & Markwald RR (1985) Protein extracts from early embryonic hearts initiate cardiac endothelial cytodifferentiation. *Dev Biol* 112(2):414-426.
24. Markwald RR, Fitzharris TP, & Manasek FJ (1977) Structural development of endocardial cushions. *Am J Anat* 148(1):85-119.
25. Henderson DJ & Copp AJ (1998) Versican expression is associated with chamber specification, septation, and valvulogenesis in the developing mouse heart. (Translated from English) *Circulation Research* 83(5):523-532 (in English).
26. Combs MD & Yutzey KE (2009) Heart valve development: regulatory networks in development and disease. *Circ Res* 105(5):408-421.
27. Delot EC (2003) Control of endocardial cushion and cardiac valve maturation by BMP signaling pathways. *Mol Genet Metab* 80(1-2):27-35.
28. Camenisch TD, Schroeder JA, Bradley J, Klewer SE, & McDonald JA (2002) Heart-valve mesenchyme formation is dependent on hyaluronan-augmented activation of ErbB2-ErbB3 receptors. *Nat Med* 8(8):850-855.
29. Keyes WM, Logan C, Parker E, & Sanders EJ (2003) Expression and function of bone morphogenetic proteins in the development of the embryonic endocardial cushions. *Anat Embryol (Berl)* 207(2):135-147.
30. Lyons KM, Pelton RW, & Hogan BL (1989) Patterns of expression of murine Vgr-1 and BMP-2a RNA suggest that transforming growth factor-beta-like genes coordinately regulate aspects of embryonic development. *Genes Dev* 3(11):1657-1668.
31. Somi S, Buffing AA, Moorman AF, & Van Den Hoff MJ (2004) Dynamic patterns of expression of BMP isoforms 2, 4, 5, 6, and 7 during chicken heart development. *Anat Rec A Discov Mol Cell Evol Biol* 279(1):636-651.
32. Bernanke DH & Markwald RR (1982) Migratory behavior of cardiac cushion tissue cells in a collagen-lattice culture system. *Dev Biol* 91(2):235-245.
33. Shepherd TG, Mujoomdar ML, & Nachtigal MW (2010) Constitutive activation of BMP signalling abrogates experimental metastasis of OVCA429 cells via reduced cell adhesion. *J Ovarian Res* 3:5.
34. Abdelwahid E, Rice D, Pelliniemi LJ, & Jokinen E (2001) Overlapping and differential localization of Bmp-2, Bmp-4, Msx-2 and apoptosis in the endocardial cushion and adjacent tissues of the developing mouse heart. *Cell Tissue Res* 305(1):67-78.
35. Jones CM, Lyons KM, & Hogan BL (1991) Involvement of Bone Morphogenetic Protein-4 (BMP-4) and Vgr-1 in morphogenesis and neurogenesis in the mouse. *Development* 111(2):531-542.
36. Yamagishi T, Nakajima Y, Miyazono K, & Nakamura H (1999) Bone morphogenetic protein-2 acts synergistically with transforming growth factor-beta3 during endothelial-mesenchymal transformation in the developing chick heart. *J Cell Physiol* 180(1):35-45.

37. Walsh EC & Stainier DY (2001) UDP-glucose dehydrogenase required for cardiac valve formation in zebrafish. *Science* 293(5535):1670-1673.
38. Koenig BB, *et al.* (1994) Characterization and cloning of a receptor for BMP-2 and BMP-4 from NIH 3T3 cells. *Mol Cell Biol* 14(9):5961-5974.
39. Yamashita H, *et al.* (1995) Osteogenic protein-1 binds to activin type II receptors and induces certain activin-like effects. *J Cell Biol* 130(1):217-226.
40. Chen D, Zhao M, & Mundy GR (2004) Bone morphogenetic proteins. *Growth Factors* 22(4):233-241.
41. ten Dijke P & Arthur HM (2007) Extracellular control of TGFbeta signalling in vascular development and disease. *Nat Rev Mol Cell Biol* 8(11):857-869.
42. Takase M, *et al.* (1998) Induction of Smad6 mRNA by bone morphogenetic proteins. *Biochem Biophys Res Commun* 244(1):26-29.
43. Imamura T, *et al.* (1997) Smad6 inhibits signalling by the TGF-beta superfamily. *Nature* 389(6651):622-626.
44. Galvin KM, *et al.* (2000) A role for smad6 in development and homeostasis of the cardiovascular system. *Nat Genet* 24(2):171-174.
45. Furthauer M, Thisse B, & Thisse C (1999) Three different noggin genes antagonize the activity of bone morphogenetic proteins in the zebrafish embryo. *Dev Biol* 214(1):181-196.
46. Lowery JW & de Caestecker MP (2010) BMP signaling in vascular development and disease. *Cytokine Growth Factor Rev* 21(4):287-298.
47. Ma LJ, Lu MF, Schwartz RJ, & Martin JF (2005) Bmp2 is essential for cardiac cushion epithelial-mesenchymal transition and myocardial patterning. (Translated from English) *Development* 132(24):5601-5611 (in English).
48. Liebner S, *et al.* (2004) Beta-catenin is required for endothelial-mesenchymal transformation during heart cushion development in the mouse. *J Cell Biol* 166(3):359-367.
49. Hurlstone AF, *et al.* (2003) The Wnt/beta-catenin pathway regulates cardiac valve formation. *Nature* 425(6958):633-637.
50. Schroeder JA, Jackson LF, Lee DC, & Camenisch TD (2003) Form and function of developing heart valves: coordination by extracellular matrix and growth factor signaling. *J Mol Med* 81(7):392-403.
51. Krug EL, *et al.* (1995) Transformation of cardiac endothelium into cushion mesenchyme is dependent on ES/130: temporal, spatial, and functional studies in the early chick embryo. *Cell Mol Biol Res* 41(4):263-277.
52. Sinning AR & McKay KJ (2004) Identification of cDNA clones that encode hLAMP-1, a component of the particulate matrix associated with cardiac mesenchyme formation. *Anat Rec A Discov Mol Cell Evol Biol* 277(2):307-311.
53. Camenisch TD, *et al.* (2000) Disruption of hyaluronan synthase-2 abrogates normal cardiac morphogenesis and hyaluronan-mediated transformation of epithelium to mesenchyme. *J Clin Invest* 106(3):349-360.
54. Toole BP (1997) Hyaluronan in morphogenesis. *J Intern Med* 242(1):35-40.
55. Bakkens J, *et al.* (2004) Has2 is required upstream of Rac1 to govern dorsal migration of lateral cells during zebrafish gastrulation. *Development* 131(3):525-537.
56. Henderson DJ & Copp AJ (1998) Versican expression is associated with chamber specification, septation, and valvulogenesis in the developing mouse heart. *Circ Res* 83(5):523-532.
57. Wu Y, Chen L, Zheng PS, & Yang BB (2002) beta 1-Integrin-mediated glioma cell adhesion and free radical-induced apoptosis are regulated by binding to a C-terminal domain of PG-M/versican. *J Biol Chem* 277(14):12294-12301.

58. Yamagata M, Suzuki S, Akiyama SK, Yamada KM, & Kimata K (1989) Regulation of cell-substrate adhesion by proteoglycans immobilized on extracellular substrates. *J Biol Chem* 264(14):8012-8018.
59. Wight TN (2002) Versican: a versatile extracellular matrix proteoglycan in cell biology. *Curr Opin Cell Biol* 14(5):617-623.
60. Mjaatvedt CH, Yamamura H, Capehart AA, Turner D, & Markwald RR (1998) The *Cspg2* gene, disrupted in the *hdf* mutant, is required for right cardiac chamber and endocardial cushion formation. (Translated from English) *Developmental Biology* 202(1):56-66 (in English).
61. Keegan BR, Meyer D, & Yelon D (2004) Organization of cardiac chamber progenitors in the zebrafish blastula. *Development* 131(13):3081-3091.
62. Stainier DY, Lee RK, & Fishman MC (1993) Cardiovascular development in the zebrafish. I. Myocardial fate map and heart tube formation. *Development* 119(1):31-40.
63. Thomas NA, Koudijs M, van Eeden FJ, Joyner AL, & Yelon D (2008) Hedgehog signaling plays a cell-autonomous role in maximizing cardiac developmental potential. *Development* 135(22):3789-3799.
64. Schoenebeck JJ, Keegan BR, & Yelon D (2007) Vessel and blood specification override cardiac potential in anterior mesoderm. *Dev Cell* 13(2):254-267.
65. Yelon D, Horne SA, & Stainier DY (1999) Restricted expression of cardiac myosin genes reveals regulated aspects of heart tube assembly in zebrafish. *Dev Biol* 214(1):23-37.
66. Yelon D (2001) Cardiac patterning and morphogenesis in zebrafish. *Dev Dyn* 222(4):552-563.
67. Kikuchi Y, *et al.* (2000) The zebrafish *bonnie and clyde* gene encodes a Mix family homeodomain protein that regulates the generation of endodermal precursors. *Genes Dev* 14(10):1279-1289.
68. Kikuchi Y, *et al.* (2001) *casanova* encodes a novel Sox-related protein necessary and sufficient for early endoderm formation in zebrafish. *Genes Dev* 15(12):1493-1505.
69. Stainier DY (2001) Zebrafish genetics and vertebrate heart formation. *Nat Rev Genet* 2(1):39-48.
70. Li YX, *et al.* (2003) Cardiac neural crest in zebrafish embryos contributes to myocardial cell lineage and early heart function. *Dev Dyn* 226(3):540-550.
71. Sato M & Yost HJ (2003) Cardiac neural crest contributes to cardiomyogenesis in zebrafish. *Dev Biol* 257(1):127-139.
72. Hove JR, *et al.* (2003) Intracardiac fluid forces are an essential epigenetic factor for embryonic cardiogenesis. *Nature* 421(6919):172-177.
73. Bartman T, *et al.* (2004) Early myocardial function affects endocardial cushion development in zebrafish. *PLoS Biol* 2(5):E129.
74. Hu N, Sedmera D, Yost HJ, & Clark EB (2000) Structure and function of the developing zebrafish heart. *Anat Rec* 260(2):148-157.
75. Serluca FC (2008) Development of the proepicardial organ in the zebrafish. *Dev Biol* 315(1):18-27.
76. Manner J (1993) Experimental study on the formation of the epicardium in chick embryos. *Anat Embryol (Berl)* 187(3):281-289.
77. Auman HJ, *et al.* (2007) Functional modulation of cardiac form through regionally confined cell shape changes. *PLoS Biol* 5(3):e53.
78. Qu X, *et al.* (2008) *Ndr4* is required for normal myocyte proliferation during early cardiac development in zebrafish. *Dev Biol* 317(2):486-496.

79. Liu J, *et al.* (2010) A dual role for ErbB2 signaling in cardiac trabeculation. *Development* 137(22):3867-3875.
80. Rohr S, Otten C, & Abdelilah-Seyfried S (2008) Asymmetric involution of the myocardial field drives heart tube formation in zebrafish. *Circulation research* 102(2):e12-19.
81. Beis D, *et al.* (2005) Genetic and cellular analyses of zebrafish atrioventricular cushion and valve development. *Development* 132(18):4193-4204.
82. Smith KA, *et al.* (2009) Dominant-negative ALK2 allele associates with congenital heart defects. *Circulation* 119(24):3062-3069.
83. Scherz PJ, Huisken J, Sahai-Hernandez P, & Stainier DY (2008) High-speed imaging of developing heart valves reveals interplay of morphogenesis and function. *Development* 135(6):1179-1187.
84. Hinton RB, Jr., *et al.* (2006) Extracellular matrix remodeling and organization in developing and diseased aortic valves. *Circ Res* 98(11):1431-1438.
85. Sato Y, *et al.* (2009) Molecular basis of the recognition of nephronectin by integrin alpha8beta1. *J Biol Chem* 284(21):14524-14536.
86. Kahai S, *et al.* (2009) MicroRNA miR-378 regulates nephronectin expression modulating osteoblast differentiation by targeting GalNT-7. *PLoS One* 4(10):e7535.
87. Brandenberger R, *et al.* (2001) Identification and characterization of a novel extracellular matrix protein nephronectin that is associated with integrin alpha8beta1 in the embryonic kidney. *J Cell Biol* 154(2):447-458.
88. Linton JM, Martin GR, & Reichardt LF (2007) The ECM protein nephronectin promotes kidney development via integrin alpha8beta1-mediated stimulation of Gdnf expression. *Development* 134(13):2501-2509.
89. Muller U, *et al.* (1997) Integrin alpha8beta1 is critically important for epithelial-mesenchymal interactions during kidney morphogenesis. *Cell* 88(5):603-613.
90. Cheng CW, *et al.* (2008) Nephronectin expression in nephrotoxic acute tubular necrosis. *Nephrol Dial Transplant* 23(1):101-109.
91. Kuphal S, Wallner S, & Bosserhoff AK (2008) Loss of nephronectin promotes tumor progression in malignant melanoma. *Cancer Sci* 99(2):229-233.
92. Miyazono A, *et al.* (2007) TGF-beta suppresses POEM expression through ERK1/2 and JNK in osteoblasts. *FEBS Lett* 581(27):5321-5326.
93. Fang L, *et al.* (2010) Transforming growth factor-beta inhibits nephronectin-induced osteoblast differentiation. *FEBS Lett* 584(13):2877-2882.
94. Kahai S, Lee SC, Seth A, & Yang BB (2010) Nephronectin promotes osteoblast differentiation via the epidermal growth factor-like repeats. *FEBS Lett* 584(1):233-238.
95. D'Amico L, Scott IC, Jungblut B, & Stainier DY (2007) A mutation in zebrafish *hmgcr1b* reveals a role for isoprenoids in vertebrate heart-tube formation. *Curr Biol* 17(3):252-259.
96. Jin SW, Beis D, Mitchell T, Chen JN, & Stainier DY (2005) Cellular and molecular analyses of vascular tube and lumen formation in zebrafish. *Development* 132(23):5199-5209.
97. Mably JD, Mohideen MA, Burns CG, Chen JN, & Fishman MC (2003) heart of glass regulates the concentric growth of the heart in zebrafish. *Curr Biol* 13(24):2138-2147.
98. Dorsky RI, Sheldahl LC, & Moon RT (2002) A transgenic Lef1/beta-catenin-dependent reporter is expressed in spatially restricted domains throughout zebrafish development. *Dev Biol* 241(2):229-237.



99. Stoick-Cooper CL, *et al.* (2007) Distinct Wnt signaling pathways have opposing roles in appendage regeneration. *Development* 134(3):479-489.
100. Westerfield M (1993) *The zebrafish book : a guide for the laboratory use of zebrafish (Brachydanio rerio)* (M. Westerfield, Eugene, OR) p 1 v. (unpaged).
101. Birnboim HC & Doly J (1979) A rapid alkaline extraction procedure for screening recombinant plasmid DNA. *Nucleic Acids Res* 7(6):1513-1523.
102. Yu PB, *et al.* (2008) Dorsomorphin inhibits BMP signals required for embryogenesis and iron metabolism. *Nat Chem Biol* 4(1):33-41.
103. Lowry OH, Rosebrough NJ, Farr AL, & Randall RJ (1951) Protein measurement with the Folin phenol reagent. *J Biol Chem* 193(1):265-275.
104. Laemmli UK (1970) Cleavage of structural proteins during the assembly of the head of bacteriophage T4. *Nature* 227(5259):680-685.
105. Okagawa H, Nakagawa M, & Shimada M (1996) Immunolocalization of vinculin in the heart of the early developing rat embryo. *Anat Rec* 245(4):699-707.
106. Zang HY, Lardelli M, & Ekblom P (1997) Sequence of zebrafish fibulin-1 and its expression in developing heart and other embryonic organs. *Development Genes and Evolution* 207:340-351.
107. Westin J & Lardelli M (1997) Three novel Notch genes in zebrafish: implications for vertebrate Notch gene evolution and function. *Dev Genes Evol* 207(1):51-63.
108. Fashena D & Westerfield M (1999) Secondary motoneuron axons localize DM-GRASP on their fasciculated segments. *J Comp Neurol* 406(3):415-424.
109. Shirai M, Imanaka-Yoshida K, Schneider MD, Schwartz RJ, & Morisaki T (2009) T-box 2, a mediator of Bmp-Smad signaling, induced hyaluronan synthase 2 and Tgfbeta2 expression and endocardial cushion formation. *Proc Natl Acad Sci U S A* 106(44):18604-18609.
110. Gaussin V, *et al.* (2002) Endocardial cushion and myocardial defects after cardiac myocyte-specific conditional deletion of the bone morphogenetic protein receptor ALK3. *Proc Natl Acad Sci U S A* 99(5):2878-2883.
111. Chi NC, *et al.* (2008) Foxn4 directly regulates tbx2b expression and atrioventricular canal formation. *Genes Dev* 22(6):734-739.
112. Sultana N, *et al.* (2008) Zebrafish early cardiac connexin, Cx36.7/Ecx, regulates myofibril orientation and heart morphogenesis by establishing Nkx2.5 expression. *Proc Natl Acad Sci U S A* 105(12):4763-4768.
113. Eisenberg LM & Markwald RR (1995) Molecular regulation of atrioventricular valvuloseptal morphogenesis. *Circ Res* 77(1):1-6.
114. Ferencz C & Boughman JA (1993) Congenital heart disease in adolescents and adults. Teratology, genetics, and recurrence risks. *Cardiol Clin* 11(4):557-567.
115. Hogan BL (1996) Bone morphogenetic proteins: multifunctional regulators of vertebrate development. *Genes Dev* 10(13):1580-1594.
116. von Bubnoff A & Cho KW (2001) Intracellular BMP signaling regulation in vertebrates: pathway or network? *Dev Biol* 239(1):1-14.
117. Jiao K, *et al.* (2003) An essential role of Bmp4 in the atrioventricular septation of the mouse heart. *Genes Dev* 17(19):2362-2367.
118. Klewer SE, *et al.* (2006) Has2 expression in heart forming regions is independent of BMP signaling. *Gene Expr Patterns* 6(5):462-470.
119. Yamada M, Revelli JP, Eichele G, Barron M, & Schwartz RJ (2000) Expression of chick Tbx-2, Tbx-3, and Tbx-5 genes during early heart development: evidence for BMP2 induction of Tbx2. *Dev Biol* 228(1):95-105.

120. Marques SR & Yelon D (2009) Differential requirement for BMP signaling in atrial and ventricular lineages establishes cardiac chamber proportionality. *Dev Biol* 328(2):472-482.
121. van de Wetering M, *et al.* (2002) The beta-catenin/TCF-4 complex imposes a crypt progenitor phenotype on colorectal cancer cells. *Cell* 111(2):241-250.
122. Kielman MF, *et al.* (2002) Apc modulates embryonic stem-cell differentiation by controlling the dosage of beta-catenin signaling. *Nat Genet* 32(4):594-605.
123. Mjaatvedt CH, Lepera RC, & Markwald RR (1987) Myocardial specificity for initiating endothelial-mesenchymal cell transition in embryonic chick heart correlates with a particulate distribution of fibronectin. *Dev Biol* 119(1):59-67.
124. Wagner M & Siddiqui MA (2007) Signal transduction in early heart development (I): cardiogenic induction and heart tube formation. *Exp Biol Med (Maywood)* 232(7):852-865.
125. Cooley MA, *et al.* (2008) Fibulin-1 is required for morphogenesis of neural crest-derived structures. (Translated from English) *Developmental Biology* 319(2):336-345 (in English).
126. Kahai S, Lee SC, Seth A, & Yang BB (2010) Nephronectin promotes osteoblast differentiation via the epidermal growth factor-like repeats. *FEBS letters* 584(1):233-238.
127. Wight TN (2002) Versican: a versatile extracellular matrix proteoglycan in cell biology. (Translated from English) *Current Opinion in Cell Biology* 14(5):617-623 (in English).
128. Zhang Y, Cao L, Yang BL, & Yang BB (1998) The G3 domain of versican enhances cell proliferation via epidermal growth factor-like motifs. *J Biol Chem* 273(33):21342-21351.
129. Chocron S, Verhoeven MC, Rentzsch F, Hammerschmidt M, & Bakkers J (2007) Zebrafish Bmp4 regulates left-right asymmetry at two distinct developmental time points. *Dev Biol* 305(2):577-588.
130. Ablooglu AJ, Kang J, Handin RI, Traver D, & Shattil SJ (2007) The zebrafish vitronectin receptor: characterization of integrin alphaV and beta3 expression patterns in early vertebrate development. *Dev Dyn* 236(8):2268-2276.
131. Inai K, Norris RA, Hoffman S, Markwald RR, & Sugi Y (2008) BMP-2 induces cell migration and periostin expression during atrioventricular valvulogenesis. *Dev Biol* 315(2):383-396.
132. Ghosh-Choudhury N, *et al.* (2001) Autoregulation of mouse BMP-2 gene transcription is directed by the proximal promoter element. *Biochem Biophys Res Commun* 286(1):101-108.
133. Kawano M, *et al.* (2011) Mechanism involved in enhancement of osteoblast differentiation by hyaluronic acid. *Biochem Biophys Res Commun* 405(4):575-580.
134. Xiao G, *et al.* (2002) Bone morphogenetic proteins, extracellular matrix, and mitogen-activated protein kinase signaling pathways are required for osteoblast-specific gene expression and differentiation in MC3T3-E1 cells. *J Bone Miner Res* 17(1):101-110.
135. Iozzo RV & Schaefer L (2010) Proteoglycans in health and disease: novel regulatory signaling mechanisms evoked by the small leucine-rich proteoglycans. *FEBS J*.
136. Gassmann M, *et al.* (1995) Aberrant neural and cardiac development in mice lacking the ErbB4 neuregulin receptor. *Nature* 378(6555):390-394.
137. Seeley RJ, Sharon LM, & Woods SC (1997) The effect of intragastric ethanol on meal size in the rat. *Pharmacol Biochem Behav* 56(3):379-382.

- 
138. Fuller SJ, Sivarajah K, & Sugden PH (2008) ErbB receptors, their ligands, and the consequences of their activation and inhibition in the myocardium. *J Mol Cell Cardiol* 44(5):831-854.

## Npnt amino acid sequence homology

```

mouse      MAVLLAAVLASSLYLQVAADFGRWRPQIVSSIGLCRYGGRIDCCGWARQSWGQCQFFY 60
Rat        MAVLLVAVLASSLYLQVAADFGRWRPQIVSSIGLCRYGGRIDCCGWARQSWGQCQFFY 60
homo       MDFLALVLVSSLYLQAAAEFDGRWRPQIVSSIGLCRYGGRIDCCGWARQSWGQCQFFY 60
Danio      -MWIIKFMMLWTCWIAVDADFGRWRSQMSSSNGLCRYGGRIDCCGWTRVSWGQCQFP-- 57
          ::  :*  :  :: . *:*:*:*:*:*:*: ** *****:*****:* *****

mouse      VLRQLARIRQCQLKAVCQPQCKHGEICVGNPKCKCHPGFAGKTCNQD----- 106
Rat        VLRQLARIRQCQLKAVCQPQCKHGEICVGNPKCKCHPGFAGKTCNQDEPFHPTPLDQGSSEQ 120
homo       VLRQRIARIRQCQLKAVCQPRCKHGEICVGNPKCKCHPGYAGKTCNQD----- 106
Danio      -----LCQHGCCKHGEICVGNPKCKCHPGYTGKTCNQD----- 88
          :** *****:*****:*****:*****

mouse      -----LNECGLKPRPKHRCMNTFGSYKCYCLNGYMLLPDGSCESSALS 149
Rat        PLFQPPDHDQATSVPSRDLNECGLKPRPKHRCMNTFGSYKCYCLNGYMLMPDGSCESSALS 180
homo       -----LNECGLKPRPKHRCMNTYGSYKCYCLNGYMLMPDGSCESSALT 149
Danio      -----LNECGLKPRPKHRCMNTFGSFICYCLNGFMLLPDGSANART 131
          *****:*****:*****:*****:*****:

mouse      CSMANCQYGC DVVKGQVRCQCPSPGLQLAPDGRITCVDIDEATGRVSCPRFRQCVENTFGS 209
Rat        CSMANCQYGC DVIKGQIRQCQCPSPGLQLAPDGRITCVDIDEATGRVSCPRFRQCVENTFGS 240
homo       CSMANCQYGC DVVKGQIRQCQCPSPGLQLAPDGRITCVDVDECATGRASCPRFRQCVENTFGS 209
Danio      CSMANCQYGC EVMKGEVRCQCPSPGLQLAPDGRITCVDVDECAAGLAVCPFRFKCINTFGS 191
          *****:*****:*****:*****:*****:

mouse      YICKCHTGF DLMYIGGKYQCHDIDEC SLGQHQCSSYARCYNIHGSYKQCQKDG YEGDGLN 269
Rat        YICKCHTGF DLMYIGGKYQCHDIDEC SLGQHQCSSYARCYNIHGSYKQCQKDG YEGDGLN 300
homo       YICKCHKGF DLMYIGGKYQCHDIDEC SLGQYQCSSFARCYNIRGSYKCKCKE GYQG DGLT 269
Danio      YICKCHDGF DLQVNGKYQCTDVNEC SLGQHQC GPPYATCYNTPGSYKCKCKE DYR GVG YD 251
          ***** *:*:*:*:*:*:*****:*****:*****:*****:*****:

mouse      CVYIPKVMIEPSGP-IHMPERNGTISKGDGGHANRIPDAGSTRWPLKTPYIPP-VITNRP 327
Rat        CVYIPKVMIEPSGP-IHMPERNGTILKGDGGYANRIPDAGSTRWPLKTPYIPPPVITNRP 359
homo       CVYIPKVMIEPSGP-IHVPKNGTILKGDITGNNNWI PDVGSTWPPKTPYIPP-IITNRP 327
Danio      CKPIPKVVIDPPRPGKTTTSSNNKGGNKIPGSDQKRITTTITRPFVTAKRISPTITTTTT 311
          * *****:*****:*****:*****:*****:

mouse      TSKP--TTRPTNPPTPQPTPPPPPLPTEPRITPLPPTPERPSTRPT----IAPATS-- 379
Rat        TSKP--TARPTNPPTPQPTPPPPPLPTELRITPLPPTPERPATSPIT----VAPAT--- 410
homo       TSKP--TTRPTPKPTPIPTPPPPPLPTELRITPLPPTPERPTITGLIT----IAPAAS-- 379
Danio      TTKPPPTKKITTPARVPVITTRKPFITRKPVPLVITKPKVPTHQHTITKVPVVTAVVVF 371
          ** * : * * . * .. * ** . . . . : * : * * : * . .

mouse      -----TTRVITVDNRIQTD PQKPRGDVFIPR-QPTNDFEI-FEIERGVSADDEVKD 430
Rat        -----QVVTVDNRIQTD PQKPRGDVFIPR-QPSNDFEI-FEIERGVSADDEAKD 458
homo       -----TPGGITVDNRVQTD PQKPRGDVFIPR-QPSNDFEI-FEIERGVSADDEAKD 430
Danio      IPTRRPFTIPFVTPIDNSIKDITQKQRGDVHIPRHHGKNVVGIDLDIELGN-TEEEKLD 430
          .:*:*: . ** *****:*****:*****:*****:*****:

mouse      DPGILHSCNFDHGLCGWIREKDSDLHWEIARDPAGGQYLTVS-AAKAPGGKAARLVLRLL 489
Rat        DPGILHSCNFDHGLCGWIREKDSDLHWEPTRD PAGGQYLTVS-AAKAPGGKAARLVLRLL 517
homo       DPGVLVHSCNFDHGLCGWIREKDNLDLHWEPIRD PAGGQYLTVS-AAKAPGGKAARLVLRLL 489
Danio      DPESGYLSCSFDHGLCGWIQRREGDLHWEI SDEPSGGRYLTISEGGEKRGGRGAQLLPL 490
          ** ** *****:*****:*****:*****:*****:*****:

mouse      GHLMHSGDLCLSFRHKVTGLHSGTLQVFRKKGHTHGAALWGRNGGHGWRQITILRGADV 549
Rat        GHLMHSGDLCLSFRHKVTGLHSGALQVFRKKGHTHGSALWGRNGGHGWRQITILRGADV 577
homo       GRLMHSGDLCLSFRHKVTGLHSGTLQVFRKKGHTHGAALWGRNGGHGWRQITILRGADI 549
Danio      KTPWNEGNLCLAFRHNMAGHHVGM LQVFFVQKGRQHS PAVWGRITGGNGWRSTQITILWGNGL 550
          :.:*:*:*:*:*:*****:*****:*****:*****:*****:*****:

mouse      KSVIFKGEKRRGHTGEI GLDDVSLKRGRC----- 578
Rat        KSVIFKGEKRRGHTGEI GLDDVSLKRGRC----- 606
homo       KSVVFKGEKRRGHTGEI GLDDVSLKKGHCSEER----- 582
Danio      ESVIVKGERRRGRKGEIALDDMSLKR EDSRKMDTLWKG TWPSPDMVMVHFLSGCKCMS 610
          :*:*: *****:*****:*****:*****:
    
```

**Figure A1:** Amino acid sequence demonstrating Npnt protein homology among zebrafish, mouse, rat and human.

**Table A1: Sequential events during zebrafish heart development**

Events	Developmental time-point
Initiation of Cardiogenesis	Early blastula (2.75 hpf/512 cells)
Cardiac progenitors located at the blastoderm margin	40 % epiboly (5 hpf)
Precardiac cells involute and migrate towards animal pole	Gastrulation (5.5 hpf to 8 hpf)
Progenitors are reached embryonic axis and form a part of ALPM (those cells are <i>NKX2.5</i> positive)	6-8 somite stage (11.5 hpf)
<i>NKX2.5</i> positive cells are migrated medially	10-16 somite stage (14-16 hpf)
Initiation of myocardial differentiation ( Cells exhibit <i>cmhc2</i> expression and ventricular cardiomyocytes are expressed <i>vmhc</i> )	13-14 somite stage (15 hpf)
Atrial progenitors exhibit <i>amhc</i> expression	19 somite stage (17 hpf)
Cardiomyocyte progenitors are formed a pair of bilateral complete tube	16 somite stage (16 hpf)
Cardiac fusion	18 somite stage
Cardiac cone is formed	21 somite stage (19 hpf)
Cardiac tube is formed	27 somite stage (22 hpf)
Initiation of cardiac contraction	27 somite stage (22 hpf)
Organization of the atrial cardiomyocytes is completed	24 hpf
Initiation of cardiac ballooning and looping morphogenesis (visibly distinct ventricular and atrial chambers)	30 hpf

Events	Developmental time-point
Initiation of endocardial cell differentiation and cardiac jelly swelling at AVC	36 hpf
Visible Proepicardial organs (PEO)	50 hpf
Cellular migration of the PEO	3 dpf to 4 dpf
Ventricular trabeculation initiation	3 dpf
Every part of the adult heart appearance	5 dpf

## ***Acknowledgements***

I am thankful to many people who gave me their immense support during my research work and even more to complete my Ph.D. thesis.

I would like to show my gratitude to Prof. Dr. Dr. Thomas Braun and Dr. Felix B. Engel for giving me the opportunity to perform my thesis work at the Max Planck Institute for Heart Lung Research in Dr. Engel's Laboratory.

My warm thanks go to my supervisor Dr. Felix B. Engel for his strong motivation and kind guidance during my Ph.D. research. I would like to thank him for providing constant guidance, contribution, encouragement, and critical reading and helpful suggestions for this thesis and manuscripts. It is difficult for me to find proper and enough words for all his support and for making this journey of mine a pleasurable and unforgettable one.

I take the honor to thank Dr. Benno Jungblut, MPI, Bad Nauheim, for his immense guidance during my research work on zebrafish and whose supervision all through the years of this study was invaluable. I also want to thank all lab members of Dr. Jungblut's laboratory for their kind help to support my research work.

I would like also to thank my colleagues in Dr. Engel's laboratory for their help and for creating a good atmosphere in the group. They became good friends during my Ph.D. study: Machteld J. van Amerongen, Florian Diehl, Tatyana Novoyatleva, Ingrid Hauck-Schmalenberger, Filomena Ricciardi, Ajit Magadum, and Subhajit Ghosh.

It is my pleasure to take the honor to thank Prof. Dr. Anna Starzinski-Powitz, Johann Wolfgang Goethe University, Frankfurt am Main, for acting as my university supervisor enabling my thesis at the MPI as well as for her creative suggestions and constructive criticism during my annual thesis committee meetings.

I want to show my gratitude also to Dr. Gilbert Weidinger and Dr. Günes Özhan-Kizil for providing me the opportunity to study Wnt/ $\beta$ -catenin signaling at the Biotechnology Center, TU Dresden.

I would like to thank all the people at the Goethe Graduate Academy (GRADE) organizing committee for providing a structured PhD program including regular workshops covering different aspects.

Finally, I would like to thank my parents Dhurjati Prasad Patra and Sandhyarani Devi, my grandparents Nabagopal Patra and Uttara Devi and my uncle Tarasankar Patra. They have always stood behind me and have inspired me to pursue my studies.

This work was supported by a grant from the Alexander von Humboldt Foundation (Sofja Kovalevskaja Award to F. B. E.) and the Excellence Cluster Cardio-Pulmonary Systems (DFG).



## **Zusammenfassung**

### **Nephronectin reguliert die Herzklappenentwicklung über den BMP4-HAS2 Signaltransduktionsweg im Zebrafisch**

#### **Einleitung**

Angeborene Herzerkrankungen sind weltweit die häufigste Todesursache aller auf Geburtsfehler zurückzuführender Todesfälle. Ungefähr 1% aller Lebendgeburten ist betroffen (1). Die Ursache für die meisten dieser Erkrankungen ist bisher unklar. Angesichts der hohen Morbidität und Mortalität angeborener Herzerkrankungen ist es wichtig deren Krankheitsursache zu bestimmen. Dafür ist ein detailliertes Wissen der Entwicklung des Herzens erforderlich.

Angeborene Herzklappenfehler stellen mit 20 bis 30% die häufigsten angeborenen Herzerkrankungen dar (3) Aus diesem Grund beschäftigt sich die vorliegende Doktorarbeit mit der Aufklärung molekularer Mechanismen, welche die Herzklappenentwicklung regulieren. In dieser Arbeit wurde der Zebrafisch als Modellsystem gewählt.

#### **Herzentwicklung**

Die Herzentwicklung im Zebrafisch beginnt 2,75 Stunden nach der Befruchtung (hours post fertilization, hpf) im Blastulastadium. Die Kardiogenese erfolgt dann über eine komplexe Serie von Schritten, die anfangs vor allem Differenzierungs- und Migrationsprozesse beinhalten. Das Herz entwickelt sich aus dem Herzblastem in der viszeralen Mesodermschicht der rechten und linken Seite zunächst getrennt voneinander. Später vereinigen sich diese beiden Herzanlagen in der Mittellinie und bilden den Herzschlauch. Dieser beginnt um 22 hpf zu kontrahieren. Die hämodynamischen Veränderungen induzieren regional spezifische Genexpression, die von entscheidender Bedeutung für die Herzklappenentwicklung und Trabekulierung sind (61, 62) (65) (66, 69) (72, 73).

Der Herzschlauch besteht aus dem Endokard und dem Myokard (Muskelschicht), die durch eine zellfreie Schicht extrazellulärer Matrix (EZM), der Herzgallerte, getrennt wird. Der Schlauch wächst und bildet die Herzschleife, in der Ventrikel und Atrium um 30 hpf unterschieden werden

können (70, 71). Am dritten Tag nach Befruchtung sind vier Herzkammern zu erkennen (Atrium, Ventrikel, Sinus Venosus, Bulbus Arteriosus), die durch Einschnürungen voneinander getrennt sind (77, 78). Zu diesem Zeitpunkt beginnt die Trabekulierung, d.h. es bilden sich kleine Gruppen ventrikulärer Herzmuskelzellen, die aus der Herzmuskelwand in die EZM ragen (79).

### **Herzklappenentwicklung**

Alle Wirbeltiere besitzen Herzklappen, um den Blutkreislauf zu regulieren und einen Rückstrom des Blutes in die falsche Richtung zu verhindern. Um 30 hpf sind ventrikuläre Herzmuskelzellen kubisch während Herzmuskelzellen des Atriums und Endokardzellen squamös (flach) sind. Herzmuskelzellen am Übergang vom Atrium zum Ventrikel, dem sogenannten atrio-ventrikulären (AV)-Kanal, haben keine besondere Form (81)

Die Herzklappenentwicklung beginnt im AV-Kanal um 36 hpf mit dem Anschwellen der EZM. Zu dem beginnen sowohl die Herzmuskelzellen als auch die Endokardzellen im AV-Kanal zu differenzieren. Zuerst differenziert nur eine Reihe von 12 Endokardzellen, die zusammen mit den Herzmuskelzellen EZM-Komponenten exprimieren. Dies führt zum Anschwellen der EZM im AV-Kanal. Die Anzahl differenzierter Endokardzellen nimmt stetig zu und am 2ten Tag nach der Befruchtung kleiden 5 bis 6 Reihen differenzierter Endokardzellen den AV-Kanal aus. Diese Zellen sind charakterisiert durch ihre kubische Form und die Expression des Zelladhäsionsproteins Alcam (Dm-grasp). Während der Differenzierung des AV-Kanals und der Herzklappenbildung werden Gene, die zuvor im gesamten Herzschlauch exprimiert wurden, nur noch im AV-Kanal exprimiert (*has2*, *bmp4*, *cspg2*, *tbx2* and *notch1b*). Um 60 hpf beginnen die differenzierten AV-Endokardzellen Herzklappenvorläufer zu bilden (81)

### **Nephronectin**

Wir haben kürzlich Nephronectin (Npnt) als transient exprimiertes Protein in der Herzentwicklung der Ratte identifiziert. Seine Expression korreliert mit der Herzklappenentwicklung. Npnt ist ein EZM-Protein mit folgender Domänenstruktur: N-terminales Signalpeptid, Ca<sup>2+</sup>-abhängigen EGF-ähnlichen Domänen, Mucin-ähnliche Domäne, RGD Sequenz und C-terminale MAM

Domäne. Diese Struktur weist daraufhin, dass es sich um ein sekretiertes, vermutlich glykolisiertes Protein mit adhäsiven Eigenschaften handelt, das mit Wachstumsfaktoren, Wachstumsfaktorrezeptoren und Integrinen interagieren kann. Mehrere Studien legen nahe, dass Npnt eine wichtige Funktion in der Nierenentwicklung und –regeneration spielt sowie in der Differenzierung von Osteoblasten. Funktionell scheint es eine wichtige Funktion in der Zellmigration zu haben (85-88) (91) (90) (93) (94).

### **Problemstellung**

Um die Entwicklung des Herzens besser zu verstehen hat Dr. Engel eine Expressionsstudie durchgeführt, welche die Expression von 28000 Genen während der Herzentwicklung der Ratte vom embryonalen Tag E11 bis zum postnatalen Tag P10,5 im Abstand von 12 Stunden beschreibt. Diese Expressionsdaten verbunden mit einem bioinformatischen Ansatz und dem Wissen über zeitliche Veränderungen der Herzmorphologie resultierte in der Hypothese: „Nephronectin ist ein neuer Regulator der Herzklappenentwicklung und/oder der Trabekulierung“.

Ziel der Arbeit war die Verifizierung dieser Hypothese. Als Modellsystem wurde der Zebrafisch gewählt, da Zebrafische alle 5 Tage mehrere hundert Embryonen produzieren, diese sich extern entwickeln, transparent sind, sich mehrere Tage ohne funktionierendes Herz entwickeln und die Herzklappenentwicklung bereits nach 36 hpf initiiert wird. Darüber hinaus lässt sich die Expression bzw. Funktion von Genen und Proteinen leicht manipulieren.

- Ziel 1:** Bestimmung des räumlich-zeitlichen Expressionsmusters von Npnt während der Herzentwicklung im Zebrafisch.
- Ziel 2:** Morpholino-basierter Knockdown von Npnt, um dessen Funktion während der Herzentwicklung im Zebrafisch zu bestimmen.
- Ziel 3:** Identifizierung der Signaltransduktionswege, die Npnt während der Herzentwicklung nutzt, um die Herzklappenentwicklung zu steuern.

## **Ergebnisse**

Anhand von RT-PCR Experimenten konnte bestätigt werden, dass *npnt* transient im Rattenherzen während der Herzklappenbildung und der Trabekulation exprimiert wird (E11 to E17). Das Protein Npnt konnte mittels Antikörperfärbungen im Myokard aber nicht im Endokard oder Epikard im Herzen von Rattenembryonen (E14) detektiert werden. Zellfraktionierungsexperimente deuten darauf hin, dass *npnt* sowohl in Herzmuskelzellen als auch in den andern Myokardzellen (z.B. Fibroblasten) exprimiert wird.

Die Expression im Zebrafisch wurde mittels *in situ* Hybridisierung bestimmt. Um 24 hpf wurde *npnt* am Schwanzende, im Kopf, am hinteren Ende des Darms und dem Endoderm der Pharynx (Rachen) detektiert. 34 hpf wurde die Expression nach wie vor im Kopf und zusätzlich in der Region der Nierenvorläufer beobachtet. Expression im Herzen wurde erst um 44 hpf detektiert. Zu diesem Zeitpunkt war *npnt* auch in den Schlundtaschen und im Mandibularknorpel exprimiert. Herzexpression war auch noch nach 48 hpf nachweisbar, konnte aber um 53 hpf nicht mehr detektiert werden. Untersuchungen an Schnitten zeigten, dass *npnt* im gesamten Herzen exprimiert wird.

Um die Funktion von Npnt für das Herz zu bestimmen, wurde die Expression von *npnt* mittels sogenannter Morpholinos unterdrückt. Morpholinos sind Oligonukleotide, die an prä-mRNA binden und das Splicing inhibieren bzw. an das Translationsstartkodon ATG binden und die Translation inhibieren. In dieser Studie wurden drei Morpholinos eingesetzt. Western Blot Versuche haben gezeigt, dass alle drei Morpholinos die Expression von Nephronectin auf Proteinebene effizient inhibieren.

Mit Hilfe dieser Morpholinos konnte gezeigt werden, dass der Npnt Knockdown 7 Tage nach Befruchtung zu  $89\% \pm 7.9\%$  lethal ist. Der erste offensichtliche Phänotyp ist ein kardiales Ödem um 75 hpf. Die Herzklappenbildung und Trabekulierung war in  $86\% \pm 3.9\%$  der Zebrafische um 110 hpf stark gestört und  $> 30\%$  dieser Fische zeigten keinerlei Hinweise auf eine Herzklappenentwicklung. Zudem wurde beobachtet, dass die Herzgallerte im gesamten Herzen angeschwollen war.

Eine nähere Analyse unter zur Hilfenahme transgener Fischlinien, in denen die Zellmembran bzw. die Zellkerne von Herzmuskelzellen mit einem Fluorochrom markiert sind, zeigte dass der AV-Kanal in *npnt* Morphanten um 52 hpf verlängert war. Anhand von Ko-Injektionen von Morpholinos und *npnt* mRNA konnte gezeigt werden, dass dieser Phänotyp spezifisch ist. Die injizierte mRNA wird nicht von den Morpholinos, die Splicing inhibieren, beeinträchtigt und wird daher genutzt, um zu testen welche Nebeneffekte die eingesetzten Morpholinos haben. Die Injektion von 30 pg *npnt* mRNA hatte keinen Effekt auf die Herzentwicklung in Wildtyp Fischen konnte aber auch nicht den Effekt der Morpholinos beeinflussen. Im Gegensatz dazu resultierte die Injektion von 50 pg *npnt* mRNA in einer Reduzierung des AV-Kanaldefekts in den Morphanten.  $40\% \pm 2.33\%$  der Embryonen wiesen nach Ko-Injektion einen AV-Kanal normaler Länge im Gegensatz zu  $11\% \pm 2.0\%$  der Embryonen nach Morpholino-Injektion. Zu dem wurde der Effekt in den übrigen Embryonen gemildert. Injektionen von 80 pg *npnt* mRNA resultierte in starken Defekten in Wildtyp Embryonen.

Nach der Charakterisierung des Phänotyps auf morphologischer Ebene wurden als nächstes molekulare und zelluläre Veränderungen im Myokard untersucht. *In situ* Hybridisierungsexperimente um 52 hpf zeigten, dass die Expression der spezifischen AV-Kanalmarker *cspg2* (*versican* Homolog im Zebrafisch), *bone morphogenetic protein 4* (*bmp4*) und *fibulin1* in den Morphanten expandiert ist. Zu dem wurde in den Morphanten ektopische *cspg2* Expression im Einflusstrakt detektiert. Die Expression der Herzkammer-spezifischen Gene *vmhc* und *amhc* waren nicht beeinflusst. Untersuchungen des Endokards um 52 hpf zeigten, dass die Expression der spezifischen AV-Kanalmarker *notch1b* und *Alcam* expandiert ist. Detaillierte Untersuchungen mittels konfokaler Lasermikroskopie zeigten, dass Morphanten anstatt 5 bis 6 Reihen 8 bis 12 Reihen an *Alcam*-positiven Endokardzellen besitzen. Diese Daten zeigen, dass *Npnt* Knockdown in einer Verlängerung des AV-Kanal auf morphologischer, zellulärer und molekularer Ebene resultiert.

Ein verlängerter AV-Kanal kann durch eine vermehrte Proliferation oder eine vermehrte Differenzierung in AV-Kanalzellen hervorgerufen werden. Zählexperimente um 52 hpf deuten daraufhin, dass sich die Gesamtzahl an Herzmuskelzellen in Wildtyp Embryonen und Morphanten nicht signifikant

unterscheiden. Auch die Anzahl von Zellen im Atrium war nicht beeinflusst. Das lässt darauf schließen, dass in den Morphanten mehr ventrikuläre Zellen in AV-Kanalzellen differenzieren.

Der AV-Kanal ist charakterisiert durch eine lokale Schwellung der Herzgallerte. Während der zuvor beschriebenen Experimente fiel auf, dass in den Morphanten die Herzgallerte im AV-Kanal, aber auch im gesamten Herzen, stark angeschwollen ist. Die lokale Schwellung wird durch die lokale Expression von *bmp4*, *tbx2* und *has2* kontrolliert. Interessanterweise war die Expression dieser Gene in den Morphanten stark expandiert, d.h. die Daten zeigen eine inverse Korrelation des BMP4-HAS2 Signaltransduktionsweges mit Nephronectin Expression. Um zu testen, ob Nephronectin tatsächlich diesen Signaltransduktionsweg reguliert und dessen Misregulation die Ursache der beobachteten Phänotypen ist, wurden HAS2- und BMP4-Inhibierungsexperimente durchgeführt. *has2* Knockdown in den Morphanten reduzierte die Anzahl Alcam-positiver endokardialer AV-Kanalzellen von  $\geq 8$  Reihen ( $183\% \pm 32.2\%$  im Vergleich zur Kontrolle) zu  $\leq 3$  Reihen ( $31\% \pm 11.9\%$  im Vergleich zur Kontrolle) und einer Reduzierung der Expression des spezifischen endokardialen AV-Markers *notch1b*. Im Gegensatz dazu war die Expression der kardialen AV-Markergene *bmp4* und *cspg2* unverändert. Diese Daten legen nahe, dass Nephronectin indirekt die Expression von HAS2 steuert. Um herauszufinden, ob Npnt möglicherweise ein Regulator von BMP4 ist, einem Regulator von HAS2, wurde dessen Rezeptor (Typ I BMP Rezeptor) pharmakologisch mit Dorsomorphin inhibiert. Die optimale Konzentration des Inhibitors wurde mittels Western Blot-Analyse anhand der Phosphorylierung des Mediators Smad bestimmt. Dorsomorphin reduzierte in den Morphanten die Anzahl Alcam-positiver endokardialer AV-Kanalzellen von  $\geq 8$  Reihen ( $166\% \pm 32.7\%$  im Vergleich zur Kontrolle) zu  $\leq 6$  Reihen ( $125.3\% \pm 10.7\%$  im Vergleich zur Kontrolle) und verursachte eine Reduzierung der Expression des spezifischen endokardialen AV Markers *notch1b*, aber auch von *has2* und *cspg2*. Diese Daten deuten daraufhin, dass Nephronectin ein Regulator des BMP4-HAS2 Signaltransduktionsweges ist.

Kürzlich wurde gezeigt, dass Nephronectin als Ligand für Integrin  $\alpha 8$  fungiert. Mittels *in situ* Hybridisierungsexperimenten konnte allerdings zu verschiedensten Zeitpunkten keine *itga8* Expression im Herzen detektiert

werden, obwohl die Expression in mehreren anderen Organen beobachtet werden konnte.

## **Diskussion**

Die Mechanismen, welche die Differenzierung des AV-Kanals kontrollieren sind kaum verstanden obwohl einige wichtige Regulatoren wie Notch, Tbx2 und BMP2 bekannt sind. Allerdings sind die Gene, die diese Regulatoren kontrollieren, weitestgehend unbekannt. Die während dieser Doktorarbeit erbrachten Daten identifizieren *Npnt* als einen neuen Regulator der frühen Herzentwicklung im Zebrafisch. Die Daten legen nahe, dass *Npnt* die Differenzierung des AV-Kanals über den BMP4-HAS2 Signaltransduktionsweg reguliert.

Es wurde gezeigt, dass die Interaktion zwischen Endokard und Myokard eine entscheidende Rolle in der Induktion der Herzklappenentwicklung spielt (23, 123, 124). Eine Veränderung der EZM, die Endokard und Myokard trennen, kann anscheinend diese Interaktion stören. Knockdown der Gene *cspg2* und *has2*, die beide für die Zusammensetzung und damit die Eigenschaften der EZM wichtig sind, resultiert in einer reduzierten EZM und dem Ausbleiben der Herzklappenbildung (53, 60). Knockdown des Gens *npnt* resultiert überraschenderweise in einer vermehrten EZM-Produktion. Darüber hinaus resultiert der *Npnt* Knockdown in einem verlängerten AV-Kanal. Diese Daten deuten darauf hin, dass *Npnt* nicht nur als strukturelles Protein fungiert sondern als negativer Regulator der Differenzierung des AV-Kanals.

Hurlstone und Mitarbeiter haben anhand ihrer Daten mit *apc* Mutanten vorgeschlagen, dass die Differenzierung des Endokards im AV-Kanal durch den Wnt/ $\beta$ -catenin Signaltransduktionsweg vermittelt wird (49). Interessanterweise sind die Phänotypen der *npnt* Morphanten und der *apc* Mutanten ähnlich. Die Herzen beider erscheinen normal um 36 hpf. Allerdings produzieren beide im Gegensatz zu Wildtyp Fischen eine erhöhte Menge an Herzgallerte. In *apc* Mutanten ist Wnt/ $\beta$ -catenin im gesamten Herzen aktiv und resultiert hier in *has2* Expression um 72 hpf. Die Daten der vorliegenden Arbeit zeigen allerdings, dass der Wnt/ $\beta$ -catenin Signaltransduktionsweg um 52 hpf nicht aktiv ist und daher dessen Misregulation vermutlich nicht die Ursache für den Phänotyp der *npnt* Mutanten ist.

Die Daten bzgl. der npnt Morphanten weisen auf die Bedeutung des BMP4-HAS2 Signaltransduktionsweges hin. Die Bedeutung von BMP wurde allerdings nur anhand von dem Inhibitor Dorsomorphin gezeigt. Es wird daher in der Zukunft wichtig sein, diese Ergebnisse mit einer transgenen Zebrafishlinie zu verifizieren, in der BMP Rezeptoren spezifisch blockiert werden können (*tg(hsp70:noggin3)*). Schließlich erscheint es wichtig herauszufinden, wie Npnt den BMP Signaltransduktionsweg genau kontrolliert. Es ist möglich, dass das Myokard im Ventrikel und im Atrium einen Rezeptor exprimiert, an den Npnt bindet und die Differenzierung in AV-Kanalzellen inhibiert. Ein möglicher Kandidat ist Integrin  $\alpha 8$ , das bisher als Npnt Rezeptor beschrieben wurde (85, 87). Allerdings konnte in dieser Arbeit keine Expression von Integrin  $\alpha 8$  im Herzen nachgewiesen werden. Alternativ könnte Integrin  $\alpha V$  als Rezeptor fungieren (130). Seine Expression wurde allerdings im Herzen bisher nicht genau charakterisiert. Aufgrund der  $Ca^{2+}$ -abhängigen EGF-ähnlichen Domänen könnte Npnt möglicherweise auch Wachstumsfaktorrezeptoren aktivieren. So wurde z.B. gezeigt, dass Npnt über seine  $Ca^{2+}$ -abhängigen EGF-ähnlichen Domänen die Differenzierung von Osteoblasten induziert (94). Ein ähnliches Phänomen wurde auch für das EZM-Protein Versican beschrieben, dass mit seinen  $Ca^{2+}$ -abhängigen EGF-ähnlichen Domänen Wachstumsfaktorrezeptoren binden kann (127, 128). Ein möglicher Rezeptor für Npnt sind die sogenannten ErbB Rezeptoren. ErbB Rezeptoren sind wichtig für die Herzklappenentwicklung als auch für die Trabekulierung (28, 136). Zudem ist bekannt, dass die  $Ca^{2+}$ -abhängigen EGF-ähnlichen Domänen mehrerer Proteine (z.B. Versican, EGF, TGF- $\alpha$ , Amphiregulin, Epiregulin, Neuregulin) an die extrazelluläre Domäne von ErbB Rezeptoren binden und diese aktivieren können (138).

Anstatt als Ligand könnte Npnt allerdings auch die Verfügbarkeit bzw. die Konzentration von BMP4 regulieren. Npnt könnte nötig sein, um die Eigenschaften der Herzgallerte so zu regulieren, dass BMP4 nicht von der exprimierenden Zelle weg diffundieren und so seine Funktion nur lokal ausüben kann. Der Knockdown von Npnt würde folglich dazu führen, dass BMP4 aus dem AV-Kanal diffundiert und in dem Ventrikel und dem Atrium, die BMP4 Rezeptoren exprimieren, ektopisch die Differenzierung des AV-Kanals verursachen. Ein ähnlicher Mechanismus wurde für die Differenzierung von



Osteoblasten beschrieben (134). Da die regulatorischen Mechanismen der Differenzierung von Osteoblasten und der Herzklappenentwicklung sich zum Teil sehr ähnlich sind (133), sollte dieser Hypothese in der Zukunft nachgegangen werden.

Die Entdeckung, dass Nephronectin für die Herzentwicklung essentiell ist, ist aus mehreren Gründen von Bedeutung. Dies ist, meines Wissens nach, die erste Studie, die zeigt, dass Npnt transient im Herzen exprimiert ist. Diese Studie zeigt, dass Npnt für die Herzklappenentwicklung und die Trabekulierung des Herzens von Bedeutung ist. Die vorliegenden Daten etablieren Npnt als neuen Regulator für den BMP4-HAS2 Signaltransduktionsweg. Die Daten bestätigen zudem im Zebrafisch, dass HAS2 eine entscheidende Rolle für die Differenzierung der Endothelzellen im AV-Kanal spielt. Schließlich könnte diese Studie von medizinischer Relevanz sein. Defekte in der Herzklappenentwicklung sind für 20% bis 30% aller angeborenen Herzerkrankungen verantwortlich (3). Die Ursache für die meisten dieser Erkrankungen ist jedoch unklar.

## Curriculum Vitae

### Personal details:

---

**Name:** Chinmoy Patra  
**Email ID:** chinmoy.patra@mpi-bn.mpg.de  
**Date of birth:** 6<sup>th</sup> September 1977  
**Nationality:** Indian  
**Gender:** Male

### Education:

---

**2007-2011:** Ph.D.  
**Thesis:** “Nephronectin regulates cardiac valve development via BMP4-HAS2 signaling in zebrafish” under the guidance of Dr. Felix .B. Engel, Max Planck Institute for Heart and Lung Research, Bad Nauheim, Germany.

**2005-2007:** Master in Technology (Biotechnology and Biochemical Engineering) from the Indian Institute of Technology (IIT), Kharagpur, India.  
**Thesis:** “Molecular interaction of natural compounds with actomyosin and there biological effects” under the supervision of Prof. Dr. H. O. Gutzeit, TU Dresden, Germany and Prof. Dr. S. C. Kundu, IIT, Kharagpur, India.

**2001-2005:** Bachelor in Pharmaceutical Science.  
Secured 76.55% (1<sup>st</sup> class Honours) from Jadavpur University, Kolkata, India.

### Achievements:

---

- **DAAD Fellowship** to complete the M. Tech. project at the TU Dresden, Germany.
- Secured **All India Rank 1** in the Graduate Aptitude Test in Engineering (GATE) – 2005 in Pharmaceutical Science.
- Stipend for two years for my M. Tech. study by the Ministry of Human Resource Development, India.
- Secured **2<sup>nd</sup> position** in M. Tech. study with a **CGPA of 9.15** out of 10 from IIT Kharagpur, India.

## Publications

### Publications related to this thesis:

#### Peer-reviewed publications:

1. **Patra C**, Diehl F, Ferrazzi F, van Amerongen MJ, Novoyatleva T, Jungblut B and Engel FB. Nephronectin regulates heart patterning via BMP4-HAS2 signaling during zebrafish development (under revision).

#### Conferences

##### Oral presentation:

##### ***Scientific Sessions of the American Heart Association, USA***

**Patra C**, Ferrazzi F, van Amerongen MJ, Diehl F, Novoyatleva T, Jungblut B, Engel FB (2009). The extracellular matrix protein nephronectin is required for zebrafish heart development. *Circulation* 120(18):S605 (Orlando, USA)

##### ***Annual meeting of the German Cardiac Society - Heart and Circulation Research, Germany***

**Patra C**, Ferrazzi F, van Amerongen MJ, Diehl F, Novoyatleva T, Jungblut B, Engel FB (2009). The extracellular matrix protein nephronectin is required for zebrafish heart development. 75. annual meeting (Mannheim, Germany); *Clin Res Cardiol* 98, Suppl 1: V382

##### Poster presentation:

##### ***Meeting of the Federation of European Connective Tissue Societies***

**Patra C**, Diehl F, Ferrazzi F, van Amerongen MJ, Novoyatleva T, Jungblut B, Engel FB (2010). Nephronectin is required to restrict the differentiation of the atrio-ventricular canal in zebrafish. XXII<sup>nd</sup> Meeting (Davos, Switzerland)

##### ***Weinstein Cardiovascular Development Conference***

**Patra C**, Diehl F, Ferrazzi F, van Amerongen MJ, Novoyatleva T, Jungblut B, Engel FB (2010). Nephronectin is essential for Proper differentiation of zebrafish cardiac atreovertricular canal. (Amsterdam, The Netherlands)

**Published work unrelated to this thesis:****Peer-reviewed publications:**

1) Kundu J<sup>a</sup>, **Patra C**<sup>a</sup> and Kundu SC. Design, fabrication and characterization of silk fibroin-HPMC-PEG blended films as vehicle for transmucosal delivery. *Mat Sci Eng C*. 2008; 28(8):1376-1380.

2) van Amerongen MJ, Diehl F, Novoyatleva T, **Patra C** and Engel FB. E2F4 is required for cardiomyocyte proliferation. *Cardiovasc Res*. 2010; 86(1):92-102.

3) Novoyatleva T, Diehl F, van Amerongen MJ, **Patra C**, Ferrazzi F, Bellazzi R and Engel FB. TWEAK is a positive regulator of cardiomyocyte proliferation. *Cardiovasc Res*. 2010; 85(4):681-690.

a: Contributed equally

**Conferences****Oral presentation:*****Annual meeting of the German Cardiac Society - Heart and Circulation Research***

1) Ferrazzi F, Diehl F, **Patra C**, van Amerongen MJ, Novoyatleva T, Mohammed A-W, Magni P, Bellazzi R, Engel FB (2009). Temporal expression analysis to elucidate regulatory mechanisms of heart development. 75. annual meeting (Mannheim, Germany); *Clin Res Cardiol* 98, Suppl 1: V683

2) Novoyatleva T, van Amerongen MJ, Diehl F, **Patra C**, Ferrazzi F, Engel FB (2009). TWEAK, via its FN14 receptor, is a novel positive regulator of cardiomyocyte proliferation. 75. annual meeting (Mannheim, Germany); *Clin Res Cardiol* 98, Suppl 1: V388

3) van Amerongen MJ, Diehl F, Novoyatleva T, **Patra C**, Engel FB (2009). E2F4 is required for cardiomyocyte proliferation. 75. annual meeting (Mannheim, Germany); *Clin Res Cardiol* 98, Suppl 1: V363

**Poster presentation:*****Weinstein Cardiovascular Development Conference***

van Amerongen MJ, **Patra C**, Jungblut B, Engel FB (2010). Knockdown of the orphan G protein-coupled receptor 126 reduces heart rate and influences ventricular morphogenesis in zebrafish. (Amsterdam, The Netherlands)

***Basic Cardiovascular Sciences Conference 2008 of the American Heart Association***

Ferrazzi F, Diehl F, **Patra C**, van Amerongen MJ, Novoyatleva T, Magni P, Bellazzi R, Engel FB (2008). Systems biology approach to elucidate fundamental mechanisms of heart growth and maturation. *Circ Res* 103:e35-e70 (P98) (Keystone, USA)

***EMBO Practical course on Networks in Biology analysis, modeling and reverse engineering***

Ferrazzi F, Diehl F, **Patra C**, van Amerongen MJ, Novoyatleva T, Mohammed A-W, Magni P, Bellazzi R, Engel FB (2009). Temporal expression analysis to elucidate regulatory mechanisms of heart development. (Bologna, Italy); Best Poster award (2nd prize)

***Annual Meeting of the German Society for Cell Biology***

Novoyatleva T, Diehl F, van Amerongen MJ, **Patra C**, Ferrazzi F, Engel FB (2010). The TWEAK/FN14 axis in cardiomyocyte proliferation. 33. annual meeting (Regensburg, Germany); **Eur J Cell Biol** 89S1, Suppl. 60(MS14-9)